Uptake of natural organic matter (NOM) fractions by anion exchangers in demineralisation and drinking water plants

DISSERTATION

zur Erlangung des akademischen Grades

Doctor rerum naturalium

(Dr. rer. nat.)

vorgelegt

der Fakultät Umweltwissenschaften

der Technischen Universität Dresden

von

Dipl.-Geoökol.

Madlen Pürschel

geboren am 21.01.1982 in Zittau

Tag der Verteidigung: 29.01.2014

Gutachter:

Herr Prof. E. Worch (TUD, UW)

Herr Prof. G. Bernhard (TUD, MN)

Herr Prof. V. Ender (HS Zittau/Görlitz)

Erklärung des Promovenden

Die Übereinstimmung dieses Exemplars mit dem Original der Dissertation zum Thema:

„Uptake of natural organic matter (NOM) fractions by anion exchangers in demineralisation and drinking water plants“

wird hiermit bestätigt.

Zittau, 31.01.2014
……
Ort, Datum

Madlen Pürschel
……
Unterschrift (Vorname Name)

Danksagung

Die vorliegende Arbeit wurde in den Jahren 2008 – 2013 an der Hochschule Zittau/Görlitz (Fakultät Naturwissenschaften/Mathematik) in Zusammenarbeit mit der Technischen Universität Dresden (Fakultät Umweltwissenschaften) und dem Helmholtz-Zentrum Dresden-Rossendorf (Institut für Ressourcenökologie) sowie den Unternehmen Vattenfall PowerConsult GmbH und Vattenfall Europe Generation AG angefertigt. An dieser Stelle bedanke ich mich herzlich bei allen Personen, die zum Gelingen dieser Arbeit beigetragen haben.

Mein ganz besonderer Dank gilt Prof. Dr. Eckhard Worch und Prof. Dr. Volker Ender für die engagierte Betreuung dieser Arbeit. Sie unterstützten mich in der Themenfindung, bei Problemen in der Laborarbeit, in Modellierungsfragen und vor allem in der Diskussion der gewonnenen Ergebnisse und Erkenntnisse. Vielen Dank dafür!

Prof. Dr. Gert Bernhard danke ich für die freundliche Bereitschaft diese Arbeit zu begutachten. Großer Dank gilt Dr. Susanne Sachs für die zuverlässige Unterstützung in der Arbeit mit radioaktiven Substanzen und ihre Hilfsbereitschaft in wissenschaftlichen Fragestellungen.

Herzlich gedankt sei der Hochschule Zittau/Görlitz und den Unternehmen Vattenfall PowerConsult GmbH und Vattenfall Europe Generation AG für die Finanzierung der vorliegenden Arbeit. Ebenso sei gedankt: Rohm und Haas, Bayer AG und Purolite für die kostenlose Bereitstellung der Anionenaustauscherharze sowie dem DOC Labor Dr. Huber für die verlässliche Analysen der NOM-Fraktionen.

Weiterhin möchte ich mich bei meinen Kollegen, speziell bei Eveline Bürger, Matthias Jeschke, Björn Kettner, Maria Meurich und Prof. Dr. Klaus Seibt, für die wissenschaftlichen Diskussionen, der praktisch-technischen Hilfe und für die angenehme Arbeitsatmosphäre bedanken. Vielen Dank auch an Heike Heidenreich, Mathias Hilsberg, René Illgen, Thomas Petrick und Christiana Schmidt für die zuverlässige Laborarbeit.

Familie und Freunden danke ich für das Interesse an meiner Arbeit und die Unterstützung mit freundlichen Worten und Taten wie auch mit willkommener Ablenkung.

List of contents

List of figures

List of tables

Abbreviations

AER	anion exchange resin
BB	building blocks
BET	Brunauer–Emmett–Teller
BP	biopolymers
BTC	breakthrough curve
CAL	calculated
CDOC	chromatographable dissolved organic carbon
DBPs	disinfection by-products
DOC	dissolved organic carbon
exp	experimental
GAC	granular activated carbon
HETP	height equivalent to a theoretical plate
HOC	hydrophobic organic carbon
HS	humic substances
HSDM	homogeneous surface diffusion model
IAST	ideal adsorbed solution theory
IC	ion chromatography
ICP-OES	inductively coupled plasma – optical emission spectrometry
LC-OCD	liquid chromatography – organic carbon detection
LDF	linear driving force
LMW	low-molecular-weight
LSC	liquid scintillation counting
MP	macroporous
MTZ	mass transfer zone
n. a.	not analysed
n. d.	not detectable
Neutr	neutrals
NOM	natural organic matter
POC	particulate organic carbon
RSSCT	rapid small-scale column test
$SUVA_{254}$	specific absorbance at 254 nm
TOC	total organic carbon
UV/VIS	ultraviolet/visible
UV_{254}	ultraviolet absorbance at 254 nm

Nomenclature

A	column cross section (m^2)
a	empirical parameter (s^{-1})
α_{AB}, R^*_{AB}	separation factors (-)
a_{VR}	area available for mass transfer related to the reactor volume (m^{-1})
Bi	Biot number (-)
BV	bed volume (input solution volume related to reactor volume) (-)
b	empirical parameter $(m^2 \cdot L)/(mg \cdot s)$
c	actual concentration in the fluid phase (mg/L)
c_i	concentration of the component *i* (mg/L)
c_s	concentration at the outer solid particle surface (mg/L)
c_0	inlet concentration (mg/L)
$c_{0,a}$	total concentration of all adsorbable NOM fractions (mg/L)
$c_{0,i}$	inlet concentration of the component *i* (mg/L)
D_L	liquid film diffusion coefficient (m^2/s or cm^2/s)
D_S	intraparticle (solid) diffusion coefficient (m^2/s or cm^2/s)
d_P	particle diameter (m)
H_H	hydrodynamic term in the height equivalent to a theoretical plate (HETP) model (m)
H_L	liquid film diffusion term in the HETP model (m)
H_S	intraparticle (solid) diffusion term in the HETP model (m)
K_d	distribution coefficient (-)
K_F	parameter of the Freundlich isotherm $(mg/g)/(mg/L)^n$
$K_{F,i}$	parameter of the Freundlich isotherm of the component *i* $(mg/g)/(mg/L)^n$
K_L	adsorption constant (parameter of the Langmuir isotherm) (L/mg)
k_F	film mass transfer coefficient (m/s)
$k_F a_{VR}$	volumetric film mass transfer coefficient (s^{-1})
k_S	mass transfer coefficient (m/s)
k_S^*	intraparticle mass transfer coefficient (s^{-1})
$k_S^*(0)$	intrinsic mass transfer coefficient (s^{-1})
L	length of the column (m)
M	molecular mass of the solute (g/mol)
m_A	adsorbent mass (g)
n	exponent of the Freundlich isotherm (-)
n_i	exponent of the Freundlich isotherm of the component *i* (-)

q	equilibrium loading corresponding to c (mg/g)
q_i	adsorbed amount of i (mg/g)
q_m	maximum loading (parameter of the Langmuir isotherm) (mg/g)
q_s	loading at the outer particle surface (in equilibrium with c_s) (mg/g)
q_T	total amount adsorbed (mg/g)
q_0	loading corresponding to c_0 (mg/g)
$\overline{q}$	mean loading of the solid phase (mg/g)
Re	Reynolds number (-)
r_P	particle radius (m)
Sc	Schmidt number (-)
Sh	Sherwood number (-)
T	temperature (K)
TVC	total volume (anion exchange) capacity (mol/L)
t	time (s)
t_b^{id}	ideal breakthrough time (s)
V_L	volume of the liquid phase (L)
V_R	(total) reactor volume (volume of the adsorbent particles plus liquid-filled void volume) (L)
V_T	throughput volume (effluent volume at which a given concentration of the adsorbate emerges from the column) (m^3)
$\dot{V}$	volumetric flow rate (L/s)
v_F	linear filter velocity (m/s)
X_A , X_B	reduced concentration of component A or B (-)
Y_A , Y_B	reduced loading of component A or B (-)
z	vertical travel distance through the adsorber (m)
z'	distance of the considered relative concentration of ion/adsorbate from the centre of gravity of the mass transfer zone (m)
z_i	adsorbed phase mol fraction of component i (-)
ε_B	bed porosity (ratio of the liquid-filled void volume between the adsorbent particles and the reactor volume) (-)
η	dynamic viscosity (Pa·s)
λ	actual conductivity in the fluid phase (µS/cm)
λ_0	inlet conductivity (µS/cm)
ρ_B	bed density (ratio of the adsorbent mass and the reactor volume) (g/L)
ρ_P	particle density (ratio of the adsorbent mass and the adsorbent volume including pores (g/L)
v	kinematic viscosity (m^2/s)

φ spreading pressure term originating from the thermodynamic approach (-)

ω empirical parameter that describes the strength of the influence of the adsorbed amount $\overline{q}$ (-)

Abstract

The elimination of natural organic matter (NOM) is an important aim of water treatment in demineralisation plants of power stations. NOM is regarded as corrosion risk factor in the steam water cycle because of its potential to decompose into low-molecular-weight (LMW) acids and carbon dioxide. Further, the removal of NOM is also one of the main objectives in the drinking water production, since it can cause i) colour, taste and odour problems, ii) formation of carcinogen halogenated disinfection by-products (DBPs) after disinfection with chlorine and iii) bacterial growth in the water distribution system.

In earlier studies, it was found that anion exchange is a successful method to remove NOM fractions. However, NOM fractions with low charge density (LMW neutrals and hydrophobic organic carbon (HOC)) and/or large molecular size (biopolymers and particulate organic carbon (POC)) could not be removed in some cases in satisfying quantities. The aim of the present work was to investigate the uptake performance of different anion exchange resins (AERs) in regard to problematic NOM fractions. The AERs differ especially in their functional groups (tertiary versus quaternary amines) and matrix material (polystyrene versus polyacrylic resins). The use of different AERs provides an option to identify possible interactions between adsorbate (NOM fractions) and adsorber (AERs) as well as the mechanism which determine the removal efficiency.

The NOM fraction adsorption onto AERs was studied in equilibrium and fixed-bed experiments with three types of starch with different molecular size distributions (model substances for biopolymer fraction) as well as 2-naphthol (model substance for the LMW neutral fraction) at acidic pH (relevant for water in demineralisation plants of power stations) and neutral pH (covering most raw waters). Furthermore, the NOM fraction uptake from “real” acidic and neutral water samples, obtained from a demineralisation plant of a power station, was estimated for different AERs. Results were discussed in terms of size-exclusion, anion exchange and hydrophilic/hydrophobic repulsion.

In case that size-exclusion influences the NOM uptake onto AERs, it was found that the smaller the size of the NOM molecules and the higher the water content of the AERs, the more effective the uptake is. Thus, for the removal of biopolymers and POC, polyacrylic resins with high water content could be a good choice. Contrary, polystyrene AERs are the most effective resins in the removal of NOM fractions, if no size-exclusion occurs. They

seem to be able to uptake more hydrophilic NOM fractions by polar/ionic interactions between acids/acidic components and tertiary/quaternary amines as well as to remove more hydrophobic NOM fractions by π-π stacking and/or hydrophobic interactions on the polystyrene matrix. Further, it was found that the higher the total volume (anion exchange) capacity of an AER, the higher its NOM removal by polar/ionic interactions can be. At acidic pH, weak/medium base AERs have higher total volume (anion exchange) capacities than strong base AERs, whereas, at neutral pH, strong base AERs have the highest ones.

In view of these results, the application of polyacrylic AERs with high water content can be recommended to remove NOM components with large molecular size in demineralisation and drinking water plants. If there is a higher amount of smaller NOM fractions, especially LMW neutrals, than polystyrene weak/medium base AERs should be favoured in demineralisation plants and polystyrene strong base AERs in drinking water treatment plants.

From the engineering point of view, breakthrough curve (BTC) prediction models are important for the design of fixed-bed filter. Therefore, two different BTC model approaches were tested in the present study to describe the single-solute adsorption onto AERs: i) the homogenous surface diffusion model (HSDM) with linear driving force (LDF) approach for surface diffusion, known from activated carbon adsorption, and ii) the Glueckauf/Helfferich formulae as an extension of the height equivalent to a theoretical plate (HETP) model, initially used to describe ion exchange processes. It was found that the Glueckauf/Helfferich approach is not only a suitable tool for the fast calculation of BTCs for ionic components, but it can also successfully be applied, after considering the Freundlich model for the mass balance, for the rapid prediction of BTCs for single-solute organic molecules. For competitive BTC predictions, the ideal adsorbed solution theory (IAST) within the LDF model was applied. All calculated BTCs fit the experimental data in a good manner. Thus, the investigated BTC models can be applied for estimating the breakthrough bed volumes of different AERs to avoid leakage of NOM in the drinking or demineralised water caused by overloading.

Zusammenfassung

Die Entfernung von natürlichen organischen Substanzen (NOM) ist ein wichtiges Ziel für die Herstellung von Reinstwasser im Kraftwerksbetrieb, da diese sich im Wasser/Dampf-Kreislauf zu niedermolekularen Säuren und Kohlenstoffdioxid zersetzen können und so ein potentielles Korrosionsrisiko darstellen. Außerdem ist die Elimination von natürlichen organischen Substanzen einer der Schwerpunkte in der Trinkwasseraufbereitung, da NOM im Trinkwasser folgende Konsequenzen verursachen können i) Farb-, Geschmacks- und Geruchsprobleme, ii) Bildung von kanzerogen halogenierten Desinfektionsnebenprodukten nach der Desinfektion mit Chlor und iii) Bakterienwachstum im Wasserverteilungssystem.

In früheren Untersuchungen wurde festgestellt, dass Anionenaustauscherharze (AERs) die NOM-Fraktionen in der Regel erfolgreich aufnehmen können. Nur NOM-Fraktionen mit geringer Ladungsdichte (niedermolekulare Neutralstoffe und hydrophober organischer Kohlenstoff) und/oder großer Molekülgröße (Biopolymere und partikulärer organischer Kohlenstoff) können unter bestimmten Bedingungen nicht in zufriedenstellender Menge entfernt werden. Ziel dieser Arbeit war es, das Aufnahmeverhalten unterschiedlicher AERs hinsichtlich problematischer NOM-Fraktionen zu untersuchen. Die AERs unterscheiden sich vor allem in ihren funktionellen Gruppen (tertiäre versus quaternäre Amine) und ihrer Matrix (Polystyren- versus Polyacryl-Harze). Die Verwendung unterschiedlicher AERs erlaubt es, mögliche Wechselwirkungen zwischen Adsorbat (NOM-Fraktionen) und Adsorber (AERs) und die Mechanismen, die die NOM-Aufnahme entscheidend bestimmen, zu identifizieren.

Die Entfernung von NOM-Fraktionen durch AERs wurde in Gleichgewichts- und Festbett-versuchen mittels dreier Stärketypen mit unterschiedlicher Molekülgrößenverteilung (Modellsubstanzen für die Biopolymere) und 2-Naphthol (Modellsubstanz für die Neutralstoffe) unter sauren pH-Bedingungen (relevant für die Herstellung von Reinstwasser im Kraftwerksbetrieb) und neutralen pH-Bedingungen (bedeutsam für die meisten Rohwässer) untersucht. Außerdem sollte das Adsorptionsverhalten von AERs bezüglich verschiedener NOM-Fraktionen unter Einsatz von „real“ neutralen und sauren Wasserproben aus einer Wasseraufbereitungsanlage eines Kraftwerksbetriebes eingeschätzt werden.

In dieser Arbeit konnte gezeigt werden, dass falls Größenausschluss die NOM-Aufnahme von AERs beeinflusst, dann ist die Adsorption der NOM-Fraktionen umso größer, je kleiner die NOM-Moleküle sind und je höher der Wassergehalt der AERs ist. Daher kann für die Entfernung von größeren Biopolymeren, der Einsatz von AERs mit Polyacryl-Matrix und

hohem Wassergehalt die beste Option sein. AERs mit Polystyren-Matrix besitzen die höchste Aufnahmekapazität für NOM-Fraktionen, falls kein Größenausschluss auftritt. Es scheint für sie möglich zu sein, sowohl hydrophile NOM-Fraktionen durch polare/ionische Wechselwirkungen zwischen NOM Säuren/sauren Komponenten und tertiären/quaternären Aminen aufzunehmen als auch hydrophobe NOM-Fraktionen durch π-π Anziehungen und/oder hydrophobe Interaktionen an die Polystyren-Matrix zu binden. Weiterhin konnte gezeigt werden, dass je höher die Gesamtvolumenkapazität eines AERs, desto größer ist die NOM-Entfernung auf Grund von polaren/ionischen Wechselwirkungen. Es gilt, dass schwach/mittel basische AERs im Vergleich zu stark basischen AERs höhere Gesamtvolumenkapazitäten unter sauren pH-Bedingungen besitzen und stark basische AERs die höchsten Gesamtvolumenkapazitäten unter neutralen pH-Bedingungen aufweisen.

Auf Grund dieser Ergebnisse ist es möglich, die Verwendung von AERs mit Polyacryl-Matrix und hohem Wassergehalt für die Entfernung von NOM-Fraktionen mit großer Molekülgröße in Reinst- und Trinkwasseraufbereitungsanlagen zu empfehlen. Falls es einen höheren Anteil von kleineren NOM-Fraktionen, im Besonderen Neutralstoffen, gibt, sollte die Verwendung von schwach/mittel basischen AERs in Vollentsalzungsanlagen von Kraftwerksbetrieben und stark basischen AERs in Trinkwasseraufbereitungsanlagen bevorzugt werden.

Vor allem im Hinblick auf technische Anwendungen ist es wichtig, Durchbruchskurven (BTC) vorausberechnen zu können. In der vorliegenden Arbeit wurden zwei Modellansätze für die Berechnung von BTCs für die Einkomponentenadsorption getestet: i) das homogene Oberflächendiffusionsmodell mit linearer Triebkraft (LDF), bekannt aus Untersuchungen zur Aufnahme von NOM an Aktivkohle, und ii) die Glueckauf/Helfferich-Formeln, primär verwendet für die Beschreibung von Ionenaustauschprozessen. Es konnte gezeigt werden, dass das Glueckauf/Helfferich-Verfahren nicht nur ein geeignetes Instrument für die schnelle Berechnung von BTCs für ionische Komponenten ist, sondern dass dieses, nach Berücksichtigung des Freundlich-Ansatzes in der Massenbilanz, auch erfolgreich angewendet werden kann, um BTCs für Einkomponentenadsorption von Organika zu berechnen. Für die Vorausberechnung von BTCs für Mehrkomponentensysteme wurde die Theorie der idealen adsorbierten Lösung im LDF-Modell genutzt. Die berechneten BTCs stimmen in guter Qualität mit den experimentell ermittelten BTCs überein. Die Ergebnisse verdeutlichen, dass die untersuchten BTC-Modelle eingesetzt werden können, um Durchbruchspunkte für die jeweiligen AERs zu bestimmen und damit die Gefahr des Schlupfes von NOM ins Trink- bzw. Reinstwasser zu minimieren.

1. Introduction

In all raw water sources for demineralised and drinking water, natural organic matter (NOM) occurs, which is a mix of organic materials such as biopolymers (proteins, amino sugars, polypeptides, polysaccharides), humic substances (humic and fulvic acids), building blocks (hydrolysates of humics) and low-molecular-weight (LMW) neutrals/acids (e.g. alcohols, ketones, aldehydes, amino acids).

First, NOM in the demineralised makeup water of power stations is considered to be a corrosion risk factor in the steam water cycle because of the possible decomposition to LMW acids and carbon dioxide (e.g., Svoboda et al., 2003; Huber, 2006). Thus, a limit of 100 ppb total organic carbon (TOC) is recommended for the makeup water of power stations (VGB standard, 2011).

Under raw water conditions with low NOM contents, this limit will be guaranteed by the use of anion exchangers in conventional demineralisation plants (Huber, 2006). In cases, where the raw water is contaminated with high concentrations of NOM and of increased amounts of colloidal particles, the combination of anion exchange with reverse osmosis was successful (Schley and Markert, 2004). Other methods to remove NOM in the makeup water have also been studied, among them ultrafiltration (Hübner, 2011) and adsorption onto activated carbon (Schönfelder and Lutat, 2000; Luukkonen et al., 2012). However, if a conventional demineralisation plant supplies water with TOC contents slightly above 100 ppb TOC, there is an ambivalent situation with three possibilities: i) to extent the present plant with a cost intensive reverse osmosis or another method, ii) to do nothing with the risk of corrosion or iii) to optimise the use of anion exchange resins (AERs) in the already installed reactors. Reasonably, the third opportunity should be checked first.

Second, NOM elimination performance of anion exchangers was also investigated successfully under neutral pH conditions in the field of drinking and waste water treatment (e.g., Heijman et al., 1999; Bolto et al., 2002; Fettig, 2005; Boyer and Singer, 2008; Cornellissen et al., 2008; Caetano et al., 2009). There are two principal reasons to improve TOC removal. Firstly, during drinking water treatment, NOM reacts with chlorine and other disinfectants to form halogenated organic disinfection by-products (DBPs). Investigations revealed that bladder or skin cancer and adverse reproductive outcomes can be attributed to consumption of water that contains DBPs (Villanueva et al., 2007; Karagas et al., 2008).

Secondly, organic pollutants (like phenolic compounds in industrial waste waters) are of particular concern due to their acute toxicity and negative environmental impacts (Jain et al., 2004).

Anion exchange processes have received increased attention in past years as a promising technique for removing NOM. The NOM uptake capacities are mostly influenced by matrix material, porosity and functional groups of the AERs (Boyer and Singer, 2008). However, it is difficult to assess the impacts of raw water composition, NOM characteristics and anion exchanger properties on the NOM removal quantitatively due to the complexity of these influence factors. As a prerequisite for that, more knowledge about the mechanisms of NOM uptake (anion exchange or adsorption) is necessary.

In the past, the NOM elimination efficiency using commercial anion exchange resins was studied mainly through measuring water quality parameters like colour, dissolved organic carbon (DOC), ultraviolet absorbance at 254 nm (UV_{254}) and specific absorbance at 254 nm ($SUVA_{254}$) (Croué et al., 1999; Bolto et al., 2002; Tan et al., 2005). Deeper insights about the selectivity of the resins to specific NOM components were obtained in studies using the liquid chromatography – organic carbon detection (LC-OCD) after Huber and Frimmel (1996) as advanced organic characterisation method, for instance by Cornelissen et al. (2008) at neutral pH or Huber (2006) at acidic pH. The LC-OCD is a relatively fast measuring method to quantify particulate organic carbon (POC) and hydrophobic organic carbon (HOC) as well as DOC fractions with respect to their molecular size (biopolymers, humic substances, building blocks, LMW neutrals and LMW acids).

Studies by several authors (e.g., Fu and Symons, 1990; Huber and Gluschke, 1998; Bolto et al., 2002) have shown that AERs possess the strongest affinity for hydrophilic NOM with small particle size and high charge density. Thus, ion exchange was supposed to be the dominant mechanism for NOM uptake onto AERs. Yet, Croué et al. (1999) suggested that a combination of ion exchange and adsorption was responsible for NOM removal. Additionally, Cornelissen et al. (2008) reported that a substantial portion of the neutral NOM fraction was removed by adsorption.

However, hydrophobic NOM as well as NOM with large molecular size cannot be removed in all cases by AERs in satisfying quantities (Huber and Gluschke, 1998). Following the LC-OCD classification, these problematic fractions are POC, HOC, biopolymers and LMW neutrals. Also, Croué et al. (1999), Hongve et al. (1999) and Humbert et al. (2005)

investigated that neutral molecules, such as polysaccharides and proteins, are less effectively removed by AERs than other NOM components. Ender et al. (2006a) have revealed that about 40 % of the remaining TOC in the makeup water of power stations comes from the POC and HOC fractions, compared to 16 % in the input water. In the remaining chromatographically detectable organic carbon, 80 % are biopolymers and neutrals. As a consequence, POC/HOC, biopolymer and neutral fractions are in focus of several investigations (Ender et al., 2006b; Tan and Kilduff, 2007; Pürschel and Ender, 2008; Pürschel et al., 2012/2013a) and have the highest potential for further studies to increase the TOC removal in water treatment processes.

The present work was performed to evaluate the NOM fraction uptake on different AERs at acidic pH (relevant for water in demineralisation plants of power stations) and neutral pH (covering most of raw waters). The investigated anion exchangers differ in their matrix material (polystyrene versus polyacrylic resins) and functional groups (tertiary versus quaternary amines). The different AER properties were used to understand the interactions between adsorbate (NOM fractions) and adsorber (AERs) as well as the mechanisms which determine the removal efficiency. The NOM adsorption onto different AERs was studied with the following adsorbates.

First, three types of starch (one of them ^{14}C-labelled) were chosen as model substances for the biopolymer NOM fraction. The use of ^{14}C-labelled starch enables a lower detection limit in relation to classic TOC analysis. Moreover, it was found that the application of ^{14}C-labelled starch – together with unlabelled starch – allows the study of the behaviour of both smaller and larger starch particles in only one experiment. As a model substance for the LMW neutral NOM fraction 2-naphthol was selected. Furthermore, 2-naphthol can also act as a model substance for phenolic organic pollutants in drinking and waste water. The uptake of different starches and 2-naphthol onto four different AERs was investigated in equilibrium, kinetic and fixed-bed experiments.

Furthermore, breakthrough curve (BTC) models can be used to predict the adsorption behaviour of different fixed-bed adsorbers, which is very important in engineering practice. In the present study, two different BTC model approaches were used to describe the single-solute adsorption (model substance at neutral pH): i) the homogeneous surface diffusion model (HSDM) with linear drive force (LDF) approach for surface diffusion (Glueckauf, 1955a; Worch, 2012), known from activated carbon adsorption, and ii) the

Glueckauf/Helfferich formulae as an extension of the height equivalent to a theoretical plate (HETP) model (Glueckauf, 1955b; Helfferich, 1962), initially used to describe ion exchange processes. The first model applies a relatively complex numerical calculation method. The second model is related to an analytical solution. Because of its simple calculation method, the Glueckauf/Helfferich formulae might also be a good alternative for the modelling of single-solute NOM adsorption processes onto AERs. The BTC model used to predict two-component uptake (model substance at acidic pH) was the LDF model with integrated ideal adsorbed solution theory (IAST) (Radke and Prausnitz; 1972; Worch, 2012).

Second, the NOM uptake capacities onto different AERs were also investigated with “real” water originating from the water treatment plant of a power station. The NOM adsorption behaviour was studied with pre-treated water (neutral pH) and pre-treated water after cation exchange (acidic pH). The pre-treatment procedure implies coagulation, neutralisation/precipitation and filtration.

Under drinking water conditions (neutral pH), the present study includes the estimation of equilibrium and kinetic parameters and subsequently the prediction of BTCs for different AERs. For the BTC modelling, the fictive component approach (adsorption analysis) by Johannsen and Worch (1994) was applied to describe the sorption equilibria of the complex NOM system. Further, the HSDM with LDF approach for surface diffusion and the IAST for competitive adsorption (Glueckauf, 1955a; Worch, 1991a/b) were used to predict NOM (fraction) uptake in fixed-bed AER columns at neutral pH. In addition, the applicability of this BTC model for competitive adsorption was verified with the experimental data of NOM uptake on one selected AER.

Under demineralised water production conditions (acidic pH), laboratory fixed-bed experiments were carried out in the present work. NOM was measured as DOC. Additionally, for some samples, the LC-OCD method was applied to investigate the behaviour of the different NOM fractions before the anion breakthrough, since NOM leaching before anion breakthrough reveals the quality of the demineralised water.

Summarising, the main aims of the present work were:

- Quantifying NOM model substance adsorption as well as NOM (fraction) adsorption from “real” water samples and to identify possible size-exclusion effects as well as

potential adsorption mechanisms for specific NOM fraction uptake by AERs to optimise the selection of AERs in water supply companies.

- Testing the applicability of different BTC model approaches to describe the single-solute and competitive NOM adsorption onto AERs to supply engineers with powerful tools to determine fixed-bed adsorber designs.

2. Theory

2.1 Natural organic matter - Background and characterisation

NOM is a mixture of naturally occurring organic compounds having diverse chemical properties. It is known that NOM in demineralised water has been implicated in the corrosion of turbines and engineering systems because of the possible decomposition to LMW acids and carbon dioxide (Svoboda et al., 2003; McDonald et al., 2004; Huber, 2006). Further, during drinking water production, NOM may i) cause colour, taste and odour problems, ii) reacts with chlorine to form halogenated DBPs and iii) promotes bacterial growth in the water distribution system (Christman and Ghassemi, 1966; Croué et al., 1999; Van der Kooij, 2003). Thus, the understanding of the impact of NOM on water treatment processes is an important requirement.

Aquatic NOM is mainly derived as degradation product of organics. NOM can be categorized into humic substances, microbial by-products and colloidal/particulate NOM, depending on their source and characteristics. It is known that humic substances constitute the more hydrophobic NOM fraction and contain a relatively high proportion of aromatic carbon, whereas microbial-derived organic matter is a more hydrophilic NOM fraction and has a higher content of aliphatic carbon (Leenheer, 1994). The colloidal/particulate NOM fraction includes relatively large proteins and polysaccharides. A review about the characterisation of NOM is given for example by Leenheer and Croué (2003).

Studying the effects of NOM properties on natural and engineering processes, the NOM fraction have to be characterised in detail. This is often done by XAD-8/XAD-4 resin chromatography as standard method for fractionating NOM by both polarity and acidity (Aiken et al., 1992). Further separation methods are tangential ultrafiltration or (high pressure) size-exclusion chromatography (Peuravuori et al., 2005). For advanced NOM characterisation ^{13}C-nuclear magnetic resonance spectroscopy and elemental analysis are often used (Peuravuori and Pihlaja, 1997; Sachs et al., 2002). Reviews on the separation methods and analytical chemistry of humic substances are given by Janoš (2003) and McDonald et al. (2004).

In general, TOC or DOC contents as well as UV_{254} and $SUVA_{254}$ values are efficient parameters used to characterise water samples and NOM isolates. TOC is the total amount of organic carbon in the water sample, whereas DOC is defined as the organic carbon

concentration of a water sample filtered through a filter with 0.45 µm pore diameter. UV_{254} is strongly correlated to the concentration of aromatic carbon within NOM. $SUVA_{254}$ is defined as the ratio of UV_{254} absorbance to the DOC concentration, and is reported to be directly proportional to the aromatic carbon content and the molecular weight of NOM.

In the present work, the detailed NOM characterisation was investigated by size-exclusion chromatography in connection with on-line, high-sensitivity organic carbon detection (LC-OCD) after Huber and Frimmel (1996). A schematic diagram of the LC-OCD system and a resulting chromatogram showing the TOC constituents of a surface water sample is presented in Figure 1.

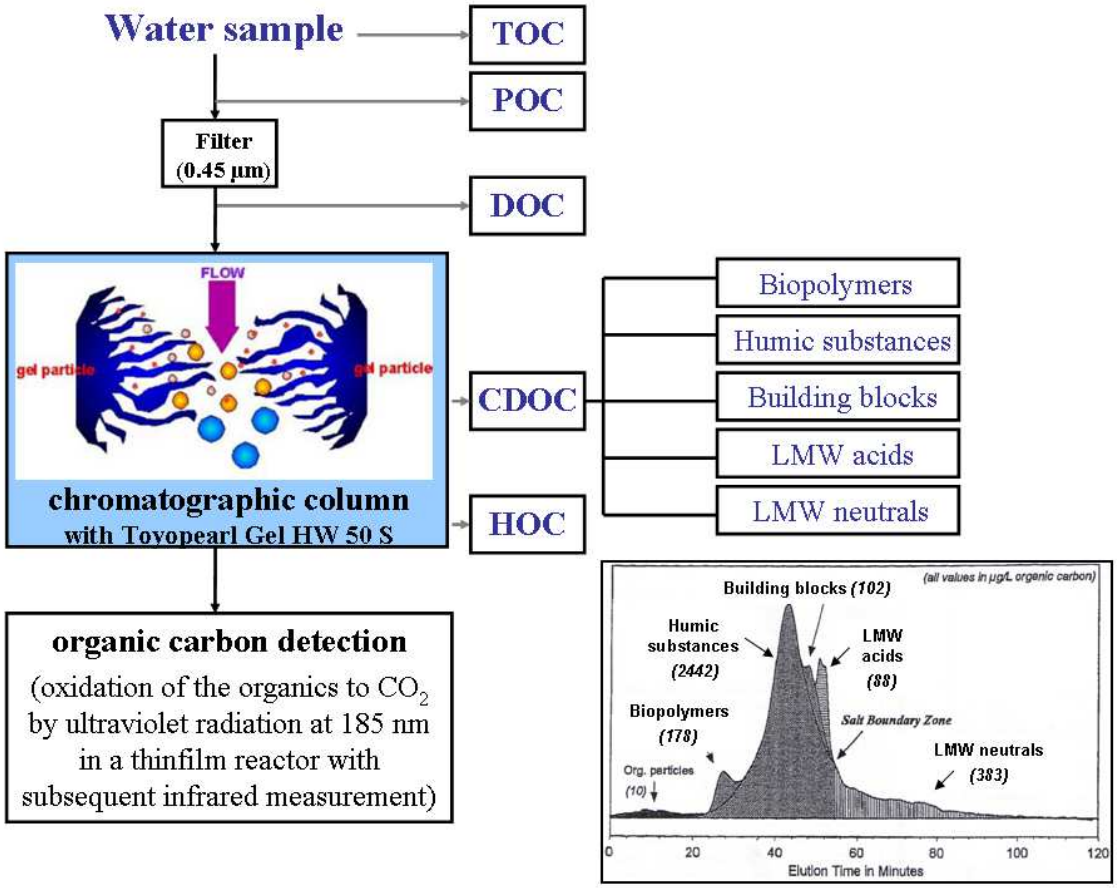

Figure 1. Outline of the NOM fractions analysed by LC-OCD method with resulting chromatogram (after Huber and Frimmel (1996) and Huber and Gluschke (1998)).

LC-OCD = liquid chromatography – organic carbon detection; TOC = total organic carbon; POC = particulate organic carbon; DOC = dissolved organic carbon; CDOC = chromatographable DOC; HOC = hydrophobic organic carbon; LMW = low-molecular-weight; CDOC fractions operational defined; calibration with polyethylene glycol standards

It can be seen in Figure 1 that LC-OCD is a method to separate DOC into fractions depending on their molecular size (biopolymers, humic substances, building blocks, LMW neutrals and LMW acids) without pre-treatment of the samples.

Precisely, the biopolymer fraction includes amino sugars, polysaccharides and proteins with molecular weight greater than 20000 g/mol. The humic substances are humic and fulvic acids with a molecular weight in the range from 500 to 1000 g/mol. The building blocks are the breakdown products of humic substances with molecular weights between 200 and 400 g/mol. The LMW acids are the aliphatic LMW organic acids fractions with molecular weight less than 350 g/mol. The LMW neutrals are accountable for alcohols, aldehydes, ketones, sugars and amino acids. They also possess molecular weight with less than 350 g/mol. The sum of these five fractions is termed chromatographable DOC (CDOC). The difference between DOC and CDOC represents the hydrophobic organic carbon (HOC). The particulate organic carbon (POC) is obtained by on-line filtration and automatic back-flushing of the filter within the “dead volume” of the chromatogram.

2.2 NOM elimination by anion exchange resins

The water treatment process sequence of coagulation/flocculation, clarification and filtration is the most common treatment approach used to decrease to some extent NOM concentrations in water (Krasner and Amy, 1995). Advanced removal of organics in water treatment plants is of considerable interest and has been studied by various methods, among them activated carbon (Boening et al., 1980; Luukkonen et al., 2012), activated alumina (Fettig, 2005), granular ferric hydroxide (Sperlich et al., 2008; Genz et al., 2008), adsorber resins (Aiken et al., 1979; Pan et al., 2005), biologically active filters (Schönfelder and Lutat, 2000), reverse osmosis (Mattaraj and Kilduff, 2000; Schley and Markert, 2004) as well as anion exchanger resins (AERs) and magnetic anion exchange resins (Goto et al., 1986; Croué et al., 1999; Bolto et al., 2002; Humbert et al., 2005; Tan et al., 2005; Boyer and Singer, 2008; Cornelissen et al., 2008). The AERs are of particular interest, since they are able to eliminate NOM fractions specifically and effectively.

The NOM uptake capacities of the anion exchangers are strongly influenced by functional groups, matrix material, porosity, water content and resin size.

Table 1 gives a short overview of the most important functional groups and matrix materials of commercially available AERs.

Table 1. Most important functional groups and matrix materials of AERs

Characteristics				
	secondary amine	**tertiary amine**	**quaternary amine, type I**	**quaternary amine, type II**
functional group	basic and neutral pH: $-HN(CH_3)$ acidic pH: $-H_2N^+(CH_3)$	basic and neutral pH: $-N(CH_3)_2$ acidic pH: $-HN^+(CH_3)_2$	basic, neutral and acidic pH: $-N^+(CH_3)_3$	basic, neutral and acidic pH: $-N^+(CH_3)_2(C_2H_4OH)$
	polystyrene resin		**polyacrylic resin**	
matrix material	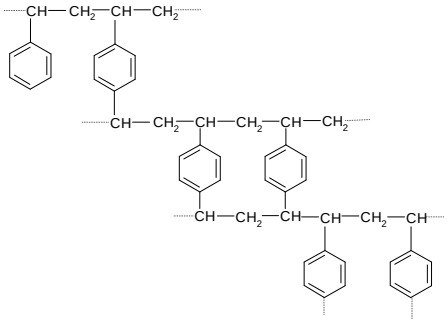		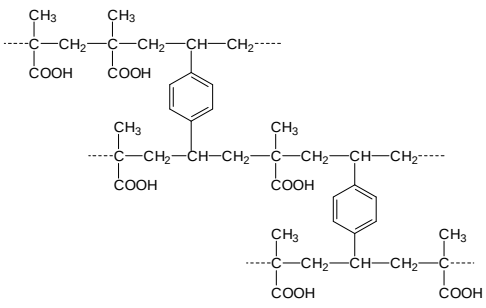	

The classification of AERs into weak, medium and strong base ones is determined by the nature of the amine functional group (see Table 1). Weak base resins contain generally secondary or tertiary amine functional groups. They show best effectiveness under acidic conditions where they tend to be protonated. Strong base resins typically have quaternary amines and are in positively charged form over a wide range of acidic and basic pH values (Helfferich, 1955). Medium AERs have both tertiary and quaternary amine functional groups. Strong base AERs have a higher total volume (anion exchange) capacity *TVC* (mol_{eq}/L) than weak/medium base AERs at neutral pH. Contrary, weak/medium base AERs exhibit a higher *TVC* than strong base AERs at acidic pH.

In earlier studies, it was found that the higher the *TVC* the higher the NOM removal is (Bolto et al., 2002). Among strong base resins, there are two types based on their functional groups: type I (trimethyl-ammonium) and type II (dimethylethanol-ammonium). Due to their lack of ethanolic content, type I resins are more hydrophobic than type II resins (Boyer and Singer, 2008). Thus, type I resins tend to remove more hydrophobic NOM than type II resins.

Also, the matrix material of the resins (see Table 1) strongly influences NOM uptake. AERs with a polystyrene matrix display an increased affinity for aromatic components than resins based on a polyacrylic matrix (Humbert et al., 2005; Gottlieb, 1996). In contrast, AERs with polyacrylic matrix exhibit a higher removal of larger molecules, like biopolymers and fulvic acid, than the polystyrene ones. The hindered uptake of larger molecules by polystyrene resins was discussed as a result of size exclusion processes (Boyer and Singer, 2008; Pürschel et al., 2013a).

The porosity of resins is given as either macroporous (MP) or gel-type. Bolto et al. (2002) investigated that AERs with a MP structure remove more NOM, since organic anions may diffuse easier within this structure, than in gel-type resins. In contrast, Tan et al. (2005) and Cornelissen et al. (2008) found a higher NOM uptake by gel-type resins, because of their higher swelling capacity in water. Consequently, the water content of the AERs is a further property influencing NOM removal. Resins with high water content remove NOM due to a more open structure allowing a better entry of larger compounds (Gottlieb, 1996). Furthermore, Cornelissen et al. (2008) showed that the resins with the smallest particle size were the best-performing AERs for the removal of NOM fractions.

At neutral pH, main mechanisms for NOM removal by AERs are supposed to be polar/ionic interactions between adsorbate and functional groups as well as hydrophobic adsorption onto

the matrix material (Croué et al., 1999; Bolto et al., 2002; Tan et al., 2005; Cornelissen et al., 2008; Li and Sengupta, 2004). At acidic pH, NOM components have a low charge density due to the undissociated form of their functional groups (Ritchie and Perdue, 2003; Boyer and Singer, 2008). Hence, NOM uptake from acidic water onto AERs occurs most likely by ion-dipole, van der Waals and/or hydrophobic interactions between NOM components and anionic resin (Croué et al., 1999).

In the present work, the NOM adsorption onto different AERs was investigated with the following adsorbates: three types of starch with different molecular size (model substances for biopolymers), 2-naphthol (model substance for LMW neutrals) and NOM from "real" water samples. Main aims are to quantify NOM (fraction) adsorption and to identify possible size-exclusion effects as well as potential adsorption mechanisms for NOM fraction uptake by AERs to optimise the selection of AERs in water supply companies.

The possible uptake mechanisms for organic ions onto AERs at neutral and acidic pH are exemplary shown for polystyrene strong base AERs in Figure 2.

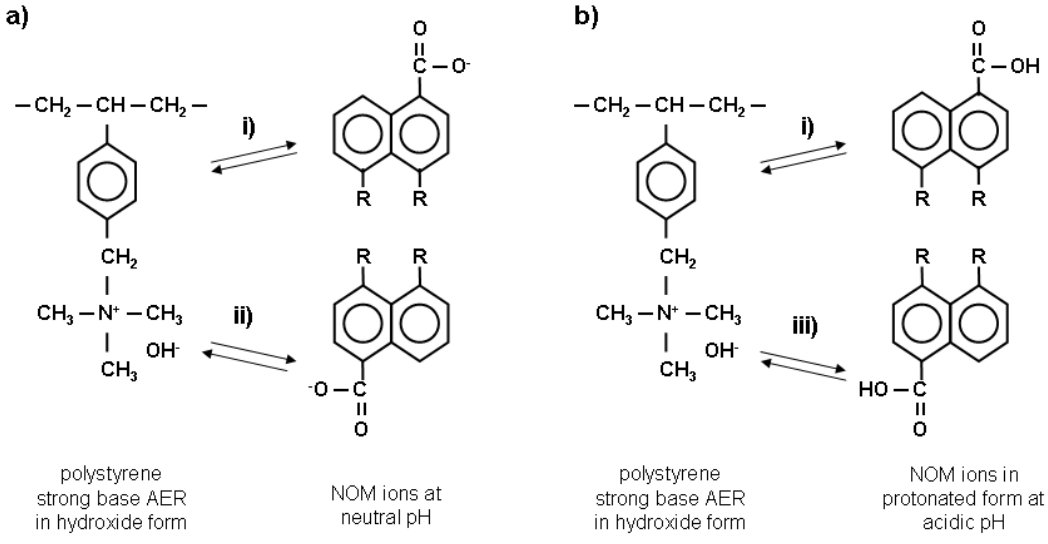

Figure 2. Possible adsorption mechanisms of NOM ions onto a polystyrene strong base AER at a) neutral pH and b) acidic pH are i) π-π stacking and/or hydrophobic interactions, ii) anion exchange and iii) ion-dipole and/or van der Waals interactions.

Figure 2 illustrates the most likely NOM ion uptake mechanisms at neutral and acidic pH. NOM ion uptake could occur at neutral and acidic pH by (i) π-π stacking and/or hydrophobic interactions between non-ionic hydrophobic moieties present on NOM components and the hydrophobic polymer backbone of the anion exchangers (Huang et al., 2012). These interactions could be based on London force between non-polar molecules caused by instantaneously induced dipoles (special form of van der Waals interactions) and/or be due to displacement of water molecules between non-polar particles by aggregating of hydrophobic molecules in order to reduce the surface area exposed to water and minimize their disruptive effect (Tan and Kilduff, 2007).

At neutral pH, the uptake could also occur by (ii) anion exchange, which involves counterion displacement from the resin phase and electrostatic interaction between functional groups (Tan and Kilduff, 2007), in Figure 2 shown as a quaternary amine and a carboxylic NOM moiety. Contrary, at acidic pH, it is known that NOM has a low charge density due to protonation of acidic functional groups (Boyer and Singer, 2008). Thus, (iii) ion-dipole and/or van der Waals interactions are proposed as further NOM uptake mechanism between hydrophilic moieties of the NOM components and functional groups of the anionic resins (Huang et al., 2012).

Furthermore, it can be assumed that less π-π stacking and/or hydrophobic interactions occur between aromatic adsorbates and polyacrylic AERs in comparison to polystyrene resins, due to the less hydrophobic polymer backbone of the polyacrylic resins. Strong base resins typically have quaternary amines, which are positively charged at acidic and basic pH values. Thus, their uptake behaviour due to anion exchange, ion-dipole and/or van der Waals interactions should not depend on the pH conditions. In contrast, weak base resins with their secondary or tertiary amine functional groups are supposed to show higher uptakes due to anion exchange, ion-dipole and/or van der Waals interactions under acidic conditions, where they tend to be protonated, than under neutral conditions. Medium base AERs have both tertiary and quaternary amine functional groups. As a consequence, strong base AERs have a higher *TVC* than weak/medium base AERs at neutral pH. Contrary, weak/medium base AERs exhibit a higher *TVC* than strong base AERs at acidic pH. It can be assumed that the higher the *TVC*, the higher the NOM uptake by anion exchange, ion-dipole and/or van der Waals interactions is.

In the following Figure 3, the possible uptake mechanisms of starch and 2-naphthol onto a strong base AER are exemplary revealed.

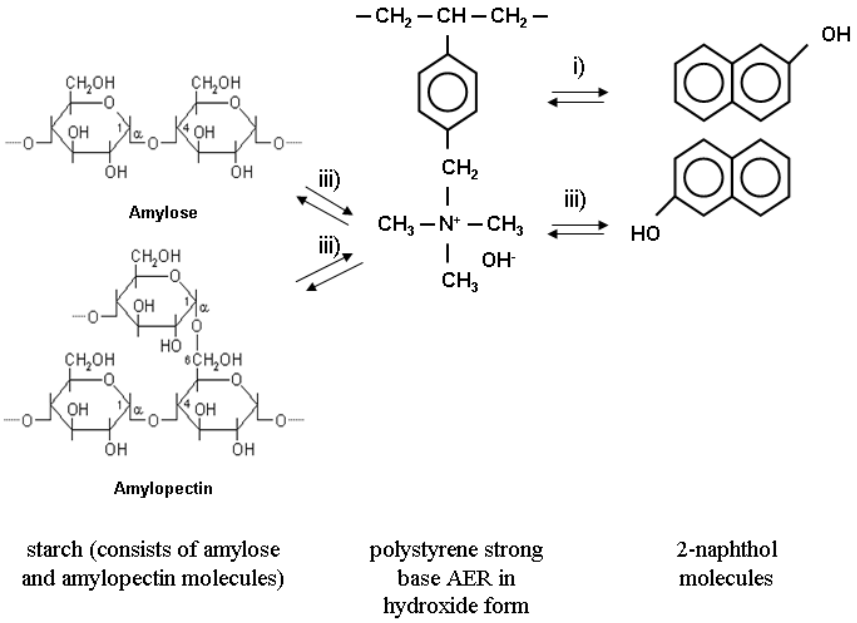

Figure 3. Possible adsorption mechanisms of starch and 2-naphthol onto a polystyrene strong base AER at both neutral and acidic pH are i) π-π stacking and/or hydrophobic interactions and iii) ion-dipole and/or van der Waals interactions.

Like shown in Figure 3, it is assumed that starch, which consists of amylose and amylopectin molecules, is primarily removed from water by (iii) ion-dipole and/or van der Waals interactions between hydrophilic organic molecules and functional groups of the AERs at neutral and acidic pH. 2-Naphthol could be removed by AERs through (i) π-π stacking and/or hydrophobic interactions as well as through (iii) ion-dipole and/or van der Waals interactions between hydroxide moiety of 2-naphthol molecules and functional groups of the anionic resins at both pH conditions.

Again, less π-π stacking and/or hydrophobic interactions should occur between 2-naphthol and polyacrylic resins in comparison to polystyrene resins, caused by the less hydrophobic polymer backbone of the polyacrylic resins. Further, it can be assumed that the higher the *TVC*, the higher the starch and 2-naphthol uptake by ion-dipole and/or van der Waals

interactions is. Thus, strong base AERs should show higher starch and 2-naphthol uptakes due to ion-dipole and/or van der Waals interactions at neutral pH and weak/medium base AERs should have higher starch and 2-naphthol adsorption capacities at acidic pH.

Finally, the anionic composition of water affects the removal of NOM by AERs. In particular, sulphate has been reported to compete with NOM for polar/anion functional sites, thereby adversely affecting removal of NOM (Anderson and Maier, 1979; Tan and Kilduff, 2007).

2.3 Breakthrough curves

BTC measurements are generally applied to study the dynamic adsorption behaviour of adsorbates onto adsorbers.

Generated breakthrough graph is a plot of reduced concentration represented as c/c_0, where c is the actual concentration of the fluid phase (output concentration) and c_0 is the inlet concentration, versus time (t) or bed volume treated (BV; throughput volume (V_T) related to reactor volume (V_R)). In Figure 4, the relation between the traveling of the mass transfer zone (MTZ), which is the boundary between loaded and unloaded adsorbent layers, and the development of the BTC is schematically shown for a single-solute system.

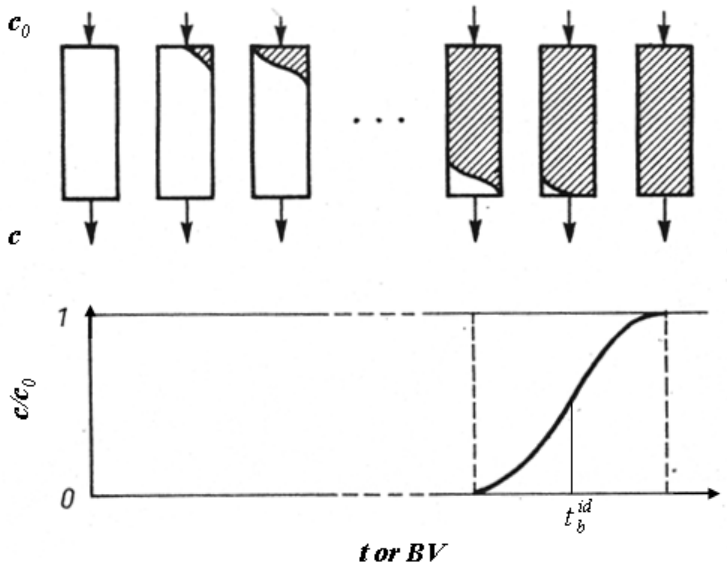

Figure 4. Travelling of the mass transfer zone through the adsorber bed and development of the breakthrough curve, which is a plot of reduced concentration (c/c_0) versus time (t) or bed volume (BV) throughput with t_b^{id} is the ideal breakthrough time (s) (after Kümmel and Worch (1990)).

It can be seen in Figure 4 that the MTZ is reflected by the BTC. The position of the BTC on the time or bed volume axis depends on the flow velocity, input concentration and strength of adsorption. The spreading of the BTC is primarily determined by the film and intraparticle (solid) mass transfer coefficients.

The film mass transfer controls the transport of the adsorbate from the bulk liquid to the external surface of the adsorbent, whereas the intraparticle mass transfer controls the transport into the interior of the adsorbent particle (Helfferich, 1962; Worch 2012). One of these mass transfer steps usually offers a higher resistance than the other, so it can be considered as the rate-limiting step of the process. The influence of film or intraparticle mass transfer controlled uptake on the BTC is revealed in Figure 5.

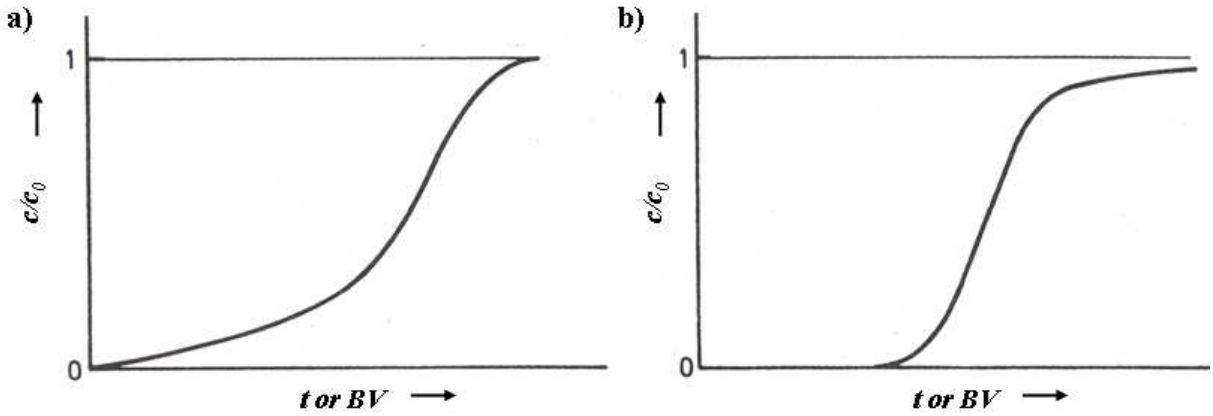

Figure 5. Single-solute breakthrough curves by a) film diffusion and b) intraparticle mass transfer controlled uptake (after Sontheimer et al. (1975)).

If film mass transfer controls the adsorption process, an earlier breakthrough can be observed (Figure 5a). Contrary, if the adsorption process depends on intraparticle mass transfer, a tailing can be found (Figure 5b).

The capacities of the AERs regarding different single-solutes can be calculated from experimental BTCs by application of the integral mass balance equations for ideal BTCs (Equation 1) or for real BTCs (Equation 2) after Worch (2012)

$$q_0 = c_0 \cdot \frac{\dot{V}}{m_A} \cdot t_b^{id} \tag{1}$$

$$q_0 = c_0 \cdot \frac{\dot{V}}{m_A} \cdot \int_{t=0}^{t=\infty} \left(1 - \frac{c}{c_0}\right) dt \tag{2}$$

where q_0 is the loading corresponding to c_0 (mg/g), $\dot{V}$ is the volumetric flow rate (L/s), m_A is the adsorbent mass (g) and t_b^{id} is the ideal breakthrough time (s).

In the case of a multisolute adsorbate system, individual MTZs for the components occur, which pass through the adsorbent with different velocities. As a result, displacement processes take place leading to different breakthrough manners in comparison to single-solute adsorption.

Figure 6 illustrates the breakthrough behaviour of a two-component system.

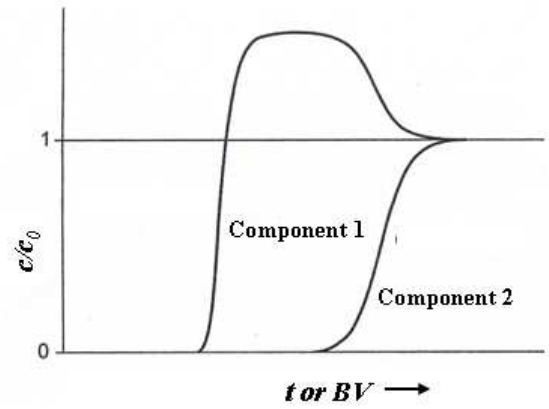

Figure 6. Breakthrough curves of a two-component system with component 1 is weaker adsorbable and component 2 is stronger adsorbable (after Worch (2012)).

In Figure 6, it can be seen that due to competition and displacement, a concentration overshoot ($c/c_0 > 1$) can be found for the weaker adsorbable component 1. In general, an adsorption of an adsorbate onto the resin is reflected by a c/c_0 ratio smaller than 1. Otherwise, $c/c_0 > 1$ indicates the elution of an adsorbate from the resin and $c/c_0 = 1$ refers to resin exhaustion.

Displacement occurs, since the travelling velocity of the MTZ depends on the adsorption strength (Worch, 2012). Component 1 is weaker adsorbable and therefore travels faster through the adsorber. It always reaches the layers of fresh adsorbent at first and is for that reason adsorbed in these layers as a single-solute. Afterward, when the stronger adsorbable component 2 reaches the same layers, a new (two-component) equilibrium state is established, which follow in a partial displacement of the previously adsorbed component 1.

For multi-component systems of unknown composition only total BTCs can be obtained like revealed in Figure 7.

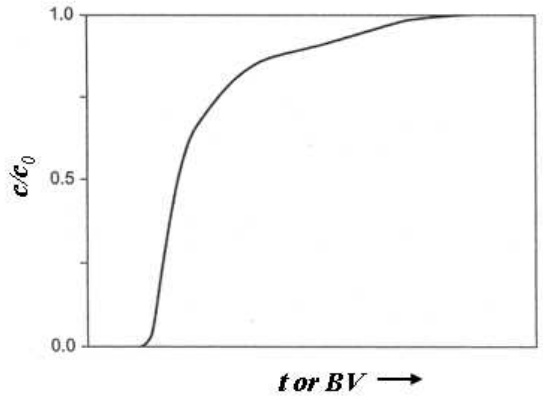

Figure 7. Total breakthrough curve of a multi-component system (after Worch (2012)).

Typically BTCs for NOM uptake (measured as DOC) can look like shown in Figure 7. Otherwise, they can also start at a reduced concentration higher than zero indicating an existence of a non-adsorbable NOM fraction.

There are different reasons to determine fixed-bed BTCs experimentally in laboratory. Experimental BTCs are useful to compare the dynamic NOM uptake of a given aqueous solution by different AERs to get deeper insights, which adsorbate and adsorbent properties have the highest impact on the adsorption without application of a complicated BTC model. If further full-size adsorbers should be designed then a simple scale-up method (for instance the rapid small-scale column test (RSSCT) developed by Crittenden et al., 1986/1987) can be used.

Additionally, experimental BTCs are necessary to verify the suitability of a BTC model for a given adsorbent/adsorbate system. They can also be used to estimate the related mass transfer coefficients for those cases that they are not known from separate kinetic measurements. The BTC model as well as the related adsorption equilibrium and kinetic data can then be used to predict the adsorption behaviour of fixed-bed adsorbers.

2.4 Breakthrough curve models for calculating single-solute adsorption

In the present study, two different BTC model approaches were used to describe the single-solute adsorption i) the HSDM with LDF approach for surface diffusion (Glueckauf, 1955a; Worch, 2012) and ii) the Glueckauf/Helfferich formulae as an extension of the HETP model (Glueckauf, 1955b; Helfferich, 1962).

The LDF model is known for activated carbon adsorption. It has been shown that the LDF model can also be used to predict single-solute NOM as well as total NOM adsorption onto AERs (e.g., Cornelissen et al. (2008)). As far as the author knows, the LDF has not been applied to calculate BTCs for single-solute NOM adsorption onto AERs at acidic pH, where the competitive uptake of the anion of the applied acid has to be considered.

In demineralisation plants, the acidic water condition in front of the anion exchanger are a result of the previous cation exchange water treatment step, which only let pass anions and release protons. Thus, the obtained solution after the cation exchanger is an acid mixture. In the present study, the acidic water composition after the cation exchanger is simulated by addition of an acid to the NOM model substance solution. H_2SO_4 was applied as acid for the following reasons: i) sulphate concentration was found to be the highest anion concentration in the studied “real” water sample after cation exchange and ii) sulphate has been reported to compete more than for example chloride with NOM for polar/anion functional sites and thereby limiting NOM removal (worst case prediction).

The prediction of BTCs for the uptake of single-solute NOM onto AERs at acidic pH is shown in the present work by considering an inverse ideal adsorbed solution theory (IAST) fitting (see sections 2.5 and 2.6).

The Glueckauf/Helfferich formulae are initially applied to describe ion exchange processes. In the present study, this model is firstly used to predict BTCs for single-solute NOM adsorption onto AERs by considering Freundlich isotherm parameters and a separation factor, which can be obtained by the dimensionless form of the Langmuir isotherm equation. The Glueckauf/Helfferich formulae are related to an analytical solution. Because of its simple calculation method, this model might also be a good alternative for the modelling of single-solute NOM adsorption onto AERs.

2.4.1 Linear driving force model

The LDF model is usually applied to describe adsorption processes in fixed-bed adsorbers. In this model, the mass balance equation can be written as:

$$v_F \frac{\partial c}{\partial z} + \varepsilon_B \frac{\partial c}{\partial t} + \rho_B \frac{\partial \overline{q}}{\partial t} = 0 \tag{3}$$

where v_F is the linear filter velocity (m/s), z is the vertical travel distance through the adsorber (m), ε_B is the bed porosity (-), ρ_B is the bed density (g/L) and $\overline{q}$ is the mean loading of the solid phase (mg/g).

The adsorption kinetics is described by simplified mass transport equations based on the LDF approach proposed by Glueckauf (1955a). The rate of film diffusion is given by Equation (4) and the intraparticle (solid) diffusion, which includes pore and surface diffusion, is expressed in Equation (5):

$$\frac{d\overline{q}}{dt} = \frac{k_F a_{VR}}{\rho_B} \cdot (c - c_s) \tag{4}$$

$$\frac{d\overline{q}}{dt} = k_S^* \cdot (q_s - \overline{q}) = \frac{k_S a_{VR}}{1 - \varepsilon_B} \cdot (q_s - \overline{q}) \tag{5}$$

where $k_F a_{VR}$ is the volumetric film mass transfer coefficient (s^{-1}), c_s is the concentration at the outer solid particle surface (mg/L), k_S^* is the intraparticle mass transfer coefficient (s^{-1}), which can be further separated into a mass transfer coefficient k_S (m/s) and a volume-related surface area a_{VR} (m^{-1}) like shown in Equation (5), and q_s is the loading at the outer particle surface (in equilibrium with c_s) (mg/g).

The Freundlich isotherm (Eq. 6) is applied to link concentration and loading at the outer particle surface

$$q_s = K_F \cdot (c_s)^n \tag{6}$$

where K_F ((mg/g)/(mg/L)^n) and n (-) are the parameters of the Freundlich isotherm.

For application of the LDF model, Equations (3)-(6) are written in dimensionless form and solved by numerical calculations (finite difference method) (Worch, 2012).

2.4.2 Glueckauf/Helfferich formulae

The Glueckauf/Helfferich formulae were initially developed to describe ion exchange processes. The integral mass balance is given by Glueckauf (1955b) as

$$V_T(X_A) = A \cdot \left(\frac{\rho_B \cdot q_0}{c_0} \right) \cdot (L - z'(X_A)) \tag{7}$$

where A is the column cross section (m²), L is the length of the column (m), and z' is the distance (m) of the considered relative concentration of ion/adsorbate A ($X_A = c/c_0$) from the centre of gravity of the MTZ.

For the calculation of q_0, related to $c = c_0$, the Freundlich (Eq. 8) or Langmuir (Eq. 9) isotherm equations can be applied

$$q = K_F \cdot c^n \tag{8}$$

$$q = \frac{K_L \cdot q_m \cdot c}{1 + K_L \cdot c} \tag{9}$$

where q is the equilibrium loading corresponding to c, q_m is the maximum loading (parameter of the Langmuir isotherm) (mg/g) and K_L is the adsorption constant (parameter of the Langmuir isotherm) (L/mg).

In general, the Freundlich equation describes very well the interesting medium concentration range for adsorption processes and the Langmuir equation is often used to predict ion exchange processes. As a further option to predict q_0 for an ion exchange process, Bosholm (1972) introduced the reciprocal addition of K_d (dimensionless distribution coefficient) and q_m/c_0.

After Glueckauf (1955b), the parameter z' is defined according to the HETP model as

$$\begin{aligned} z'(X_A) = {} & \frac{H_H + H_S}{2} \cdot \left(\frac{1}{\alpha_{AB} - 1} \cdot \ln \frac{1}{X_A} - \frac{\alpha_{AB}}{\alpha_{AB} - 1} \cdot \ln \frac{1}{1 - X_A} + 1 \right) \\ & + \frac{H_H + H_L}{2} \cdot \left(\frac{\alpha_{AB}}{\alpha_{AB} - 1} \cdot \ln \frac{1}{X_A} - \frac{1}{\alpha_{AB} - 1} \cdot \ln \frac{1}{1 - X_A} - 1 \right) \end{aligned} \tag{10}$$

Here, H_H is the hydrodynamic term, H_S is the intraparticle (solid) diffusion term and H_L is the liquid film diffusion term in the HETP model (all three terms in m), given as

$$H_H = 1.64 \cdot r_P \quad H_S = \frac{c_0}{\rho_B \cdot q_0} \cdot \frac{0.142 \cdot r_P^2 \cdot v_F}{D_S} \quad H_L = \frac{0.266 \cdot r_P^2 \cdot v_F}{D_L \cdot (1 + 70 \cdot r_P \cdot v_F)} \tag{11}$$

where r_P is the particle radius (m), D_S is the intraparticle (solid) diffusion coefficient and D_L is the liquid film diffusion coefficient (both in m²/s).

The separation factor α_{AB} (-) represents the quotient of the concentration ratios of the two counter ions/adsorbates *A* and *B* in the adsorbent and the solution (Helfferich 1962). In general, a dimensionless separation factor, which is not affected by the choice of the concentration unit, is calculated with the dimensionless concentrations ($X = c/c_0$) and loadings ($Y = q/q_0$).

$$\alpha_{AB} = \frac{Y_A \cdot X_B}{Y_B \cdot X_A} \tag{12}$$

with $X_A + X_B = 1$ and $Y_A + Y_B = 1$.

For practical calculations, the reciprocal α_{AB} value (called separation factor R_{AB}^* (-)) is used

$$R_{AB}^* = \frac{X_A \cdot (1 - Y_A)}{Y_A \cdot (1 - X_A)} = \frac{X_A \cdot Y_B}{Y_A \cdot X_B} = \frac{1}{\alpha_{AB}} \tag{13}$$

Thus, for the uptake of ion/adsorbate *A*, a dimensionless form of the Langmuir isotherm equation is obtained

$$Y_A = \frac{X_A}{R_{AB}^* + (1 - R_{AB}^*) \cdot X_A} \tag{14}$$

with $$R_{AB}^* = \frac{1}{1 + K_L \cdot c_0} = \frac{q_m - q_0}{q_m} \tag{15}$$

Equation (15) allows the estimation of R_{AB}^* and subsequently of α_{AB}.

2.5 Breakthrough curve model for predicting competitive adsorption

In the present work, the IAST is applied for predicting mixture adsorption isotherms on the basis of single-solute adsorption parameters. The IAST was developed by Myers and Prausnitz (1965) for gas adsorption and by Radke and Prausnitz (1972) for liquid-phase adsorption. It is widely accepted as the standard model for mixture adsorption modelling. If the single-solute equilibrium data of the mixture components can be described by the Freundlich isotherm, the following set of equations can be derived from the IAST (Worch, 2012):

$$\sum_{i=1}^{N} z_i = \sum_{i=1}^{N} \frac{c_i}{\left(\frac{\varphi \cdot n_i}{K_{F,i}} \right)^{1/n_i}} = 1 \tag{16}$$

$$q_T = \left[\sum_{i=1}^{N} \frac{z_i}{\varphi \cdot n_i} \right]^{-1} \tag{17}$$

$$q_i = z_i \cdot q_T \tag{18}$$

where z_i is the adsorbed phase mol fraction of component i (-), c_i is the concentration of i (mg/L), φ is a spreading pressure term originating from the thermodynamic approach (-), $K_{F,i}$ ((mg/g)/(mg/L)^n) and n_i (-) are the Freundlich isotherm parameters of i, q_T is the total amount adsorbed (mg/g) and q_i is the adsorbed amount of i (mg/g).

The IAST can be integrated into batch and fixed-bed adsorber models. The use of IAST in BTC modelling was described for instance by Moon and Lee (1986) and Worch (1991a/b) for LDF. Furthermore, the inverse IAST can be applied to fit Freundlich parameters for the uptake of single-solute NOM onto AERs at acidic pH (see section 2.6.1).

2.6 Parameter estimation for breakthrough curve modelling

The required input parameters for the adsorption models applied in the present study are summarised in Figure 8.

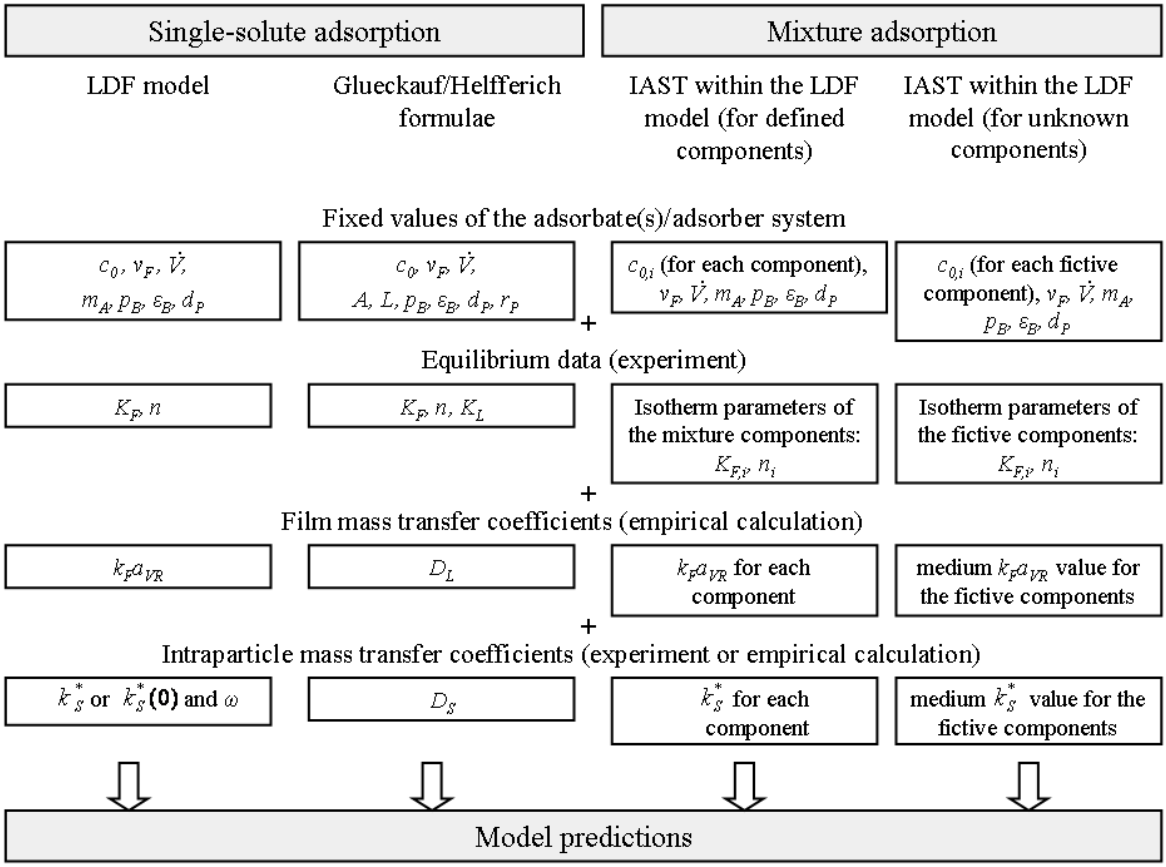

Figure 8. Required input parameters for single-solute and mixture adsorption models.

LDF = linear driving force; IAST = ideal adsorbed solution theory; c_0 = inlet concentration (mg/L); v_F = linear filter velocity (m/s); $\dot{V}$ = volumetric flow rate (L/s), m_A = adsorbent mass (g), p_B = bed density (-); ε_B = bed porosity (-); d_P = particle diameter (m); A = column cross section (m²), L = length of the column (m), r_P = particle radius (m); K_F = parameter of the Freundlich isotherm (mg/g)/(mg/L)^n; n = parameter of the Freundlich isotherm (-); K_L = parameter of the Langmuir isotherm (L/mg); k_Fa_{VR} = volumetric film mass transfer coefficient (s^{-1}); D_L = liquid film diffusion coefficient (m²/s); k_S^* = intraparticle mass transfer coefficient (s^{-1}), $k_S^*(0)$ = intrinsic mass transfer coefficient (s^{-1}); ω = empirical parameter that describes the strength of the influence of the adsorbed amount (-); D_S = intraparticle solid diffusion coefficient (m²/s)

Figure 8 shows that each model needs fixed values for the adsorbate(s)/adsorber system, equilibrium isotherm parameters as well as film and intraparticle mass transfer coefficients. In the following, the determination of the equilibrium isotherm parameters and kinetic coefficients is described in more detail.

2.6.1 Equilibrium isotherm parameters

To determine equilibrium data, the bottle-point (batch) method is usually applied. The time required to reach equilibrium is typically between some hours and some weeks and has to be investigated in preliminary kinetic studies. After the equilibrium is established, the adsorbed mass can be calculated using the material balance equation for batch adsorption processes:

$$q = \frac{V_L}{m_A} \cdot (c_0 - c) = \frac{V_L}{V_R \cdot \rho_B} \cdot (c_0 - c) \tag{19}$$

with V_L is the volume of the liquid phase (L).

In case of single-solute uptake, Freundlich parameters (K_F and n) can be obtained by linear regression analysis of log q values versus log c values, whereas Langmuir parameters (K_L and q_m) can be gained by linear regression analysis of c/q values versus c values.

Single-solute NOM uptake at acidic pH is a two-component system due to the anion of the applied acid. The Freundlich parameters for the single-solute NOM at acidic pH can be estimated from equilibrium experiment results with constant c_0 and varying m_A/V_L ratios. The equilibrium data are plotted in the form of c/c_0 values versus m_A/V_L ratios. Then, the IAST can be applied in an inverse mode, which implies fitting Freundlich parameters to the measured single-solute NOM equilibrium data.

BTC modelling for multi-solute systems requires knowledge of the concentrations and isotherm parameters of all components. In the case of water treatment, NOM is not a defined mixture. Therefore, the concentrations and the isotherm parameters of the different NOM fractions cannot be directly derived from DOC measurements. Applying the LC-OCD analysis for each equilibrium experiment could be a possible, but time-consuming and expensive solution. Another method, which is used in the present work, is to apply a fictive component approach, the so-called adsorption analysis, after Sontheimer et al. (1988) and Johannsen and Worch (1994). The principle of adsorption analysis consists in defining NOM fractions (mostly 3-5) with different adsorption performances characterised by individual Freundlich isotherm parameters (K_F and n). For simplification, n is normally held constant and only different K_F values are used to characterise the graduation of the adsorption strength. Further, a search routine based on the IAST is used to find that concentration distribution of the NOM fractions which allows the best fitting of the experimental data of the DOC isotherm.

2.6.2 Kinetic parameters

The volumetric film mass transfer coefficient $k_F a_{VR}$ (s^{-1}) strongly depends on the hydrodynamic conditions within the reactor. Thus, if the $k_F a_{VR}$ value is needed as input parameter for a BTC model, it cannot be determined using batch experiments. Consequently, $k_F a_{VR}$ values are often estimated by empirical correlations, which relate the film mass transfer coefficient to hydrodynamic conditions, adsorption characteristics and adsorbate properties.

In the present work, each $k_F a_{VR}$ value is obtained by empirical correlations from the dimensionless Reynolds (*Re*) and Schmidt (*Sc*) numbers after Williamson et al. (1963) or Wilson and Geankoplis (1966) (see Equations (20) and (21), respectively). First, the dimensionless Sherwood number (*Sh*) is calculated and subsequently the film mass transfer k_F (m/s) is found from the definition of *Sh*.

$$Sh = 2.4\varepsilon_B \cdot Re^{0.34} \cdot Sc^{0.42} \qquad \text{(for } 0.08 < \text{Re} < 125 \text{ and } 150 < \text{Sc} < 1300\text{)} \tag{20}$$

$$Sh = 1.09 \cdot \varepsilon_B^{-2/3} \cdot Re^{1/3} \cdot Sc^{1/3} \quad \text{(for } 0.0016 < \varepsilon_B Re < 55 \text{ and } 950 < Sc < 70{,}000\text{)} \tag{21}$$

The dimensionless numbers are defined as:

$$Sh = \frac{k_F \cdot d_P}{D_L},\ Re = \frac{v_F \cdot d_P}{\varepsilon_B \cdot \nu} \text{ and } Sc = \frac{\nu}{D_L} \tag{22}$$

where d_P is the particle diameter (m) and v is the kinematic viscosity (m^2/s).

The liquid phase diffusion coefficient D_L (m^2/s) is either known from the literature or can also be obtained by the empirical correlation (Worch, 1993)

$$D_L = \frac{3.595 \cdot 10^{-14} \cdot T}{\eta \cdot M^{0.53}} \tag{23}$$

where T is the temperature (K), η is the dynamic viscosity (Pa·s) and M is the molecular mass of the solute (g/mol).

Additionally to k_F, the volumetric mass transfer area a_{VR} (m^{-1}) is needed for the calculation of the $k_F a_{VR}$ value. It can be calculated by Equation (24) for spherical adsorber materials.

$$a_{VR} = \frac{6 \cdot (1 - \varepsilon_B)}{d_P} \tag{24}$$

The intraparticle (solid) mass transfer coefficient k_S^* (s^{-1}) as well as the respective diffusion coefficient D_S (m^2/s) can be obtained by separate batch kinetic experiments under conditions where only the surface diffusion is rate-determining (high shaking velocity). For the analysis of the kinetic curves (c/c_0 versus time), the balance equation (19) is combined with the LDF kinetic approach proposed by Glueckauf (1955a) and solved numerically.

In some cases, the linear solid-phase concentration gradient (LDF approach) is a too rough simplification to calculate the k_S^* value. Then, a better approximation can be reached, if the k_S^* value is not considered as a constant but as a parameter that depends on the adsorbed amount. This dependence can be described after Worch (2012) with the following equation

$$k_S^* = k_S^*(0) \cdot \exp(\omega \cdot \bar{q}) \tag{25}$$

where $k_S^*(0)$ is the intrinsic mass transfer coefficient (s^{-1}) and ω is a dimensionless empirical parameter that describes the strength of the influence of the adsorbed amount $\bar{q}$. The parameter ω must be negative under the realistic assumption that the intraparticle mass transfer resistance increases with increasing loading.

Further, to avoid time-consuming experiments, the intraparticle (solid) mass transfer coefficient can be approximately predicted by an empirical equation after Hesse and Worch (1997) with

$$k_S^* = 0.00129 \cdot \sqrt{\frac{D_L \cdot c_0}{r_P^2 \cdot q_0}} \tag{26}$$

The correlation gives acceptable results for defined micropollutants. Contrary, the calculated values for NOM containing water are often too high in comparison with parameters estimated by BTC fitting (Worch, 2012). Therefore, a specific correlation was proposed for NOM under the assumption that the mass transfer coefficients are the same for all NOM fractions (Hess, 2001), which is defined as

$$k_S^* = a + b \cdot \frac{c_{0,a}}{r_P^2} \tag{27}$$

where a = 3 x 10^{-6} s^{-1} and b = 3.215 x 10^{-14} $(m^2 \cdot L)/(mg \cdot s)$ are empirical parameters and $c_{0,a}$ is the total concentration of all adsorbable NOM fractions expressed as DOC (mg/L).

Further, D_S can be derived from the k_S^* value following the Glueckauf (1955a) approach

$$D_S = \frac{k_S^* \cdot r_P^2}{15} \tag{28}$$

Finally, the dimensionless Biot numbers *Bi* (-), can be calculated in order to check which mass transfer (film-phase, solid-phase or both) controls the uptake process.

$$Bi = \frac{k_F \cdot r_P \cdot c_0}{D_S \cdot \rho_P \cdot q_0} \tag{29}$$

where ρ_P is the density of the (AER) particle (g/L).

Hand et al. (1984) stated that the adsorption is controlled a) for $Bi \leq 0.5$ by the film mass transfer, b) for $0.5 < Bi \leq 30$ by the film and intraparticle mass transfer and c) for $Bi > 30$ by the intraparticle mass transfer. The influence of *Bi* on the BTCs is shown in Figure 9.

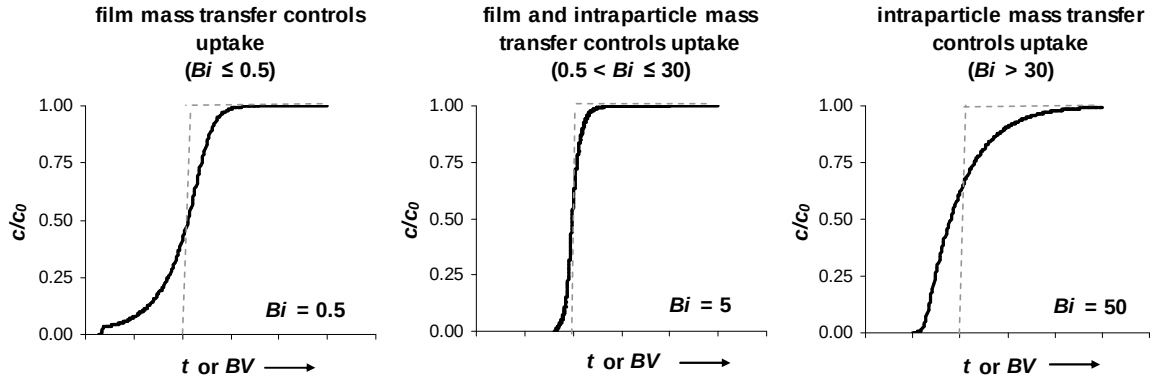

Figure 9. Influence of Biot numbers (*Bi*) on the breakthrough curves calculated by LDF model (--- ideal breakthrough curve).

It can be seen in Figure 9 that low *Bi* values refer to film mass transfer controlled uptake with an earlier breakthrough in comparison to the ideal BTC. High *Bi* numbers indicate an intraparticle mass resistance control on the adsorption process, which results in a long tailing of the BTC. Medium values point to both film and intraparticle mass transfer controlled uptake and leads to symmetrical BTC.

3. Materials and methods

3.1 Anion exchange resins

In the present work, starch and 2-naphthol uptake as well as NOM (fraction) adsorption from "real" water samples, obtained from a demineralisation water supply company, was studied on four fresh AERs (Table 2). The resins were selected in order to cover a broad range in matrix material and functional groups. All four AERs hold a MP structure and were used in the hydroxide form, which is the application form in demineralisation plants of power stations after the cation exchange unit.

AERs characteristics were obtained from product data sheets of the manufacturers. The total volume (anion) capacity *TVC* (mol_{eq}/L) of an AER, which is the sum of functional groups present on the resin material per volume, was calculated from the experimental sulphate BTC (up to $c/c_0 = 1$) by application of the integral mass balance equation for real BTCs (see Equation (2)). Sulphate BTCs were obtained from fixed-bed studies with 0.01 M Na_2SO_4 from KMF (neutral condition with pH 6) and 0.01 M H_2SO_4 from Merck (acidic condition with pH 1.9). The solutions were prepared with Millipore water (pH ≈ 6, conductivity < 1 µS/cm, and TOC < 50 µg/L) obtained from a Millipore ultrapure water system (Elix/Milli-Q Academics). The effluents were analysed by titration measurements with 0.02 M HCl or NaOH as titration solutions (both from Merck) and bromothymol blue as indicator (also from Merck). The detection limit was determined to be 0.0015 M. The evaluation of the *TVC* based on three column experiments for each resin. The relative standard deviation of the *TVC* values was determined to be about 2.9 %.

Significantly different *TVC* values were found under neutral and acidic conditions for the resins (see Table 2). AERs with tertiary amine functional groups need acidic conditions for their optimal function (see section 2.2). This is the reason for very low *TVC* values at neutral pH for weak and medium base AERs IRA96 and AP246. Also, for the strong base AERs IRA900 and A860 about 17 % lower capacities were found under neutral conditions compared to acidic ones. This indicates that the investigated strong base AERs hold not only quaternary amine functional groups, but also few tertiary ones.

Furthermore, four additionally fresh AERs (also in hydroxide form) were investigated under acidic pH conditions for NOM adsorption from the "real" water sample after cation exchange (Table 3).

Table 2. Properties of AERs investigated for starch and 2-naphthol adsorption as well as for NOM uptake from "real" water samples

Parameters	Resin type			
	MP weak and medium base AERs		MP strong base AERs, type I	
	IRA96[a)]	**AP246**[b)]	**IRA900**[a)]	**A860**[c)]
functional group	tertiary amine	tertiary/quaternary amine, type I	quaternary amine, type I	quaternary amine, type I
matrix material	polystyrene	polyacrylic	polystyrene	polyacrylic
structure	MP	MP	MP	MP
water content (%)	57-63	60-65	58-64	66-72
$TVC_{pH\ 6}$ (mol_{eq}/L)	0.10 ± 0.01	0.39 ± 0.01	0.62 ± 0.02	0.63 ± 0.07
$TVC_{pH\ 1.9}$ (mol_{eq}/L)	1.46 ± 0.07	1.44 ± 0.08	0.81 ± 0.11	0.78 ± 0.06
ρ_B (g/L)	670	710	700	700
ρ_P (g/L)	1050	1080	1065	1080
ε_B (-)	0.362	0.343	0.343	0.352
d_P (mm)	0.73	0.47	0.735	0.725
r_P (mm)	0.365	0.235	0.3675	0.3625

[a)] Rohm and Haas, France S.A.S., Chauny Cedex, France; [b)] Bayer AG, Leverkusen, Germany; [c)] Purolite, Bala Cynwyd, USA; AERs = anion exchange resins; NOM = natural organic matter; MP = macroporous; *TVC* = total volume (anion exchange) capacity (median value ± measurement uncertainty after student t-distribution); ρ_B = bed density; ρ_P = particle density; ε_B = bed porosity; d_P = particle diameter; r_P = particle radius

Table 3. Properties of further AERs tested for NOM uptake from "real" water sample after cation exchange

Parameters	Resin type			
	MP medium base AER	MP strong base AER, type I	MP strong base AER, type II	Gel-type strong base AER, type I
	MP64[d)]	**MP500**[d)]	**MP600**[d)]	**VPOC1071**[d)]
functional group	tertiary/quaternary amine, type I	quaternary amine, type I	quaternary amine, type I	quaternary amine, type I
matrix material	polystyrene	polystyrene	polystyrene	polyacrylic
structure	MP	MP	MP	gel
water content (%)	61-66	62-67	45-50	66-72
$TVC_{pH\ 1.9}$ (mol_{eq}/L)	1.36 ± 0.19	0.84 ± 0.19	1.14 ± 0.06	1.10 ± 0.13
ρ_B (g/L)	620	660	680	700
ρ_P (g/L)	1040	1070	1100	1080
ε_B (-)	0.404	0.383	0.382	0.352
d_P (mm)	0.59	0.64	0.62	0.725
r_P (mm)	0.295	0.32	0.31	0.3625

[d)] Lewatit, Lanxess GmbH, Leverkusen, Germany; AERs = anion exchange resins; NOM = natural organic matter; MP = macroporous; *TVC* = total volume (anion exchange) capacity (median value ± measurement uncertainty after student t-distribution); ρ_B = bed density; ρ_P = particle density; ε_B = bed porosity; d_P = particle diameter; r_P = particle radius

The cleaning procedure of the resins was optimised to minimise organic leachables from the AERs in batch and column experiments. Best results were found for the following procedure applied for 100 mL resin: washing with Millipore water, threefold shaking (200 rpm) for 1 h

with 500 mL 0.1 M NaOH, sequenced treatment in a soxhlet reactor first with 250 mL methanol and after that with 250 mL acetonitril (each for 24 h), washing with Millipore water and rinsing with 400 mL 1 M NaOH, 300 mL 1.4 M HCl and again twice with 400 mL 1 M NaOH (each step with 4 BV/h), and final washing with Millipore water. NaOH were obtained from VWR and HCl, methanol and acetonitril from Merck. All AERs were stored in Millipore water.

The success of the cleaning procedure by soxhlet-extraction was tested subsequently in batch experiments. For this, 50 mg untreated as well as soxhlet-treated resins were shaken (200 rpm) for 24 h with 100 mL Millipore water. The amount of organic leachables (analysed as DOC using a TOC analyzer multi N/C UV HS from Analytik Jena AG) in the decanted water solutions was measured. The DOC concentrations in the water samples for the experiments with untreated as well as soxhlet-treated resins are given in Table 4.

Table 4. DOC content in the water samples after batch experiment with untreated and soxhlet-treated AERs

Parameters	**Resin type**		
	MP weak base AER	MP strong base AERs, type I	
	IRA96	**IRA900**	**A860**
Experiment with untreated resins			
DOC (µg/L)	630.3	245.8	29.3
Experiment with soxhlet-treated resins			
DOC (µg/L)	352.3	76.2	5.7

DOC = dissolved organic carbon; MP = macroporous; AER = anion exchange resin

As can be seen in Table 4, considerably lower DOC concentrations were found with soxhlet-treated resins. This is valid for all investigated AERs.

Several methods were compared to dose accurately small quantities of resin without loss of *TVC* as a consequence of drying processes. It was found that preparation methods for anion exchangers from other authors like vacuum filtration and storing in a desiccator for 24 h (Boyer et al., 2008) or desiccation in vacuum at 325 K for 24 h (Zhang et al., 2009), could not be applied for the AERs without a significant loss of *TVC*. Therefore, the Millipore water, in which the AERs were stored, was merely decanted before the resins were weighted (1.00 ± 0.02 g wet resin is equal to 1.11 ± 0.05 mL resin volume, which is herein after referred to as reactor volume V_R).

3.2 Adsorbates

3.2.1 Model substances

Two types of starch (from Chemapol and Merck) as well as 2-naphthol (from Merck) were used in analytical grade. In addition, a ^{14}C-labelled starch, obtained from Biotrend as uniform ^{14}C-labelled product (1.5 mCi/g = 55.5 MBq/g), was applied. All TOC solutions were prepared with Millipore water (pH ≈ 6, conductivity < 1 µS/cm, and TOC < 50 µg/L) from a Millipore ultrapure water system (Elix/Milli-Q Academics).

Analytical grade H_2SO_4 (from KMF) was used for pH adjustment. It is known that H_2SO_4 dissociate as strong acid to H^+ and HSO_4^-. Further, HSO_4^- reacts to H^+ and SO_4^{2-} (pK_a = 1.92 (Küster and Thiel, 2008)). Therefore, a measured pH of 2.2 is equal to 260 mg/L SO_4^{2-} and 140 mg/L HSO_4^-. In the present work, the simplified dissociation reaction of H_2SO_4 to 2 H^+ and SO_4^{2-} was assumed. In the following, the measured pH of about 2.2 refers to about 400 mg/L SO_4^{2-}.

Unlabelled starch and 2-naphthol solutions (with c = 5.62 mg/L) were checked by LC-OCD analysis with regard to their belonging to problematic NOM fractions (Table 5). The LC-OCD allows the separation of DOC into fractions depending on their molecular size (biopolymers, humic substances, building blocks, LMW neutrals and LMW acids). The evaluation for Chemapol starch based on three measurements, whereas for Merck starch and 2-naphthol single measurements were carried out. The LC-OCD measurements were done in the DOC Labor Dr. Huber (Karlsruhe, Germany).

Table 5. LC-OCD results of unlabelled starch and 2-naphthol solutions at different pH values

Model solution	POC (%)	HOC (%)	Biopolymers (%)	Building Blocks, LMW Neutrals (%)
Chemapol starch (pH 6)	20 ± 12	4 ± 5	69 ± 17	7 ± 4
Chemapol starch (pH 2.2)	26 ± 6	15 ± 10	39 ± 15	19 ± 7
Merck starch (pH 6)	4	0	96	0
Merck starch (pH 2.2)	2	0	85	13
2-naphthol (pH 6 and 2.2)	n. d.	n. d.	n. d.	about 100

LC-OCD = liquid chromatography – organic carbon detection; POC = particulate organic carbon; HOC = hydrophobic organic carbon; LMW = low-molecular-weight; n. d. = not detectable

Table 5 shows that all starches are mainly identified by LC-OCD as biopolymers at neutral pH. However, the Chemapol starch presents higher amounts of other LC-OCD fractions, especially POC, pointing to a broader distribution of molecular weights. On the other hand,

Merck starch has a dominant part of the biopolymer fraction (96 and 94 %, respectively), indicating that this starch has a lower median molecular weight than Chemapol starch. Compared to neutral conditions, the percentage of the neutral fraction of the Chemapol starch arises from 7 to 19 % at pH 2.2. The same result was obtained for Merck starch (arising from 0 to 13 %). These changes could be caused by an acid hydrolysis reaction followed by a degradation of larger starch molecules to smaller ones.

The results for 2-naphthol (pH 6 and 2.2) prove that this model substance belongs - as expected - to the LMW NOM fraction of neutrals. In the 2-naphthol solutions, no POC content was estimated by LC-OCD analysis. Thus, measured TOC (2-naphthol) contents are equal to DOC (2-naphthol) concentrations.

3.2.2 "Real" water samples

The "real" water samples were obtained from the demineralisation plant of the power station Boxberg, Germany (Vattenfall Europe Generation AG). The raw water, a mixture from the rivers Schwarze Schöps and Spree, was treated by coagulation ($Al_2(SO_4)_3$ and coagulant aid on polyacrylamide basis), neutralisation/precipitation ($Ca(OH)_2$) and filtration (multi-layer filter containing anthracite and silica sand). This pre-treatment procedure is able to reduce the DOC concentration significant depending on the NOM content and composition of the input water (Huber 2006; Hübner 2011).

Thereafter, the water was treated with cation exchanger, trickling degasser, anion exchanger and mixed-bed exchanger in the demineralisation plant. The NOM content in the water was measured as DOC after each treatment unit with the aim to quantify the impact of each step in regard to NOM removal. The results are shown in Figure 10. The DOC measurements were done in the DOC Labor Dr. Huber (Karlsruhe, Germany).

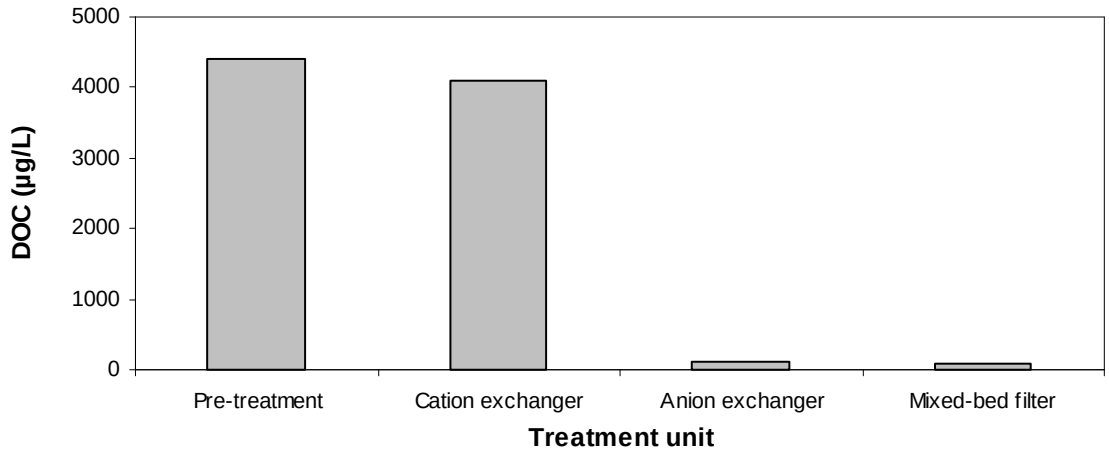

Figure 10. DOC content in the "real" water samples after each treatment unit.

It can be seen in Figure 10 that the anion exchange process has the main impact on the TOC removal in demineralisation plants. Thus, optimising the use of AERs has the highest potential to increase the TOC uptake in water treatment processes.

For this reason, the “real” water samples have been collected after passing the pre-treatment (experiments under neutral conditions) and cation exchanger (experiments under acidic pH conditions). Both water samples were stored at 5 °C to prevent bacterial growth.

The composition of the NOM fractions was analysed by LC-OCD (DOC Labor Dr. Huber, Karlsruhe, Germany); pH, conductivity and ion concentration values were obtained from the laboratory of the power plant Boxberg (details given in the following chapter). Chemical properties of the “real” water samples are listed in Table 6.

Table 6. Characterisation of “real” water samples after pre-treatment and cation exchange

Parameters	after pre-treatment	after cation exchange
DOC (µg/L)	4083	3956
HOC (µg/L)	465	426
Biopolymers (µg/L)	49	29
Humic substances (µg/L)	2231	1875
Building blocks (µg/L)	872	883
LMW neutrals (µg/L)	458	686
LMW acids (µg/L)	9	56
pH (-)	7.01	2.24
conductivity (µS/cm)	570	1635
Ca^{2+} (mg/L)	83.8	0.006
Mg^{2+} (mg/L)	14.0	n. d.
Na^{+} (mg/L)	19.1	1.060
K^{+} (mg/L)	6.55	n. d.
Cl^{-} (mg/L)	29.6	28.6
NO_3^{-} (mg/L)	15.9	15.9
SO_4^{2-} (mg/L)	167	163
HCO_3^{-} (mg/L)	274.50	n. a.
SiO_2 (mg/L)	9.85	9.75

DOC = dissolved organic carbon; HOC = hydrophobic organic carbon; LMW = low-molecular-weight; n. d. = not detectable; n.a. = not analysed

Table 6 shows that the DOC concentrations of the “real” water samples after pre-treatment and cation exchange were relatively high (4.08 and 3.96 mg/L, respectively), which reveals the requirement for further NOM removal.

The pH of the water after pre-treatment was neutral (pH ≈ 7). Under neutral pH condition, NOM has a medium charge density due to partly deprotonation of their acidic functional group (Boyer and Singer, 2008). Thus, uptake could occur by anion exchange, mainly onto strong base AERs with their quaternary amines, as well as by ion-dipole and/or van der Waals interaction onto all AERs (Bolto et al., 2002). Further, hydrophobic NOM components

could be adsorbed by π-π stacking and/or hydrophobic interactions onto the resin hydrophobic matrix, primarily onto polystyrene material (Li and Sengupta, 2004; Cornellisen et al., 2008). Also, high sulphate and hydrogen carbonate concentrations were estimated in the "real" water sample after pre-treatment. These ions could compete with weaker adsorbable NOM for polar anion exchange sites and thereby limiting NOM removal (Anderson and Maier, 1979).

In contrast to the pre-treated water, the pH of the water after cation exchange was found to be very acidic (pH ≈ 2.2). It is proposed that NOM has a low charge density under acidic condition due to protonation of their acidic functional groups (Boyer and Singer, 2008; Ritchi and Perpedue, 2003). Hence, NOM uptake from acidic water onto AERs occurs most likely by ion-dipole and/or van der Waals interactions as well as π-π stacking and/or hydrophobic interactions (Croué et al., 1999). High sulphate content was also found in the "real" water sample after cation exchange. In contrast to NOM adsorption, the uptake of sulphate ions by AERs is supposed to be due to stronger anionic interactions. One consequence could be that stronger adsorbable sulphate ions compete with weaker adsorbable NOM for polar anion exchange sites and by doing so restraining NOM elimination (Anderson and Maier, 1979).

3.3 Analyses

The concentration of Chemapol and Merck starch in solution was quantified by UV/VIS spectrometry (Lambda 2, Perkin Elmer, Cary 50 Bio, Varian or Helios Omega, Thermo Scientific) at 590 nm (after 1:1 starch reaction with 1 mmol/L iodine-potassium iodide solution from Apolda and analytical grade H_3PO_4 from Carl Roth; detection limit 0.04 mg/L TOC (starch), which is equal to about 0.09 mg/L starch). The relative error of the starch concentration due to preparation of the input solutions was determined to be about 2.5 %. ^{14}C-labelled starch was measured by LSC (liquid scintillation counting) using a scintillation cocktail (Ultima Gold, Perkin Elmer) and a counting system from Perkin Elmer (Wallac Winspectral α/β 1414; detection limit at 0.02 Bq/mL, relative error caused by setting up the input solutions (42 Bq/mL) at 0.75 %).

Furthermore, starch solutions (c_0 = 10 mg/L TOC (Chemapol and Merck starch; pH 6), 0.3 mg/L TOC (^{14}C-labelled starch; pH 6), 10 mg/L TOC (Chemapol starch) and 400 mg/L sulphate; pH 2.2) were ultrafiltered with Microsep^{TM}-filters (Pall) of five different pore sizes (1000 kDa, 300 kDa, 50 kDa, 10 kDa, and 1 kDa) with the aim to get deeper insights into the molecular size distribution of the different types of starch, especially of the ^{14}C-labelled starch for which no LC-OCD results were available. Solutions in the filtration tubes were centrifuged for 30 minutes (60 minutes for the 1 kDa filter) at 4000 rpm (Megafuge 1.0, Heraeus Sepatech). Subsequently, the Chemapol and Merck starch filtrates were quantified for their starch contents by UV/VIS spectrometry, whereas the ^{14}C-labelled starch filtrates were analysed by LSC.

The concentration of 2-naphthol in aqueous solution was analysed by ultraviolet absorption (273 nm) using a Helios Omega UV/VIS-spectrophotometer (Helios Omega, Thermo Scientific). The limit of detection was 0.12 mg/L TOC (2-naphthol), which is equal to 0.14 mg/L 2-naphthol. The relative error of the 2-naphthol concentration because of inaccuracy in the setting up of the input solutions was determined to be about 2.0 %.

In experiments under acidic pH conditions, the sulphate concentrations were calculated from sulphate-hydroxide exchange data, which were indirectly measured by titration of hydrogen ions (titration solution: 0.02 M NaOH; indicator: bromothymol blue (both from Merck); detection limit: 0.0015 M). The relative error due to preparation of input solutions was determined to be 2.6 %.

The concentration of NOM was measured as DOC using a TOC analyzer multi N/C UV HS (Analytik Jena AG), based on wet chemical reactions, an oxidation agent (natriumperoxodisulphate) and ultraviolet radiation with subsequent infrared detection. Each sample was measured twice. The two-sample standard derivation was about 1.4 %.

Advanced NOM characterisation was carried out using LC-OCD following the method of Huber and Frimmel (1996). The analyzer was equipped with a column (2 x 25 cm) filled with Toyopearl Gel HW 50S from Topo, which allows the separation of DOC into fractions depending on their molecular size (biopolymers, humic substances, building blocks, LMW neutrals and LMW acids). The oxidation was performed in a thin film reactor with subsequent infrared detection. For determination of the amount of each fraction, polyethylene glycol standards were used. The calculated fraction that remained on the chromatography column is the HOC. LC-OCD measurements of the model substances and "real" water samples were carried out by DOC Labor Dr. Huber (Karlsruhe, Germany).

The pH was measured by a WTW pH 340-meter using a Sentix 41-electrode, the conductivity by a WTW cond. 340-meter using a TetraCon 325-electrode. Ion concentration and SiO_2 determinations were performed in the analytical laboratory of the power plant Boxberg. Cation concentrations (Ca^{2+}, Mg^{2+}, Na^{+}, K^{+}) were determined by inductively coupled plasma – optical emission spectrometry (ICP-OES) analysis (Optima 3300 DV, Perkin Elmer), whereas anion concentrations (Cl^{-}, NO_3^{-}, SO_4^{2-}) were measured by ion chromatography (IC) analysis (Dionex ICS-1100, Thermo Scientific). The SiO_2 content in the water samples was investigated by photometric measurements (Lasa 100, Dr. Lange).

3.4 Experimentally obtained breakthrough curves

All fixed-bed adsorption runs were carried out in glass columns with an inside diameter of 1.0 cm. For each experiment, the column was filled with 5 mL of freshly regenerated and rinsed resin.

Different starch model solutions with 5.62 mg/L starch (between about 2.05 and 2.45 mg/L TOC, depending on the median molecular weight of the different starches) at pH 6 (obtained with Millipore water) or 2.2 (gained with Millipore water and acidification with 232 µL/L concentrated H_2SO_4 (96-98 %; analytical grade; Merck) were fed to the top of the column at a constant flow rate of about 75 mL/h (equal to 0.96 m/h) regulated by a constant speed tubing pump (IPC, Ismatec). In experiments where ^{14}C-labelled starch and Chemapol starch were used both in one solution, their concentration ratio $c_{labelled}/c_{unlabelled}$ amounted to 0.13. Additionally, column experiments with 10 and 100 mg/L TOC (Merck starch; pH 6) were performed to study the applicability of the LDF model for the prediction of BTCs. The column effluents were collected regularly once per hour and analysed by UV/VIS spectrometry or LSC to monitor the breakthrough of starch as well as by titration measurements to examine the breakthrough of sulphate. The overall error of a single measured value in the BTCs was about 4.9 % (starch) and 5.5 % (sulphate).

For 2-naphthol studies, solutions with 10 and 100 mg/L TOC (2-naphthol) at pH 6 (obtained with Millipore water) or 2.2 (attained with Millipore water and acidification with 232 µL/L concentrated H_2SO_4 (96-98 %; analytical grade; Merck) were fed to the top of the column at a constant flow rate of about 82 mL/h (equal to 1.05 m/h) adjusted by a constant-speed tubing pump system (IPC, Ismatec). The effluent was sampled repeatedly once per hour and analysed by UV/VIS spectrometry (2-naphthol) and titration measurement (sulphate). The overall error of a single measured value in the BTCs was about 3.9 % (2-naphthol) and 5.5 % (sulphate).

Further, “real” water samples after pre-treatment and cation exchange were given to the top of the column at a constant flow rate of about 75 mL/h (0.96 m/h) and 80 mL/h (1.02 m/h), respectively, regulated by a constant-speed tubing pump (IPC, Ismatec). The effluent samples were collected once per hour and NOM concentration was measured as DOC. For acidic water, conductivity measurements were also carried out in the AER filtrates. LC-OCD studies were additionally applied for effluent samples at 25 and 100 *BV* throughput to control the water quality before the breakthrough point.

3.5 Adsorption isotherm and kinetic parameter estimation

3.5.1 Adsorption isotherm parameters

Adsorption equilibrium data for single-solute Merck starch (pH 6) uptake were obtained for a constant amount of AER (V_R = 0.55 mL equal to m_A = 0.37 g (IRA96) and 0.39 g (AP246, IRA900, A860)) and solution volume (0.05 L), but varying Merck starch concentrations between 1.00 – 100 mg/L in batch experiments. For that, the AER was weighted into glass flasks and 50 mL of the appropriate solution were added. The flasks were shaken at room temperature for 4 days with 325 rpm, which was proved to be enough time for establishing the equilibrium. After this contact time the samples were decanted to separate the Merck starch solutions from the AERs. Subsequently, the Merck starch solutions were analysed by UV/VIS spectrometry. To validate the results, isotherm experiments have been conducted for three times. Overall error of a single measured value in the batch experiment with Merck starch was about 5.0 %.

Under neutral pH conditions (pH 6), adsorption isotherms for the single-solute 2-naphthol were developed for constant 2-naphthol concentration (50 mg/L TOC) and solution volume (0.25 L) and varying AER mass (m_A between 0.19-0.74 g for IRA96, 0.16-0.44 g for AP246, 0.08-0.31 g for IRA900 and 0.15-0.44 g for A860).

Under acidic pH conditions (pH 2.2), adsorption isotherms were investigated for constant 2-naphthol concentration (100 mg/L TOC), sulphate concentration (400 mg/L; adjusted with 232 µL/L concentrated H_2SO_4 (96-98 %; analytical grade; Merck)) and solution volume (0.05 L) and varying AER mass (m_A between 0.04-0.67 g for IRA96, 0.40-0.78 g for AP246, 0.04-0.62 g for IRA900 and 0.52-0.85 g for A860).

For 2-naphthol equilibrium analysis (pH 6 and 2.2), the flasks were shaken at room temperature with 325 rpm for 2-4 hours (AP246, IRA900 and A860) and 3 days (IRA96), which, in preliminary kinetic studies, was found to be a sufficient time for equilibration. After that the aqueous solutions were separated from the AERs. Then, 2-naphthol concentrations were analysed by UV/VIS spectrometry and sulphate contents were indirectly quantified by titration measurements.

For the determination of the Freundlich parameters for the single-solute sulphate at acidic pH, samples with a constant amount of AER (0.5 g) and solution volume (0.05 L), but varying sulphate concentrations (0.00375-0.02500 M; adjusted with H_2SO_4 from Merck)

were shaken at room temperature for 2 hours with 325 rpm, which has been shown in kinetic studies to be enough time for establishing the equilibrium. Subsequently, the sulphate solutions were decanted and the sulphate concentrations were indirectly analysed by titration measurements.

To validate the adsorption equilibrium results of 2-naphthol and sulphate, isotherm experiments were carried out two (2-naphthol at acidic pH) or three times (2-naphthol at neutral pH as well as sulphate at acidic pH). The overall error of a single measured value in the batch experiment was about 8.0 % for 2-naphthol (pH 6), 9.7 % for 2-naphthol (pH 2.2) and 4.0 % for sulphate (pH 2.2).

Under acidic pH conditions, the loading of 2-naphthol depends strongly on the uptake of the anion of the applied acid (in the present work sulphate). Given that acid is necessary to set the pH to 2.2, no single-component equilibrium data for 2-naphthol could be measured at this pH. For this reason, the software BATCH 2.2 was applied (© E. Worch 2009). This software is based on the IAST and was primarily developed to calculate the necessary m_A/V_L-ratio to reach given equilibrium concentrations in batch reactors (input parameters for all components: c_0, K_F and n). However, it can also be used in an inverse mode, which means fitting Freundlich values to the measured equilibrium concentrations for different m_A/V_L-ratios and constant inlet concentrations. Since, the Freundlich parameters for the single-solute sulphate can be obtained by single-solute experiments, only the Freundlich parameters for the single-solute 2-naphthol (pH 2.2) had to be fitted to the experimental data.

The required adsorption equilibrium data for water after pre-treatment (neutral pH) were obtained for constant solution volume (1.0 L) and varying AER resin volume and mass, respectively (V_R of 11, 27.5, 55, 110, 220, 330, 440 and 550 mL related to m_A of about 8, 19, 38, 76, 153, 229, 306, 382 mg). For equilibrium analysis, the flasks were shaken at room temperature with 200 rpm for 7 d, which proved to be a sufficient time in preliminary kinetic studies. After this contact time the samples were decanted to separate the NOM solutions from the AERs. Next, concentration of NOM was measured as DOC. To validate the results, equilibrium experiments have been carried out twice. The two-sample standard deviation of one measurement was about 2.0 %.

The concentrations of the different NOM fractions were obtained by adsorption analysis after Sontheimer et al. (1988) and Johannsen and Worch (1994). In the present study, the Freundlich parameter n was set to be 0.5 for all adsorbable NOM fractions, whereas the K_F

values were defined to be 0 (mg/g)/(mg/L)^n for the non-adsorbable NOM fraction and 5, 20 and 80 (mg/g)/(mg/L)^n for the weakly, moderately and strongly adsorbable NOM fractions. It is known that for a given value of n, a higher K_F directly reflects a higher capacity. A search routine in the software AdsAna 1.4 (© E. Worch 2009) based on the IAST was used to find the concentration distribution of the NOM fractions which allows the best fitting of the experimental DOC equilibrium isotherm data.

3.5.2 Adsorption kinetic parameters

All liquid film diffusion coefficients D_L (m²/s) were calculated by the empirical correlation after Worch (1993) with T = 22°C = 295 K. For this correlation, the medium molecular mass was defined to be 10000 g/mol for Merck starch (pH 6) and 1000 g/mol for NOM (pre-treated water; pH 7).

The volumetric film mass transfer coefficients $k_F a_{VR}$ (s^{-1}) for Merck starch (pH 6) were obtained by the empirical correlation after Wilson and Geankoplis (1966). The $k_F a_{VR}$ values for 2-naphthol (pH 6 and 2.2), sulphate (pH 2.2) and NOM (pre-treated water; pH 7) were calculated by the empirical correlation after Williamson et al. (1963). The required linear filter velocities v_F were defined to be 0.96 m/h for Merck starch (pH 6) and NOM (pre-treated water; pH 7) and 1.05 m/h for 2-naphthol (pH 6 and 2.2).

The intraparticle (solid) mass transfer coefficients k_S^* (s^{-1}) for Merck starch (c_0 = 2.25, 10 and 100 mg/L; pH 6) uptake on different AERs were obtained by the empirical correlation after Heese and Worch (1997). It is expected that the correlation gives acceptable results for defined micropollutants and avoids time-consuming kinetic experiments.

For 2-naphthol (pH 6 and 2.2) and sulphate (pH 2.2), the k_S^* values were also calculated by the empirical correlation after Heese and Worch (1997) with c_0 = 100 mg/L TOC (2-naphthol; pH 6 and 2.2) and c_0 = 400 mg/L sulphate (pH 2.2).

In addition, the applicability of the empirical correlation was checked with experimental obtained kinetic parameters. Therefore, the liquid phase concentration of 2-naphthol (pH 6) was measured over time for a given amount of AER mass (0.30 g for IRA96 and AP246, 0.15 g for IRA900 and 0.25 g for A860) per 0.25 L of an initial 50 mg/L TOC (2-naphthol; pH 6) solution. The k_S^* values for the uptake of 2-naphthol (pH 2.2) were obtained by measuring the liquid phase concentration of 2-naphthol over time for AERs mass of 0.6 g (IRA96 and IRA900), 1.0 g (AP246) and 0.9 g (A860) per 0.05 L of an initial 100 mg/L TOC (2-naphthol; pH 2.2) solution.

Further, the k_S^* values for the uptake of sulphate (pH 2.2) were obtained by measuring the liquid phase concentration of sulphate over time for 0.5 g (IRA96 and AP246), 0.6 g (IRA900) and 1.0 g (A860) per 0.1 L of an initial 400 mg/L sulphate (pH 2.2) solution.

For 2-naphthol (pH 6 and 2.2), the analysis of the aqueous-phase concentrations as a function of time was carried out after 0.25, 0.5, 0.75, 1, 1.5, 2, 3 and 4 h for (IRA900, AP246 and A860) and additionally after 5, 6, 9, 24, 48 and 72 h for (IRA96). For sulphate (pH 2.2), the analysis of the aqueous-phase concentrations as a function of time was carried out after 0.25, 0.5, 0.75, 1, 1.5 and 2 h for (IRA900, AP246 and A860) and additionally after 3, 4 and 5 h for (IRA96). The samples were shaken at room temperature with 325 rpm. The resulting data were plotted according to c/c_0 versus time and were evaluated using the software KIN 3.1 (© E. Worch 2009).

The k_S^* values for NOM adsorption from pre-treated water were estimated by an empirical equation after Hess (2001), which was proposed for NOM under the assumption that the mass transfer coefficients are the same for all NOM fractions.

Finally, all corresponding intraparticle diffusion coefficients D_S (m²/s) were derived from the k_S^* values following the Glueckauf (1955a) approach.

4. Results and discussion

4.1 Uptake of starches as model substances for the biopolymer NOM fraction by anion exchange resins

4.1.1 Molecular size distribution of starches

So far, the molecular size distribution of Chemapol and Merck starch was investigated by LC-OCD, which is based on size-exclusion chromatography (see results Table 5). Due to its radioactivity, ^{14}C-labelled starch could not be analysed by LC-OCD analysis in the DOC Labor Huber (Karlsruhe, Germany). As a consequence, the ultrafiltration method was applied to get deeper insights into the molecular size distribution of all three types of starch. Figure 11 shows the molecular size distribution of the starches measured by ultrafiltration.

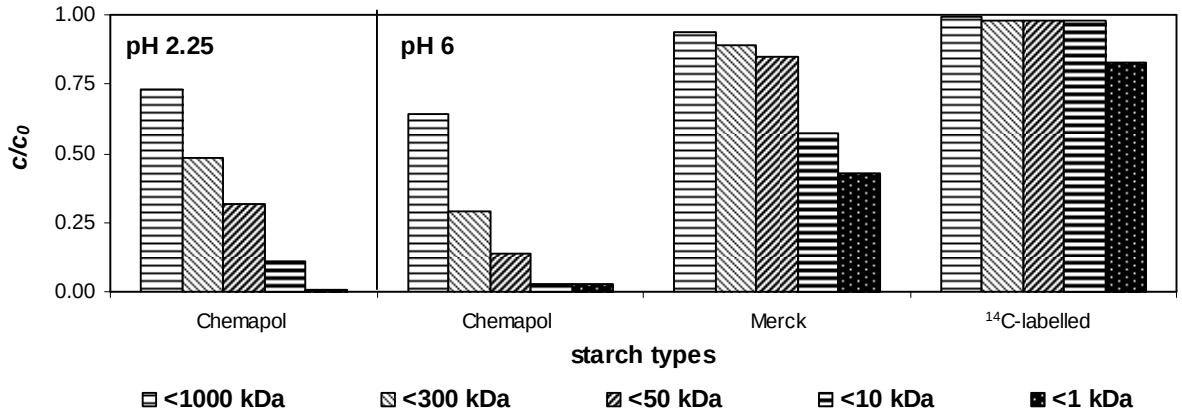

Figure 11. Molecular size distribution of three starches at pH 6 (for Chemapol starch also at pH 2.2) shown as reduced concentration c/c_0, where c is the actual concentration of the fluid phase and c_0 is the inlet concentration, after each ultrafiltration step (c_0 = 10 mg/L TOC (Chemapol and Merck starch; pH 6), 0.3 mg/L TOC (^{14}C-labelled starch; pH 6), 10 mg/L TOC (Chemapol starch) and 400 mg/L sulphate; pH 2.2).

It can be seen that Chemapol starch shows a different molecular size distribution in comparison to the other starches (Figure 11; see also Pürschel et al., 2013a). Merck and ^{14}C-labelled starch mainly consists of particles smaller than 50 kDa, which corresponds to the biopolymer fraction at the LC-OCD analysis, whereas Chemapol starch solutions have higher amounts of larger particles. So, for instance, 71 % of the Chemapol starch particles (pH 6) belongs to the fraction > 300 kDa in comparison to less than 17 % of the other starches.

Furthermore, at acidic pH, Chemapol starch shows a higher amount of smaller particles, possibly caused by an acid hydrolysis reaction followed by a degradation of larger starch molecules to smaller ones. Nevertheless, Chemapol starch solutions (pH 6 and 2.2) consist of larger aggregates than Merck and ^{14}C-labelled starch solutions (at pH 6).

These Chemapol and Merck starch results are in coincidence with the LC-OCD measures, not surprisingly, because the LC-OCD method is based on size-exclusion chromatography. Summarised, the mean molecule sizes of the starch particles decrease in the following order: Chemapol, Merck and ^{14}C-labelled starch.

4.1.2 Parameter estimation for breakthrough curve modelling of single-solute Merck starch adsorption

Equilibrium parameters for single-solute adsorption of Merck starch at neutral pH

Under neutral condition, experimentally obtained single-solute equilibrium data for Merck starch uptake onto four different AERs as well as fitted Freundlich isotherms are shown in Figure 12.

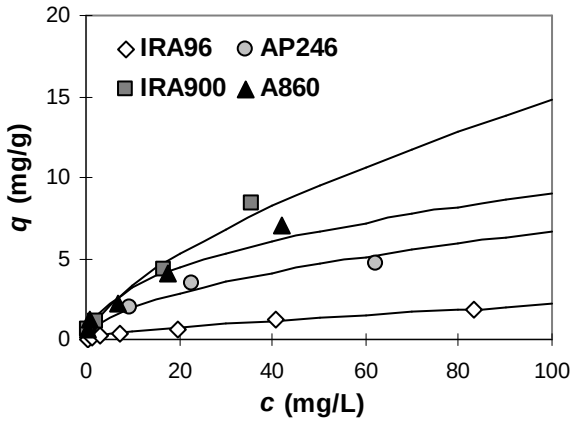

Figure 12. Equilibrium data as well as Freundlich (—) fits for TOC (Merck starch) adsorption at neutral pH onto four different AERs.

Table 7 summarises the Freundlich parameters corresponding to the isotherms presented in Figure 12 together with q_0 values for c_0 = 2.25, 10 and 100 mg/L TOC (Merck starch) calculated with these Freundlich parameters.

Table 7. Freundlich parameters (K_F and n) as well as correlation coefficients (R^2) for TOC (Merck starch) adsorption at neutral pH onto four AERs and calculated q_0 values for c_0 = 2.25, 10 and 100 mg/L TOC

AERs	K_F ((mg/g)/(mg/L)^n)	n (-)	R^2 (-)	q_0 (mg/g) related to c_0 = 2.25 mg/L TOC	q_0 (mg/g) related to c_0 = 10 mg/L TOC	q_0 (mg/g) related to c_0 = 100 mg/L TOC
IRA96	0.09	0.68	0.98	0.16	0.45	2.17
AP246	0.60	0.52	0.99	0.92	2.00	6.67
IRA900	0.78	0.64	0.99	1.30	3.38	14.77
A860	1.16	0.45	0.98	1.67	3.24	9.06

Overall, the Freundlich isotherms fit the equilibrium data of Merck starch (pH 6) for all investigated AERs in a very good manner (Figure 12 and Table 7). The equilibrium data indicate that AERs are not only able to remove anions, but can also be used to eliminate to some degree Merck starch, which act as model substance for the biopolymer NOM fraction. For Merck starch uptake onto four AERs, K_F values between 0.09-1.16 (mg/g)/(mg/L)^n and n data in the range of 0.45-0.68 were found.

Applying the determined Freundlich parameters for Merck starch (pH 6) adsorption, it can be estimated that at an equilibrium concentration of 2.25 mg/L TOC, the loading capacities of IRA96, AP246, IRA900 and A860 are about 0.2, 0.9, 1.3 and 1.7 mg/g, respectively, following the order of q(IRA96) < q(AP246) < q(IRA900) < q(A860). In contrast, at higher equilibrium concentrations, the equilibrium capacities of IRA96, AP246, IRA900 and A860 are about 0.5, 2.0, 3.4 and 3.2 mg/g (c_0 = 10 mg/L TOC) and 2.2, 6.7, 14.8 and 9.1 mg/g (c_0 = 100 mg/L TOC), respectively, which results in an uptake order in the form of q(IRA96) < q(AP246) < q(A860) < q(IRA900).

These results prove that strong base AERs (IRA900 and A860) have higher Merck starch (pH 6) uptake capacities than the medium base AER (AP246) and the weak base AER (IRA96). This might be due to their quaternary amine functional groups, which are at pH 6 in positively charged form with corresponding counterion and could favour starch uptake by ion-dipole and/or van der Waals interactions (see also Figure 3). Contrary, at this pH, the tertiary amines of the weak and medium base AERs tend to be in uncharged form and should be less able to perform ion-dipole and/or van der Waals interactions.

The comparison between MP polystyrene strong base AER IRA900 and MP polyacrylic strong base AER A860 for Merck starch uptakes at pH 6 indicate that IRA900 is able to remove a higher amount of Merck starch at c_0 = 100 mg/L TOC, about the same amount at c_0 = 10 mg/L TOC and lower amount at c_0 = 2.25 mg/L TOC than A860. It is known that AERs with MP polyacrylic matrix exhibit higher removal of larger NOM particles, like biopolymers and fulvic acid, than the AERs with MP polystyrene matrix (Boyer and Singer, 2008). This is probably due to their more hydrophilic character, so they tend to have a more open structure and higher water content. As a consequence, AER A860 should not only be able to uptake the smaller Merck starch molecules, but also the larger ones. However, it could also occur that larger Merck starch particles, which are retarded in the resin pores, block possible reaction sites and pores for smaller Merck starch particles. This could be one reason that at higher

equilibrium concentrations the overall uptake capacities of AER A860 were found to be some extent lower than those of AER IRA900. This effect was investigated in subsequent fixed-bed studies in more detail.

Kinetic parameters for single-solute adsorption of Merck starch at neutral pH

Additionally to the adsorption equilibrium parameters, the kinetic parameters are needed for BTC modelling. For Merck starch (pH 6) uptake on four different AERs, the volumetric film and intraparticle (solid) mass transfer coefficients ($k_F a_{VR}$ and k_S^*) were calculated by empirical correlations after Wilson and Geankoplis (1966) and Hess (2001) for M = 10000 g/mol, v_F = 0.96 m/h and c_0 = 2.25, 10 and 100 mg/L TOC. The estimated mass transfer coefficients are given in Table 8 together with the calculated Biot numbers (*Bi*), which can be used to check which mass transfer (film-phase, solid-phase or both) controls the uptake process under the given hydrodynamic conditions.

Table 8. $k_F a_{VR}$ and k_S^* values as well as *Bi* numbers for TOC (Merck starch) uptake at neutral pH onto four AERs (M = 10000 g/mol and v_F = 0.96 m/h)

Parameters	**Resin type**			
	MP weak and medium base AERs		MP strong base AERs, type I	
	IRA96	**AP246**	**IRA900**	**A860**
$k_F a_{VR}$ (s^{-1}) for c_0 = 2.25, 10 and 100 mg/L TOC	2.4×10^{-2}	5.5×10^{-2}	2.6×10^{-2}	2.5×10^{-2}
k_S^* (s^{-1}) for c_0 = 2.25 mg/L TOC	1.2×10^{-4}	0.5×10^{-4}	0.4×10^{-4}	0.4×10^{-4}
k_S^* (s^{-1}) for c_0 = 10 mg/L TOC	1.5×10^{-4}	0.7×10^{-4}	0.6×10^{-4}	0.6×10^{-4}
k_S^* (s^{-1}) for c_0 = 100 mg/L TOC	2.2×10^{-4}	1.3×10^{-4}	0.8×10^{-4}	1.1×10^{-4}
Bi (-) for c_0 = 2.25 mg/L TOC	2.1	0.8	0.8	0.6
Bi (-) for c_0 = 10 mg/L TOC	2.6	1.1	1.0	1.0
Bi (-) for c_0 = 100 mg/L TOC	3.8	1.9	1.5	1.8

After Hand et al. (1984), adsorption is controlled for $Bi \leq 0.5$ by the film mass transfer, for $0.5 < Bi \leq 30$ by the film and intraparticle mass transfer and for $Bi > 30$ by the intraparticle mass transfer.

The volumetric film mass transfer coefficients for Merck starch (pH 6) adsorption were found to be between 0.02 s^{-1} and 0.05 s^{-1} (Table 8). A significantly higher $k_F a_{VR}$ value was found for Merck starch uptake on AP246 than for the other three investigated AERs. This is due to its smaller particle diameter (0.47 mm in comparison to 0.725-0.735 mm).

The intraparticle mass transfer coefficients for Merck starch (pH 6) uptake were estimated to be about 0.4-2.2 x 10^{-4} s^{-1}. These values are comparable with known data from literature for

other organic compounds at neutral pH. For instance, Cornelissen et al. (2008) found experimental k_S^* values of about 1.2-3.2 x 10^{-4} s^{-1} for NOM adsorption onto strong base AERs.

For BTC predictions, k_S^* was not considered as a constant but as a parameter that depends on the adsorbed amount. Satisfactory BTC fits were achieved for $k_S^* = k_S^*(0)$ as well as $\omega = 0$ for the weak base AER (IRA 96) and $\omega = -0.25$ for the medium and strong base AERs (AP246, IRA900, A860).

For the uptake of c_0 = 2.25, 10 and 100 mg/L TOC (Merck starch; pH 6) onto the four investigated AERs, *Bi* values (after Equation (29)) between 0.6 and 3.8 were estimated. Thus, the Merck starch (pH 6) adsorption onto all resins in this concentration range and under the given hydrodynamic conditions is supposed to be controlled by both liquid film and intraparticle mass transfer rates.

4.1.3 Fixed-bed adsorption of Merck starch at neutral pH

Figure 13 shows experimental Merck starch (pH 6) BTCs for four different AERs in comparison with curves calculated by the linear driving force (LDF) model. In the following figures the x-axis refers to the throughput in bed volume (*BV*) and the y-axis depicts the actual concentration of the fluid phase (output concentration) divided by the input concentration (c/c_0). In general, an adsorption of an adsorbate onto the AER is reflected by a c/c_0 ratio smaller than 1. Otherwise, $c/c_0 > 1$ indicates the elution of an adsorbate from the resin and $c/c_0 = 1$ refers to resin exhaustion.

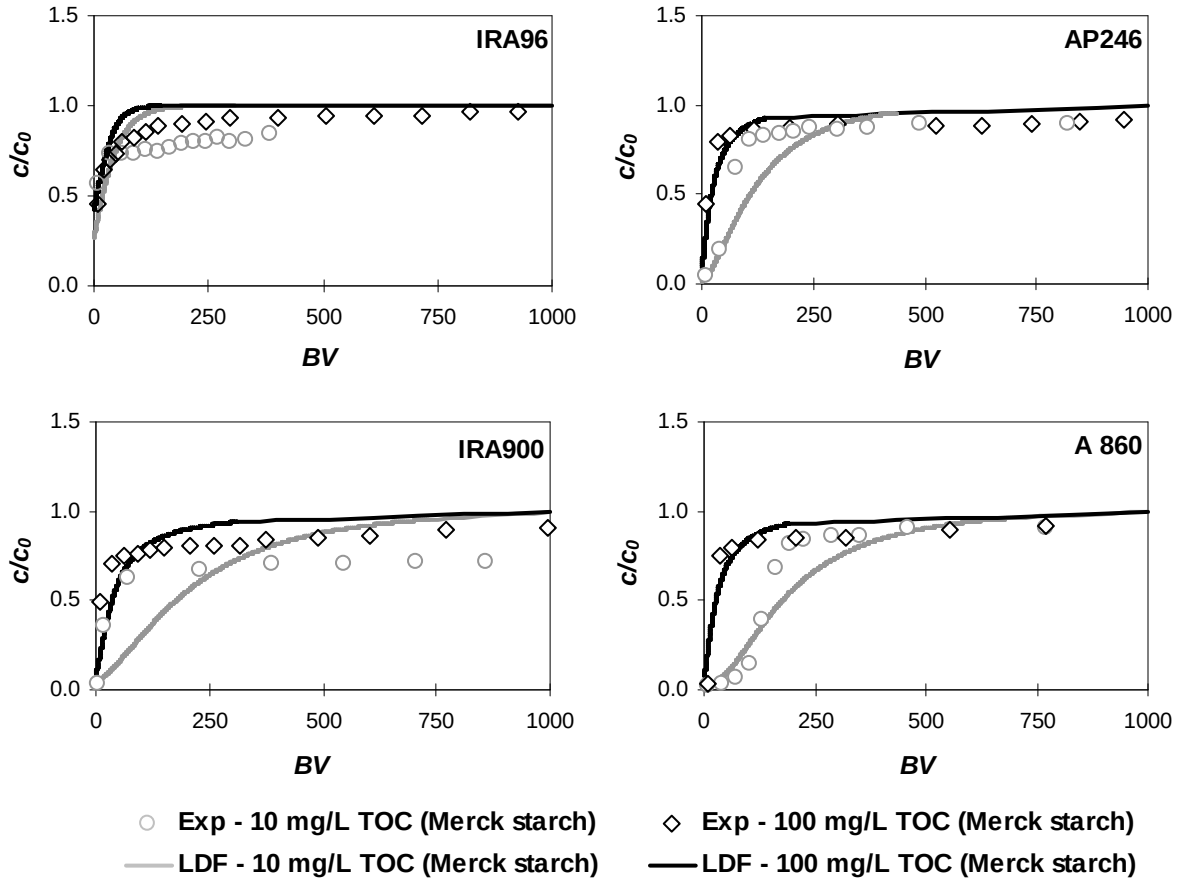

Figure 13. Breakthrough curves for TOC (Merck starch) onto four AERs (experimentally (Exp) determined and predicted by linear driving force (LDF) model; c_0 = 10 and 100 mg/L TOC; pH 6).

BTCs in Figure 13 demonstrate that overall dynamic Merck starch adsorption (up to $c/c_0 = 1$) is very low onto the weak base AER IRA96, medium onto the medium base AER AP246 and somewhat higher onto the strong base AERs IRA900 and A860. Thus, it seems that Merck

starch adsorption is clearly affected by the functional groups of the resins. At pH 6, the quaternary amines of the medium and strong base AERs (AP246, IRA900 and A860) are in positively charged form and could favour starch uptake by ion-dipole and/or van der Waals interactions, whereas the tertiary amines of the weak and medium base AERs (IRA96 and AP246) tend to be in uncharged form and should be rarely able to perform ion-dipole and/or van der Waals interactions.

Additionally, BTCs for strong base AERs IRA900 and A860 indicate that the Merck starch removal is influenced by the resin material. The MP polystyrene strong base AER IRA900 is almost not able to adsorb 65 % of the Merck starch molecules (see initial breakthrough of the Merck starch BTC up to c/c_0 = 0.65 with c_0 = 10 mg/L TOC for IRA900 in Figure 13), probably due to size-exclusion of the larger Merck starch molecules. The remaining smaller Merck starch particles are strongly adsorbed, most likely by ion-dipole and/or van der Waals interactions. Contrary, the MP polyacrylic strong base AER A860 is able to remove all Merck starch molecules up to 70 BV (for c_0 = 10 mg/L TOC). This indicates that the MP polyacrylic resin has a more open structure, which allows the uptake of both smaller and larger Merck starch particles. In sum, the overall dynamic uptake capacities (up to c/c_0 = 1) for Merck starch molecules (with c_0 = 10 and 100 mg/L TOC) are higher for the MP polystyrene strong base AER IRA900 than for the MP polyacrylic AER A860, although their total volume (anion) exchange capacities (*TVC* values) are almost equal (see Table 2). One reason could be that larger Merck starch particles, which penetrate into the polyacrylic resin pores, block possible reaction sites and pores for the other Merck starch particles.

Furthermore, Figure 13 shows that the LDF model yields results which are in good agreement with the experimental BTCs for c_0 = 100 mg/L TOC (Merck starch) uptake onto all four studied AERs. Also, for c_0 = 10 mg/L TOC (Merck starch) adsorption onto MP polystyrene weak base AER IRA96 as well as onto MP polyacrylic medium and strong base AERs AP246 and A860, the experimentally obtained and modelled BTC are in acceptable agreement. However, some variations were recognised between experimentally determined and predicted BTC for c_0 = 10 mg/L TOC (Merck starch) adsorption onto the polystyrene strong base AER IRA900. It seems that the LDF model predicts the Merck starch BTC for IRA900 in that manner that initial breakthrough of large particles and strong adsorption of small particles are to some extent counterbalanced. However, the results in Figure 13 indicate that the LDF model can further be applied to predict BTCs for Merck starch adsorption also for lower TOC inlet concentrations.

4.1.4 Fixed-bed adsorption of different types of starch at neutral pH

Figure 14 shows experimental BTCs for Chemapol starch onto weak, medium and strong base AERs as well as BTCs for Merck starch uptake calculated by the LDF model and exemplarily measured up to 250 BV for the strong base AERs IRA900 and A860. All BTCs were experimentally obtained or calculated with c_0 = 5.62 mg/L starch (equal to 2.25 ± 0.20 mg/L TOC) under neutral conditions.

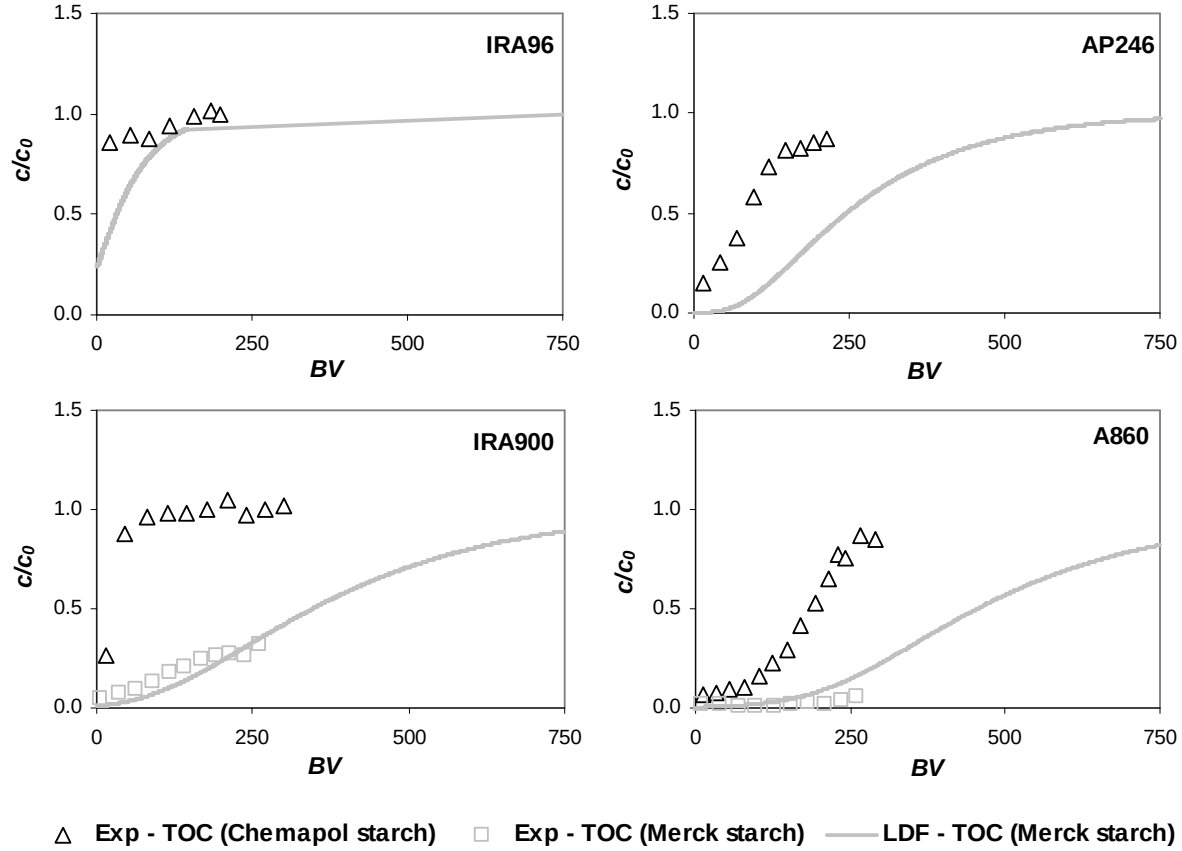

Figure 14. Breakthrough curves for TOC (Chemapol starch) and TOC (Merck starch) onto four AERs (experimentally (Exp.) determined and/or predicted by the linear driving force (LDF) model; c_0 = 2.25 ± 0.20 mg/L TOC; pH 6).

Figure 14 illustrates Chemapol and Merck starch (c_0 = 2.25 ± 0.20 mg/L TOC) BTCs at neutral pH, which where experimentally determined and/or predicted by the LDF model.

The calculated Merck starch BTCs by the LDF model fit in a good manner the experimentally obtained data for the Merck starch adsorption onto the strong base AERs IRA900 and A860 up to about 250 BV. Therefore, it can be assumed that the LDF model is

also able to describe the total BTCs for Merck starch (c_0 = 2.25 ± 0.20 mg/L TOC) uptake onto all four AERs in a satisfying quality.

Figure 14 demonstrates that the Merck starch is to some extent higher removed onto the four different AERs at neutral pH than Chemapol starch. The two types of starch do not vary in their chemical structure, but in their molecular size distribution. It was found by LC-OCD and ultrafiltration measurements (see Table 5 and Figure 11) that Merck starch consists of smaller particles than Chemapol starch. Thus, it can be stated that starch uptake is clearly affected by size-exclusion of starch molecules. The smaller the particles, the higher their removal is.

Furthermore, it can be seen in Figure 14 that MP polyacrylic resins AP246 and A860 adsorb the larger Chemapol starch at pH 6 to a significantly higher degree than MP polystyrene resins IRA96 and IRA900. Since their *TVC* values are about equal (see Table 2) only the different matrix structures can induce the different uptakes. Both MP polystyrene resins have a water retention of approximately 60-61 %, whereas the MP polyacrylic resins show a water retention ability of about 63 % and 69 %. High water retention of resins increases the porosity of the beads, so that larger Chemapol starch molecules can permeate into the resin to a higher extent. This result has also been found for high-molecular-weight NOM fractions by several authors (e. g., Croué et al., 1999; Bolto et al., 2002; Humbert et al., 2005; Cornelissen et al., 2008).

Figure 14 shows also different Merck and Chemapol starch breakthrough behaviours between weak, medium and strong base exchangers. The results indicate once more that starch adsorption is to some degree affected by the functional groups of the resins. It can be assumed that at pH 6, the quaternary amines of the medium and strong base AERs (AP246, IRA900 and A860) are in positively charged form and could favour starch uptake by ion-dipole and/or van der Waals interactions, whereas the tertiary amines of the weak and medium base AERs (IRA96 and AP246) tend to be in uncharged form and should be rarely able to perform ion-dipole and/or van der Waals interactions. However, to some extent this effect is superimposed by size-exclusion limitations (higher Chemapol starch uptake was found for the weak base AER AP246 than for the strong base AER IRA900).

In sum, higher adsorption capacities were estimated by applying the integral mass balance equation for predicted (Merck starch) or experimentally obtained (Chemapol starch) BTCs for Merck starch (with 0.12, 0.87, 1.17 and 1.67 mg/g for IRA96, AP246, IRA900 and A860,

respectively) than for Chemapol starch (with 0.04, 0.28, 0.08 and 0.59 mg/g for IRA96, AP246, IRA900 and A860, respectively).

The influence of size-exclusion on the starch uptake by AERs was additionally investigated by using smaller particles (^{14}C-labelled starch) and larger ones (unlabelled Chemapol starch) in one experiment. For this, the fixed-bed filter eluates from two strong base AERs IRA900 and A860 were measured by UV/VIS (all starch molecules) and LSC analysis (only ^{14}C-labelled molecules). Experimentally determined BTCs with $c_{labelled}/c_{unlabelled}$ = 0.13 and c_0 = 5.62 mg/L starch equal to 2.25 ± 0.20 mg/L TOC are shown in Figure 15.

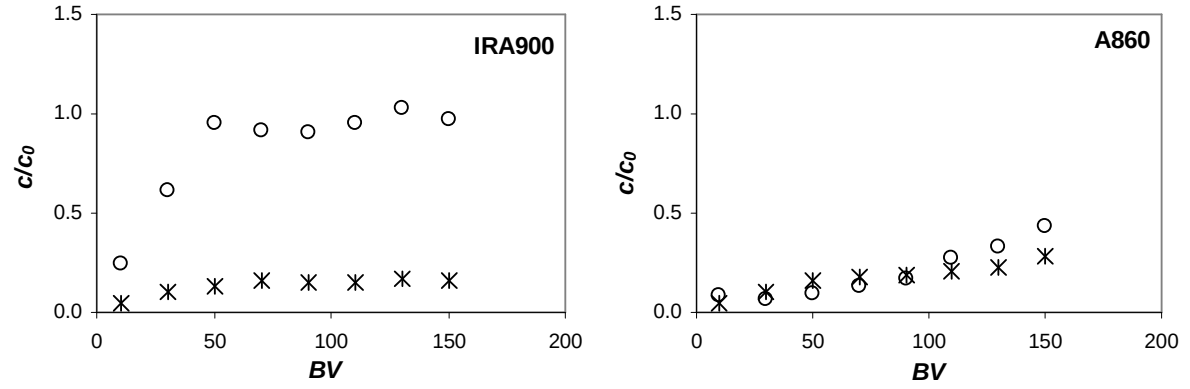

Figure 15. Experimentally (Exp) determined breakthrough curves for TOC (^{14}C-labelled starch in combination with Chemapol starch) onto two strong base AERs, where all starch molecules were measured by ultraviolet/visible (UV/VIS) spectrometry and ^{14}C-labelled starch by liquid scintillation counting (LSC) (c_0 = 2.25 ± 0.20 mg/L TOC; $c_{labelled}/c_{unlabelled}$ = 0.13; pH 6).

For the MP polystyrene AER IRA900, it can be seen in Figure 15 that large Chemapol starch molecules are eluted after a short time, since they are not able to diffuse into the resin beads. Contrary, higher uptake capacities were estimated for the smaller ^{14}C-labelled starch molecules, since they are able to penetrate into the beads and thus, higher effective adsorption surfaces are available. In contrast to that, no different uptake was observed for ^{14}C-labelled and unlabelled starch onto the polyacrylic AER A860 in Figure 15. Here, the pores are large enough to uptake also the larger Chemapol starch particles.

For starch uptake at neutral pH, it can be stated that the MP polyacrylic strong base AER A860 is the best tested resin in the overall removal of the three types of starch.

4.1.5 Fixed-bed adsorption of different types of starch at acidic pH

Figure 16 shows the BTCs for Chemapol and Merck starch, which were obtained for four different AERs under acidic experimental conditions (c_0 = 5.62 mg/L starch equal to 2.25 ± 0.20 mg/L TOC; 400 mg/L sulphate; pH 2.2).

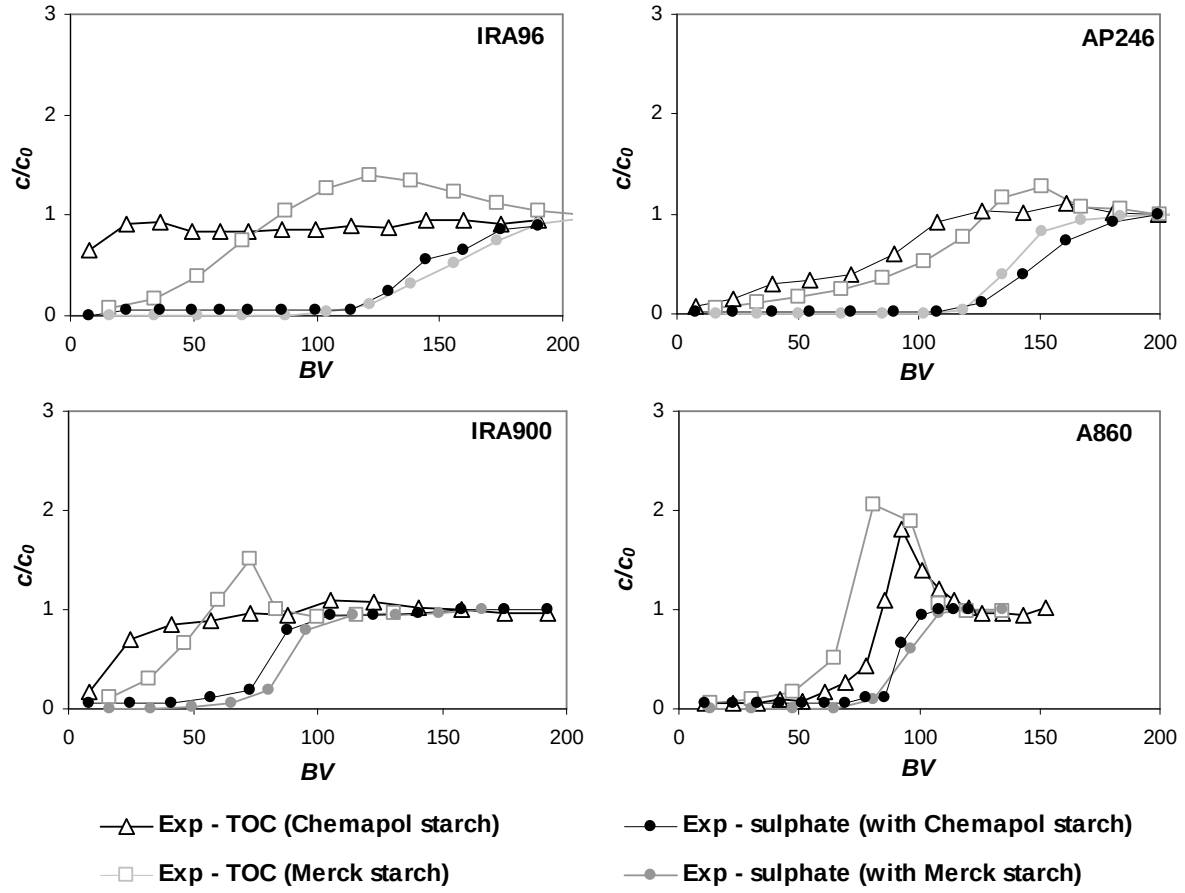

Figure 16. Experimentally (Exp) determined breakthrough curves for TOC (Chemapol starch) and TOC (Merck starch) as well as for sulphate onto four AERs (c_0 = 2.25 ± 0.20 mg/L TOC and 400 mg/L sulphate; pH 2.2).

Under acidic conditions, the loading of Chemapol and Merck starch onto the AERs depends strongly on the competitive uptake of the anion of the sulphuric acid (Figure 16). The sulphate ions have a much stronger affinity to the resins than starch molecules, which results in displacement effects and leads to elution peaks ($c/c_0 > 1$) of the weaker adsorbed starch molecules. Consequently, the breakthrough point of starch is influenced by the *TVC* of the AER. At acidic pH, the *TVC* values of the weak/medium base AERs IRA96 and AP246 are

higher than of the strong base AERs IRA900 and A860 (see Table 2). Thus, higher overall starch uptake capacities would be expected for the weak/medium base AERs IRA96 and AP246. However, the effect of the higher *TVC* values is strongly superimposed by size-exclusion effects.

Figure 16 shows that Chemapol starch is less adsorbed onto the polystyrene resins IRA96 and IRA900 than Merck starch, probably due to size-exclusion effects of the larger Chemapol starch molecules. Contrary, polyacrylic AERs AP246 and A860 vary to less extent in their Chemapol and Merck starch uptake behaviours, surely caused by their higher water contents and thus higher porosity of the beads for the large molecular size of the biopolymer fraction.

The breakthrough bed volumes ($BV = V_L/V_R$) at $c/c_0 = 0.15$, for the adsorption of different types of starch ($c_0 = 2.25 \pm 0.20$ mg/L TOC) onto IRA96, AP246, IRA900 and A860 at acidic pH, were found to be < 8, 23, < 8 and 60 *BV* for Chemapol starch and 34, 51, 16 and 48 *BV* for Merck starch, respectively. Therefore, up to the starch and anion breakthroughs, higher bed volumes, and thus longer running times, were obtained for MP polyacrylic AERs AP246 and A860 than for MP polystyrene AERs IRA96 and IRA900. Among the MP polyacrylic AERs, the strong base AER A860 outperforms the medium base AER AP246 in the uptake of Chemapol starch. This can be explained by its higher water content and thus higher porosity for large biopolymers. Contrary, little higher Merck starch breakthrough bed volumes were estimated for the AER AP246 than for the AER A860, probably due to its higher *TVC* and the lower impact of size-exclusion by this smaller biopolymer.

Like under neutral conditions, the influence of size-exclusion on the starch uptake by AERs at acidic pH was additionally investigated by using smaller particles (^{14}C-labelled starch) and larger ones (unlabelled Chemapol starch) in one experiment. Figure 17 shows BTCs experimentally obtained under acidic experimental conditions for the strong base AERs IRA900 and A860 ($c_{labelled}/c_{unlabelled} = 0.13$; $c_0 = 5.62$ mg/L starch equal to 2.25 ± 0.20 mg/L TOC; 400 mg/L sulphate; pH 2.2).

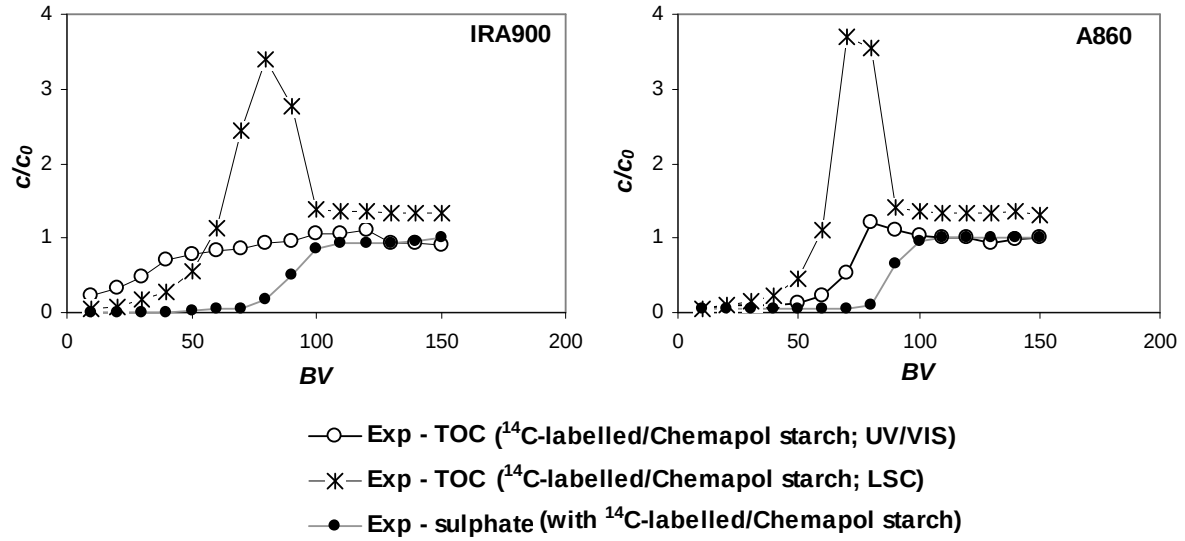

Figure 17. Experimentally (Exp) determined breakthrough curves for TOC (^{14}C-labelled starch in combination with Chemapol starch) as well as for sulphate onto two strong base AERs, where all starch molecules were measured by ultraviolet/visible (UV/VIS) spectrometry and ^{14}C-labelled starch by liquid scintillation counting (LSC) (c_0 = 2.25 ± 0.20 mg/L TOC and 400 mg/L sulphate; $c_{labelled}/c_{unlabelled}$ = 0.13; pH 2.2).

It can be seen in Figure 17 that the weaker adsorbed ^{14}C-labelled/Chemapol starch molecules were displaced by the stronger adsorbed anion component from both strong base AERs IRA900 and A860. It was found that the smaller ^{14}C-labelled starch molecules were adsorbed onto the resins, probably by ion-dipole and/or van der Waals interactions, and displaced from the resins by sulphate ions in the same manner, which might be due to the comparable *TVC* values of both strong base AERs (see Table 2). Contrary, Chemapol starch was adsorbed to smaller amounts onto the MP polystyrene AER IRA900 than ^{14}C-labelled starch, probably caused by size-exclusion effects of the larger Chemapol starch molecules. However, the polyacrylic AER A860 varied to less extent in its Chemapol and ^{14}C-labelled starch uptake behaviours, surely caused by its higher water content and thus higher porosity of the beads for the large molecular size of the biopolymer fraction.

In conclusions, at acidic pH, the most effective AER type tested for the elimination of the three types of starch, and probably also for more substances of the biopolymer NOM fraction with medium to high molecular size, was found to be the MP polyacrylic strong base AER A860.

4.2 Uptake of 2-naphthol as model substance for the neutral NOM fraction by anion exchange resins

4.2.1 Parameter estimation for breakthrough curve modelling of single-solute and competitive 2-naphthol adsorption

Equilibrium parameters for single-solute adsorption of 2-naphthol at neutral pH

Single-component equilibrium data for TOC (2-naphthol) at pH 6 as well as fitted Freundlich and Langmuir isotherms are shown in Figure 18.

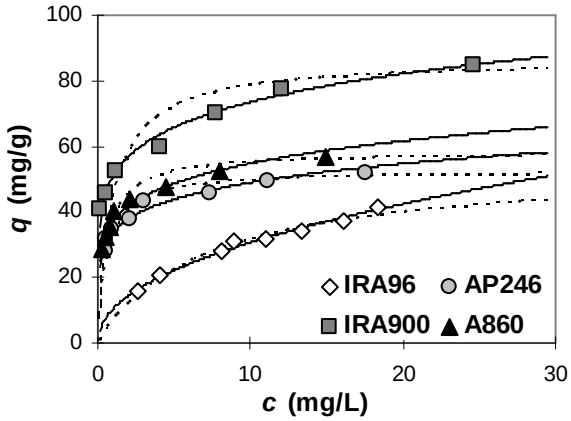

Figure 18. Equilibrium data as well as Freundlich (—) and Langmuir (---) fits for TOC (2-naphthol) at neutral pH onto four different AERs.

The corresponding Freundlich and Langmuir parameters are listed in Table 9.

Table 9. Freundlich (K_F and n) and Langmuir (K_L and q_m) parameters as well as correlation coefficients (R^2) for TOC (2-naphthol) adsorption at neutral pH onto four AERs and calculated q_0 values for c_0 = 10 and 100 mg/L TOC

AERs	K_F ((mg/g)/(mg/L)^n)	n (-)	R^2 (-)	q_0 (mg/g) related to c_0 = 10 mg/L TOC	q_0 (mg/g) related to c_0 = 100 mg/L TOC	K_L (L/mg)	q_m (mg/L)	R^2 (-)
IRA96	10.46	0.47	0.99	30.87	91.10	0.14	54.05	0.98
AP246	33.88	0.16	0.96	48.97	70.79	1.64	52.63	0.99
IRA900	50.89	0.16	0.99	73.56	106.32	1.02	86.21	0.99
A860	37.06	0.17	0.97	54.82	81.08	1.79	58.14	0.99

The Freundlich and Langmuir isotherms fit the equilibrium data of 2-naphthol (pH 6) for all investigated AERs in a very good quality (Figure 18). The equilibrium results point out that AERs are efficient in the adsorption of aromatic organic compounds like 2-naphthol (pH 6). For the 2-naphthol (pH 6) uptake by the investigated AERs, K_F values between 10.46-50.89 (mg/g)/(mg/L)^n and n data in the range of 0.16-0.47 were found. Further, K_L values between 0.14 and 1.79 L/mg and q_m values from 52.63 to 86.21 mg/g were estimated (see Table 9).

There are three main factors influencing adsorption of 2-naphthol onto different AERs: i) the surface area of the AER with respect to the pore size, ii) π-π stacking and/or hydrophobic interactions between AER and 2-naphthol molecules and iii) ion-dipole and/or van der Waals interactions between hydrophilic functional groups of the anionic resins and hydroxide moiety of 2-naphthol molecules (see also Figure 3).

The surface areas of AERs IRA96 and IRA900 are known to be between 16 and 31 m²/g (BET method measurements by Schumann, 2005). Those of AERs AP246 and A860 should be in the same magnitude, having in mind their only slightly different water content values (see Table 2). Thus, for all investigated AERs, the BET surface areas are comparable and play only a minor role in the uptake differences of 2-naphthol at pH 6. Consequently, the different adsorption mechanisms have to be discussed in more detail.

The MP polystyrene AERs IRA96 and IRA900 show higher 2-naphthol loadings at pH 6 compared to the MP polyacrylic AERs AP246 and A860. This might be due to stronger π-π stacking and/or hydrophobic interactions between 2-naphthol and the more hydrophobic polystyrene matrix. Furthermore, at pH 6, the quaternary amines of the medium base AER AP246 and the strong base AERs IRA900 and A860 are in positively charged form. Therefore, they should be able to adsorb 2-naphthol additionally by ion-dipole and/or van der Waals interactions. In contrast, the tertiary amines of the weak and medium base AERs IRA96 and AP246 tend to be in uncharged form at this pH and should be less able to perform ion-dipole and/or van der Waals interactions with 2-naphthol molecules.

Using the obtained Freundlich parameters for 2-naphthol (pH 6) adsorption, it can be calculated that at an equilibrium concentration of 10 mg/L TOC, the equilibrium capacities of IRA96, AP246, IRA900 and A860 follow an order of q(IRA96) < q(AP246) < q(A860) < q(IRA900). At higher equilibrium concentration (100 mg/L TOC), the equilibrium capacities of IRA96, AP246, IRA900 and A860 were found to be in a changed uptake order in the form of q(AP246) < q(A860) < q(IRA96) < q(IRA900). Thus, it could be assumed that at higher

equilibrium concentrations π-π stacking and/or hydrophobic interactions seem to be to some extent more important than at lower equilibrium concentrations. Possibly, the number of hydrophilic functional groups is a limiting factor for the uptake of higher 2-naphthol (pH 6) equilibrium concentrations by ion-dipole and/or van der Waals interactions.

In the following, the uptake performances of 2-naphthol (pH 6) onto AERs were compared to those obtained onto conventional and hypercrosslinked adsorber resins as well as onto granular activated carbon (GAC) reported in the literature, which are more frequently applied for the removal of organic compounds in drinking water plants (Table 10).

Table 10. Freundlich parameters (K_F and n) for TOC (2-naphthol) adsorption at neutral pH onto conventional and hypercrosslinked adsorber resins as well as activated carbon and calculated q_0 values for c_0 = 10 and 100 mg/L TOC

Adsorbent	**Data source**	**K_F ((mg/g)/(mg/L)^n)**	**n (-)**	**q_0 (mg/g) related to c_0 = 10 mg/L TOC**	**q_0 (mg/g) related to c_0 = 100 mg/L TOC**
XAD2 (non-polar, BET = 330 m²/g)	Zhaoyi et al. (1997)	2.96	0.56	11	40
XAD4 (non-polar, BET = 750 m²/g)	Huang et al. (2012)	12.45	0.53	42	143
XAD7 (intermediate-polar, BET = 450 m²/g)	Huang et al. (2012)	7.42	0.65	33	145
XAD8 (intermediate-polar, BET = 140 m²/g)	Zhaoyi et al. (1997)	16.02	0.43	43	117
HJ-1 (intermediate-polar, hyper-crosslinked, BET = 727 m²/g)	Huang et al. (2012)	23.77	0.43	64	172
granular activated carbon (GAC)	Nouri et al. (2012)	123.00	0.40	309	776

Adsorption of organic pollutants from aqueous solution by adsorber resins has been shown to be an economical and effective method due to the high uptake capacity, relatively high selectivity and easy regeneration for repeated use of the adsorbers (Huang et al., 2012). In Table 10, it can be seen that for 2-naphthol adsorption onto conventional and hypercrosslinked adsorber resins the Freundlich values range for K_F between 2.96 and 23.77 (mg/g)/(mg/L)^n and for n between 0.43-0.56.

In comparison to the Freundlich parameters obtained for 2-naphthol uptake onto AERs, the K_F values for the 2-naphthol adsorption onto conventional and hypercrosslinked adsorber

resins were generally found to be to some extent lower, whereas the *n* values were estimated to be a little higher for the most part. As consequence, higher 2-naphthol uptakes should be generally observed onto AERs for low inlet concentrations, whereas for higher inlet concentrations, 2-naphthol adsorption should be favoured onto conventional and hypercrosslinked adsorber resins.

It was found that the calculated adsorption capacities for c_0 = 10 and 100 mg/L TOC (2-naphthol) of the non-polar XAD2 resin were lower than of all investigated AERs (compare Table 9 and Table 10). Furthermore, at low equilibrium concentration of 10 mg/L TOC, higher 2-naphthol (pH 6) adsorption capacities were found for the medium AER AP246 and strong base AERs IRA900 and A860 than for all conventional macroporous resins under consideration. In this concentration range, the strong base AER IRA900 exceeded even the uptake performance of the hypercrosslinked resin HJ-1. This phenomenon could be attributed to ion-dipole and/or van der Waals interactions as well as to π-π stacking and/or hydrophobic interactions.

In view of these results, it can be concluded that MP polystyrene strong base AERs represent an alternative to the conventional and hypercrosslinked adsorber resins for the removal of relative low concentrations of aromatic organic compounds from aqueous solutions in drinking water plants. On the other hand, Nouri et al. (2012) found an outstanding 2-naphthol adsorption capacity for GAC, due to its high surface area, pore structure and surface chemical properties. Therefore, the economical advantages/disadvantages of NOM elimination in drinking water treatment applying AERs (medium adsorption capacities, but easy and low cost regenerations for repeated use) instead of GAC (high uptake capacities, but require complex and expensive regeneration procedures) have to be surveyed in detail before application.

Equilibrium parameters for competitive adsorption of 2-naphthol at acidic pH

In demineralisation plants, the AER adsorption performance under acidic conditions is important. In this case, the loading of 2-naphthol (pH 2.2) depends strongly on the uptake of the anion of the applied acid (in the present study sulphate). Given that acid is necessary to set the pH to 2.2, no single-component equilibrium data for 2-naphthol could be measured at this pH. For this reason, the IAST is applied in an inverse mode, which implies fitting 2-naphthol (pH 2.2) Freundlich parameters to the measured equilibrium concentrations for different m_A/V_L-ratios and constant inlet concentrations. In Figure 19, the experimental and

calculated reduced concentrations (c/c_0) of TOC (2-naphthol) and sulphate (both solutes at pH 2.2) as a function of the adsorbent dosage (m_A/V_L-ratio) are presented together with the Freundlich values for both components.

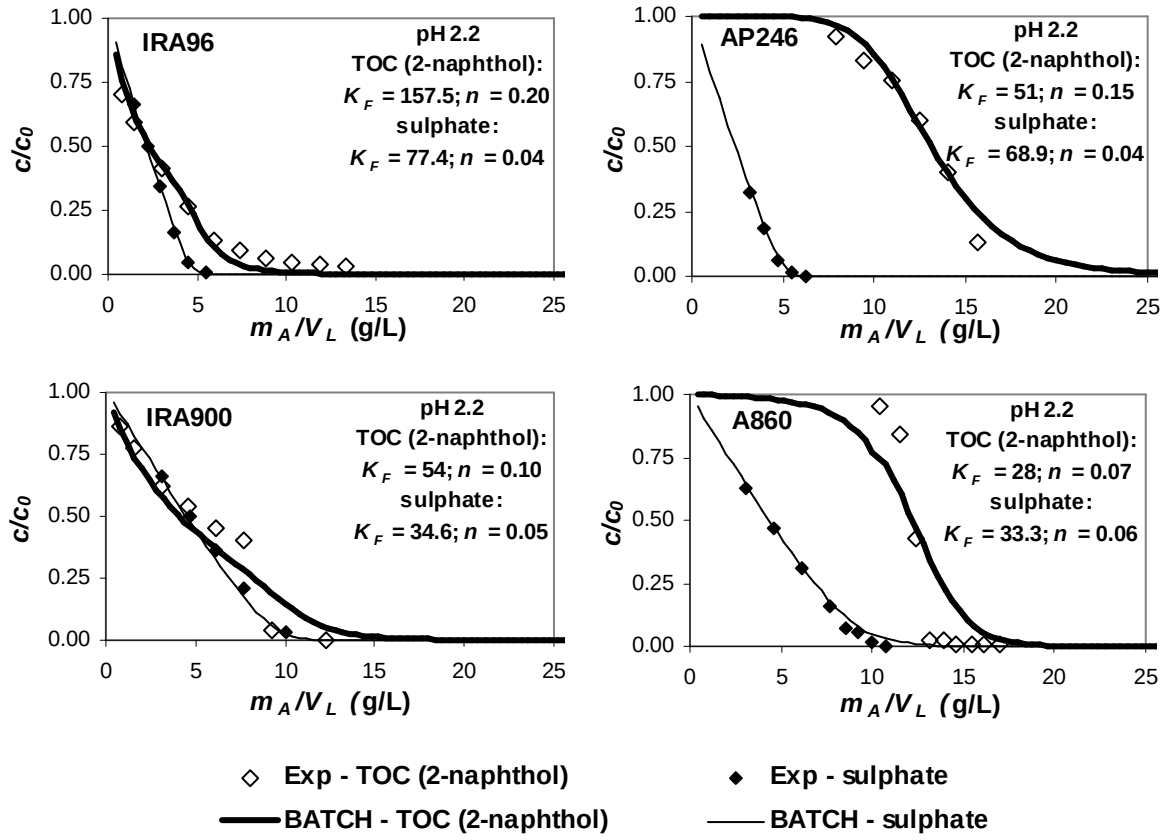

Figure 19. Reduced concentrations of TOC (2-naphthol) and sulphate as a function of the m_A/V_L-ratio for four AERs (experimental (Exp) data and calculated curves by inverse IAST fitting (software BATCH 2.2); K_F in (mg/g)/(mg/L)^n; c_0 = 100 mg/L TOC and 400 mg/L sulphate; pH 2.2).

It can be seen in Figure 19 that MP polyacrylic AERs AP246 and A860 have a high selectivity in respect of sulphate uptake. At low adsorbent dosage (m_A/V_L < 5 and 10 for AP246 and AP860, respectively), mainly the sulphate anions were removed by strong ionic interactions. Only, at higher m_A/V_L ratios, the weaker adsorbable 2-naphthol and the stronger adsorbable sulphate could both be eliminated by the resins. In contrast, MP polystyrene AERs IRA96 and IRA900 have almost an equal selectivity regarding 2-naphthol and sulphate. Thus, for equal adsorbent dosage, comparable concentration declines can be expected. Since the strong base AERs IRA900 and A860 have lower *TVC* values at pH 2.2

than the weak and medium base AERs IRA96 and AP246 (Table 2), it follows that their sulphate and 2-naphthol (pH 2.2) uptakes decrease at somewhat higher adsorbent dosage.

In sum, for the uptake of 2-naphthol at pH 2.2, K_F values between 28-157.5 (mg/g)/(mg/L)^n and n data in the range of 0.07-0.20 were found (see Figure 19). For the 2-naphthol (pH 2.2) adsorption, equilibrium loadings were found to be in the order q(A860) < q(AP246) < q(IRA900) < q(IRA96) for c_0 = 10 and 100 mg/L TOC. For the sulphate uptake at acidic conditions, K_F values of 69-77 (mg/g)/(mg/L)^n for the weak and medium base AERs IRA96 and AP246 and of about 34 (mg/g)/(mg/L)^n for the strong base AERs IRA900 and A860 were estimated (Figure 19). All n values were found to be very low with about 0.05. Thus, the obtained n values are evidence for favourable adsorption of sulphate, which should result in steep sulphate BTCs for all AERs. Because of the differences in the adsorption capacities, the sulphate (pH 2.2) uptake order is q(A860) ≈ q(IRA900) < q(AP246) ≈ q(IRA96).

It can be concluded that the MP polystyrene AERs IRA96 and IRA900 remove 2-naphthol (pH 2.2) more effectively than the MP polyacrylic AERs, possibly caused by stronger π-π stacking and/or hydrophobic interactions in addition to ion-dipole and/or van der Waals interactions. Further, MP polystyrene weak base AER IRA96 has a higher 2-naphthol (pH 2.2) uptake than the MP polystyrene strong base AER IRA900, since it has a higher *TVC* at pH 2.2 and, thus, certainly more polar sites for ion-dipole and/or van der Waals interactions.

As a result, under acidic conditions in demineralisation plants, the most effective AER type for the removal of 2-naphthol and probably also of other neutral substances from water was found to be the MP polystyrene weak base AER IRA96.

Kinetic parameters of 2-naphthol adsorption at neutral and acidic pH

Volumetric film mass transfer coefficients ($k_F a_{VR}$) and liquid film diffusion coefficients (D_L) for 2-naphthol (pH 6 and 2.2) and sulphate (pH 2.2) uptake onto AERs (v_F = 1.05 m/h) were estimated by empirical correlations after Williamson et al. (1963) and Worch (1993) (Table 11).

Table 11. $k_F a_{VR}$ and D_L values for TOC (2-naphthol; pH 6 and 2.2) and sulphate (pH 2.2) uptakes onto four AERs (v_F = 1.05 m/h)

Parameters	**Resin types**			
	MP weak and medium base AERs		MP strong base AERs, type I	
	IRA96	**AP246**	**IRA900**	**A860**
2-naphthol (pH 6 and 2.2)				
$k_F a_{VR}$ (s^{-1})	0.83×10^{-1}	1.71×10^{-1}	0.81×10^{-1}	0.84×10^{-1}
D_L (cm^2/s)		8.0×10^{-6}		
sulphate (pH 2.2)				
$k_F a_{VR}$ (s^{-1})	0.94×10^{-1}	1.94×10^{-1}	0.92×10^{-1}	0.95×10^{-1}
D_L (cm^2/s)		9.9×10^{-6}		

For 2-naphthol (pH 6 and 2.2) adsorption onto different AERs, $k_F a_{VR}$ values between 0.08 and 0.17 s^{-1} and a D_L value of 8.0×10^{-6} cm^2/s were estimated. For sulphate (pH 2.2), comparable $k_F a_{VR}$ and D_L values were found (0.09-0.19 s^{-1} and 9.9×10^{-6} cm^2/s). In the present work, significantly higher $k_F a_{VR}$ values were found for 2-naphthol (pH 6 and 2.2) and sulphate (pH 2.2) on AP246 than on the other three investigated AERs. This is due to its smaller particle diameter (0.47 mm in comparison to 0.725-0.735 mm).

The intraparticle mass transfer coefficients (k_S^*) and corresponding intraparticle diffusion coefficients (D_S) for 2-naphthol (pH 6 and 2.2) and sulphate (pH 2.2) adsorption onto AERs were evaluated using a kinetic model based on the LDF approach. The experimental and calculated kinetic curves together with the derived k_S^* and D_S values are exemplary shown for 2-naphthol uptake at pH 6 in Figure 20.

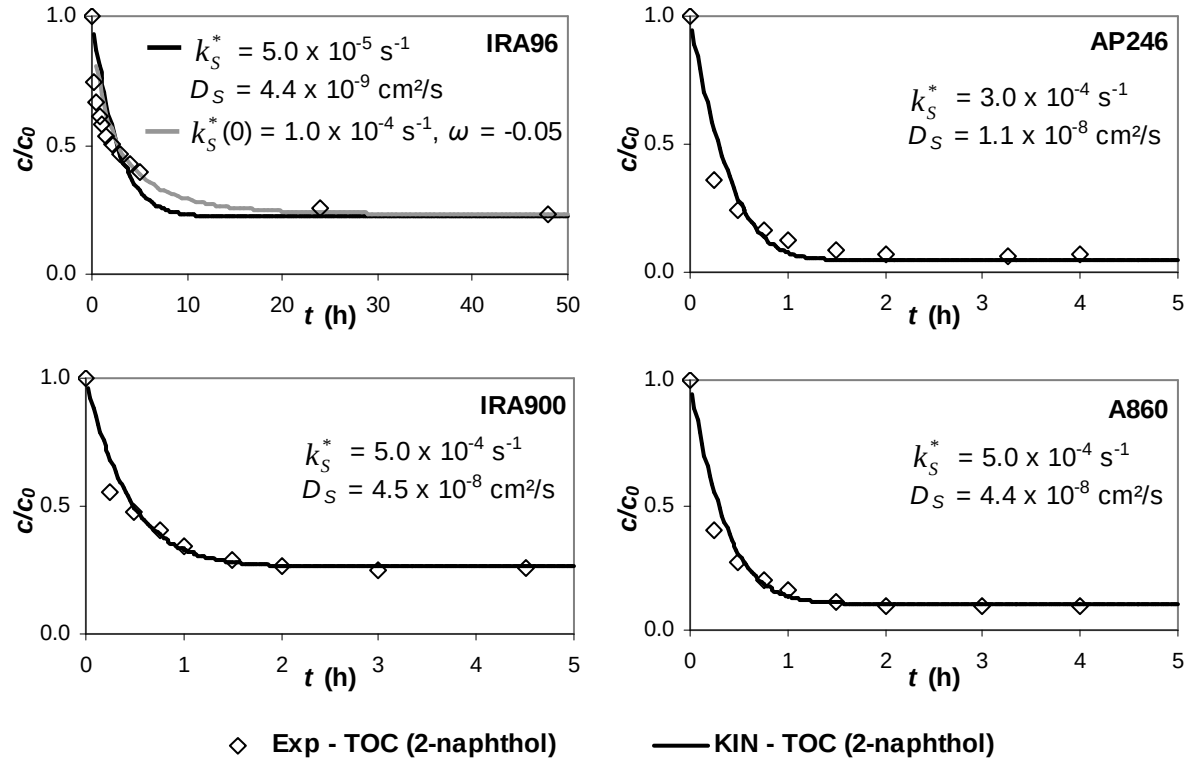

Figure 20. Reduced concentrations of TOC (2-naphthol; pH 6) as a function of time for four AERs (c_0 = 50 mg/L TOC; k_S^* and corresponding D_S as well as $k_S^*(0)$ and ω were found from a kinetic model based on the LDF approach (software KIN 3.1)).

It can be seen in Figure 20 that for medium and strong base AERs AP246, IRA900 and A860, the adsorption of 2-naphthol (pH 6) is very fast in the first hour. It reaches an equilibrium within about 150-180 min, implying that these AERs exhibit excellent intraparticle kinetic properties. Intraparticle kinetic rates for the uptake of 2-naphthol (pH 6) on the weak AER IRA96 are found to be slower by a factor of 10.

For medium and strong base AERs AP246, IRA900 and A860, the k_S^* evaluation with the LDF simplification fits the reduced concentration versus time curves in a good manner (Figure 20). Contrary, for the weak base AER IRA96 a better approximation for the c/c_0 versus time curve can be obtained, if the k_S^* value is not considered as a constant but as a parameter that depends on the amount adsorbed. This dependence can be described by the intrinsic mass transfer coefficient ($k_S^*(0)$) and the dimensionless empirical parameter (ω) according to Equation (25). All experimentally obtained k_S^* and corresponding D_S values for 2-naphthol (pH 6 and 2.2) and sulphate (pH 2.2) are summarised in Table 12. Additionally,

the calculated k_S^* values for 2-naphthol (pH 6 and 2.2) and sulphate (pH 2.2) uptake by empirical correlation after Heese and Worch (1997) are listed in Table 12.

Table 12. Experimentally (Exp) obtained and calculated (cal) k_S^* and D_S values for TOC (2-naphthol; pH 6 and 2.2) and sulphate (pH 2.2) adsorption onto four AERs

Parameters	**Resin types**			
	MP weak and medium base AERs		MP strong base AERs, type I	
	IRA96	**AP246**	**IRA900**	**A860**
2-naphthol (pH 6)				
Cal - k_S^* (s^{-1})	1.0×10^{-4}	1.8×10^{-4}	1.0×10^{-4}	1.1×10^{-4}
Exp - k_S^* (s^{-1}) or $k_S^*(0)$ (s^{-1}) and ω(-)	0.5×10^{-4} or 1.0×10^{-4} and -0.05	3.0×10^{-4}	5.0×10^{-4}	5.0×10^{-4}
Exp - D_S (cm^2/s)	0.4×10^{-8}	1.1×10^{-8}	4.5×10^{-8}	4.4×10^{-8}
2-naphthol (pH 2.2)				
Cal - k_S^* (s^{-1})	0.2×10^{-3}	8.4×10^{-3}	0.2×10^{-3}	2.0×10^{-3}
Exp - k_S^* (s^{-1})	0.2×10^{-3}	1.0×10^{-3}	2.0×10^{-3}	1.0×10^{-3}
Exp - D_S (cm^2/s)	0.1×10^{-7}	0.4×10^{-7}	1.8×10^{-7}	0.9×10^{-7}
sulphate (pH 2.2)				
Cal - k_S^* (s^{-1})	0.2×10^{-3}	0.4×10^{-3}	0.3×10^{-3}	0.3×10^{-3}
Exp - k_S^* (s^{-1})	0.5×10^{-3}	0.8×10^{-3}	2.0×10^{-3}	2.0×10^{-3}
Exp - D_S (cm^2/s)	0.4×10^{-7}	0.3×10^{-7}	1.8×10^{-7}	1.8×10^{-7}

Calculated values: c_0 = 100 mg/L TOC (2-naphthol; pH 6 and 2.2) and 400 mg/L sulphate (pH 2.2); experimentally obtained values: c_0 = 50 mg/L TOC (2-naphthol; pH 6), 100 mg/L TOC (2-naphthol; pH 2.2) and 400 mg/L sulphate (pH 2.2)

As can be seen in Table 12, slightly higher k_S^* and D_S values were found for 2-naphthol uptake onto all investigated AERs at pH 2.2 than at pH 6. Like for 2-naphthol adsorption at pH 6, the k_S^* evaluation with the LDF simplification fits the reduced concentration versus time curves in a good quality for the 2-naphthol uptake onto medium and strong base AERs AP246, IRA900 and A860 at pH 2.2, whereas for the weak base AER IRA96 a better approximation can be obtained if the k_S^* is considered as a parameter that depends on the amount adsorbed. However, since the loading dependence of k_S^* is relatively small for 2-naphthol (pH 2.2) uptake onto IRA96, a mean k_S^* value can be applied in BTC calculations for simplification. In future BTC model predictions, this mean k_S^* value will be slightly varied in dependence of the input concentration.

In conclusion, the investigated solid-phase diffusion coefficients (k_S^* and D_S) are comparable with known data from literature for other organic compounds, in which values of 1.2-3.2 x 10^{-4} s^{-1} for NOM/strong base AERs (Cornelissen et al., 2008) and values between 1 x 10^{-7} and 5 x 10^{-8} cm^2/s for phenol/strong base AERs (Goto et al., 1986) were estimated (under neutral pH conditions). Like in the present study, Cornelissen et al. (2008) found the fastest intraparticle diffusion rates for NOM on strong base AERs, whereas the intraparticle diffusion rates for NOM on weak base AER is to some extent slower.

For sulphate uptake (pH 2.2), the estimated intraparticle diffusion coefficients (see Table 12) are of the same order of magnitude as the values found in earlier studies. For instance, Guimarães and Leão (2011) estimated a k_S^* value of 1.2 x 10^{-3} s^{-1} (equivalent to D_S = 1.1 x 10^{-7} cm^2/s) for the intraparticle mass transfer for sulphate on the strong base AER IRA458.

The experimentally obtained volumetric intraparticle mass transfer coefficients for 2-naphthol (pH 6 and 2.2) uptake onto AERs were compared with the k_S^* values obtained by empirical calculation after Heese and Worch (1997). It was found that experimentally estimated and calculated k_S^* values for 2-naphthol (pH 6) uptake onto the four investigated AERs are in good agreement (Table 12). For 2-naphthol uptake at pH 2.2, equal k_S^* values were found for AERs IRA96 and A860 by experimentally studies and empirical calculations, but a somewhat higher k_S^* value and a little lower k_S^* value were experimentally estimated for AP246 and IRA900 than found by empirical calculations. For sulphate uptake somewhat higher k_S^* values were experimentally estimated for all AERs than found by empirical calculations. In conclusion, the empirical equation after Heese and Worch (1997), which is based on the results of more than 100 kinetic experiments with single organic adsorbate and different activated carbons, calculates acceptable k_S^* values for 2-naphthol uptake onto AERs at pH 6 and 2.2, but should not be applied to predict k_S^* values for anion uptake onto AERs.

For the adsorption of c_0 = 10 and 100 mg/L TOC (2-naphthol; pH 6) on the weak/medium base AERs IRA96 and AP246, Biot numbers (*Bi*) between 0.5 and 30 were estimated after Equation (29) under the given hydrodynamic conditions. Thus, the 2-naphthol adsorption onto both resins in this concentration range is expected to be controlled by liquid film and intraparticle mass transfer rates. Otherwise, for the uptake of 10 mg/L TOC (2-naphthol; pH 6) on the strong base AERs IRA900 and A860, *Bi* values less than 0.5 were found, suggesting

that the uptake is only liquid film diffusion controlled. However, at higher equilibrium concentrations (100 mg/L TOC), the 2-naphthol (pH 6) uptake on strong base AERs is comparable to those of for weak/medium base AERs supposed to be controlled by both kinetic processes.

In addition, the *Bi* values for the uptake of 2-naphthol and sulphate (both at pH 2.2) were calculated. For the adsorption of 10 and 100 mg/L TOC (2-naphthol) at acidic pH, it was found that the uptake is assumed to be film and solid-phase diffusion influenced for the polystyrene AERs IRA96 and IRA900 ($0.5 < Bi \leq 30$) as well as solid-phase controlled for the polyacrylic AERs AP246 and A860 ($Bi > 30$). For the sulphate adsorption in experiments with 10 and 100 mg/L TOC (2-naphthol; pH 2.2), it was estimated that the sulphate uptake is supposed to be both film and solid-phase diffusion influenced for all four studied AERs ($0.5 < Bi \leq 30$).

In conclusion, the *Bi* value characterises the relative influence of the film and intraparticle mass transfer on the overall mass transfer rate. Under the given experimental conditions, 2-naphthol (pH 6 and 2.2) and sulphate (pH 2) adsorption is expected to be mainly controlled by both kinetic processes ($0.5 < Bi \leq 30$). Since, the film mass transfer depends on the hydrodynamic conditions of the system, the in this study calculated *Bi* results for single-solute NOM and sulphate uptake cannot be simply adopted to industrial scale anion exchange units, except hydrodynamic conditions are comparable.

4.2.2 Fixed-bed adsorption of 2-naphthol at neutral pH

Figure 21 shows experimental BTCs of 2-naphthol (pH 6) in comparison with curves calculated by the LDF model and the Glueckauf/Helfferich formulae.

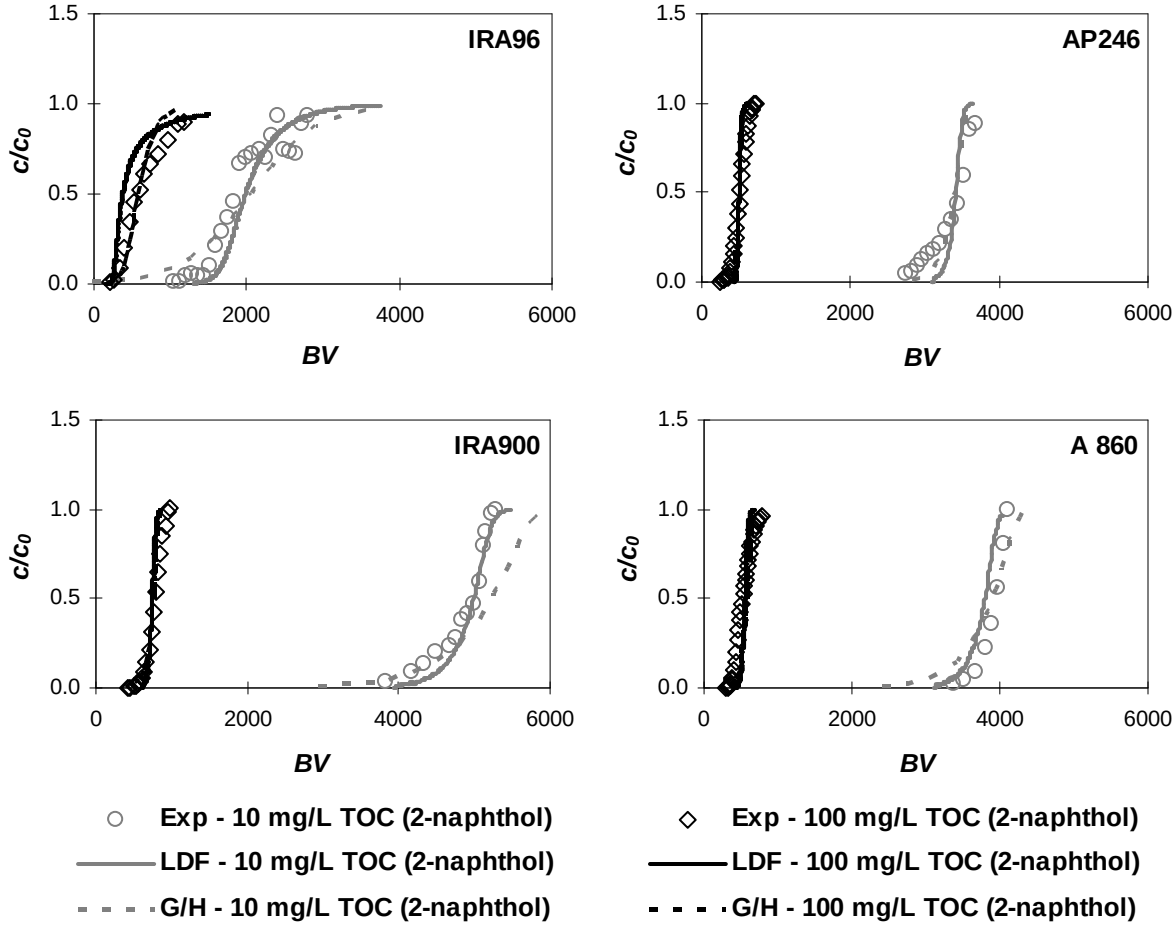

Figure 21. Breakthrough curves for TOC (2-naphthol) onto four AERs (experimentally (Exp) determined as well as predicted by the linear driving force (LDF) model and Glueckauf/Helfferich (G/H) formulae; c_0 = 10 and 100 mg/L TOC; pH 6).

The LDF model and the Glueckauf/Helfferich formulae yield almost equal BTC model results which are in good agreement with the experimental data (Figure 21). Both models are able to describe very well the equilibrium capacities and the rapid breakthrough, due to fast film and intraparticle mass transfer rates. Only little differences between experimental data and single-solute model predictions were obtained for the following BTCs. 2-Naphthol uptake (c_0 = 10 mg/L TOC) on AP246 and IRA900 shows a slightly increased impact of the

film mass transfer rate, which result in a breakthrough at little lower V_L/V_R values than calculated by the LDF model. Here, the Glueckauf/Helfferich formulae are able to account to some extent better for the leakage of 2-naphthol in front of the comparatively sharp breakthrough. Otherwise, the Glueckauf/Helfferich formulae overestimate the impact of the intraparticle mass transfer on the uptake of 2-naphthol (c_0 = 10 mg/L TOC) on IRA96 and IRA900, which results in a later breakthrough compared to the experimental data. In addition, for the 2-naphthol adsorption (c_0 = 100 mg/L TOC) on IRA96, it was found that the LDF model overestimates the intraparticle mass transfer for some degree, whereas the Glueckauf-Helfferich formulae show a somewhat lower impact of the intraparticle mass transfer. Nevertheless, it can be stated that both models are able to describe the dynamic single-solute uptake of 2-naphthol for different inlet concentrations in a good quality.

The dynamic adsorption results for 10 mg/L TOC (2-naphthol; pH 6) prove that the strong base AERs IRA900 and A860 have higher 2-naphthol capacities compared to the medium base AER AP246 and weak base AER IRA96. 2-Naphthol (pH 6) adsorption capacities were estimated from experimental BTCs by the integral mass balance equations for real BTCs to be about 69 and 59 mg/g for IRA900 and A860, respectively, 47 mg/g for AP246 and 35 mg/g for IRA96. This could be explained by the quaternary amines of the medium and strong base AERs, which are in positively charged form at pH 6 and should be able to adsorb 2-naphthol by ion-dipole and/or van der Waals interactions, whereas the tertiary amines of the weak and medium base AERs tend to be in uncharged form at this pH and should be less able to perform ion-dipole and/or van der Waals interactions. Further, the more hydrophobic MP polystyrene AERs IRA96 and IRA900 should be able to adsorb a higher amount of 2-naphthol by additionally π-π stacking and/or hydrophobic interactions in comparison to the more hydrophilic MP polyacrylic AERs AP246 and A860.

These results are consistent with conclusions from earlier studies at neutral pH. For instance, Bolto et al. (2002) and Cornelissen et al. (2008) found that strong base AERs with quaternary amines remove NOM and phenolic compounds to a higher extent than weak/medium base AERs with tertiary amines. Further, Gottlieb (1996) and Humbert et al. (2005) evaluated that polystyrene AERs display a higher affinity for aromatic components than polyacrylic AERs.

Furthermore, the dynamic adsorption results for 100 mg/L TOC (2-naphthol; pH 6) show that MP polystyrene AERs IRA96 and IRA900 have somewhat higher 2-naphthol capacities than MP polyacrylic AERs AP246 and A860. 2-Naphthol (pH 6) adsorption capacities were

estimated from experimental BTCs and were found to be about 93 and 109 mg/g for IRA96 and IRA900, respectively, as well as 71 and 82 mg/g for AP246 and A860, respectively. These results indicate that at higher inlet concentrations ion-dipole and/or van der Waals interactions become less important than π-π stacking and/or hydrophobic interactions. One reason could be that the number of hydrophilic functional groups is a limiting factor for 2-naphthol (pH 6) uptake by ion-dipole and/or van der Waals interactions at higher 2-naphthol inlet concentrations.

In conclusion, the most effective AER type for 2-naphthol removal from aqueous solutions in drinking water plants was found to be the MP polystyrene strong base AER IRA900. For fixed-bed design evaluation, both the LDF model as well as the Glueckauf/Hellferich formulae can be applied.

4.2.3 Fixed-bed adsorption of 2-naphthol at acidic pH

The breakthrough curves of 2-naphthol at acidic pH on the four AERs are shown in Figure 22.

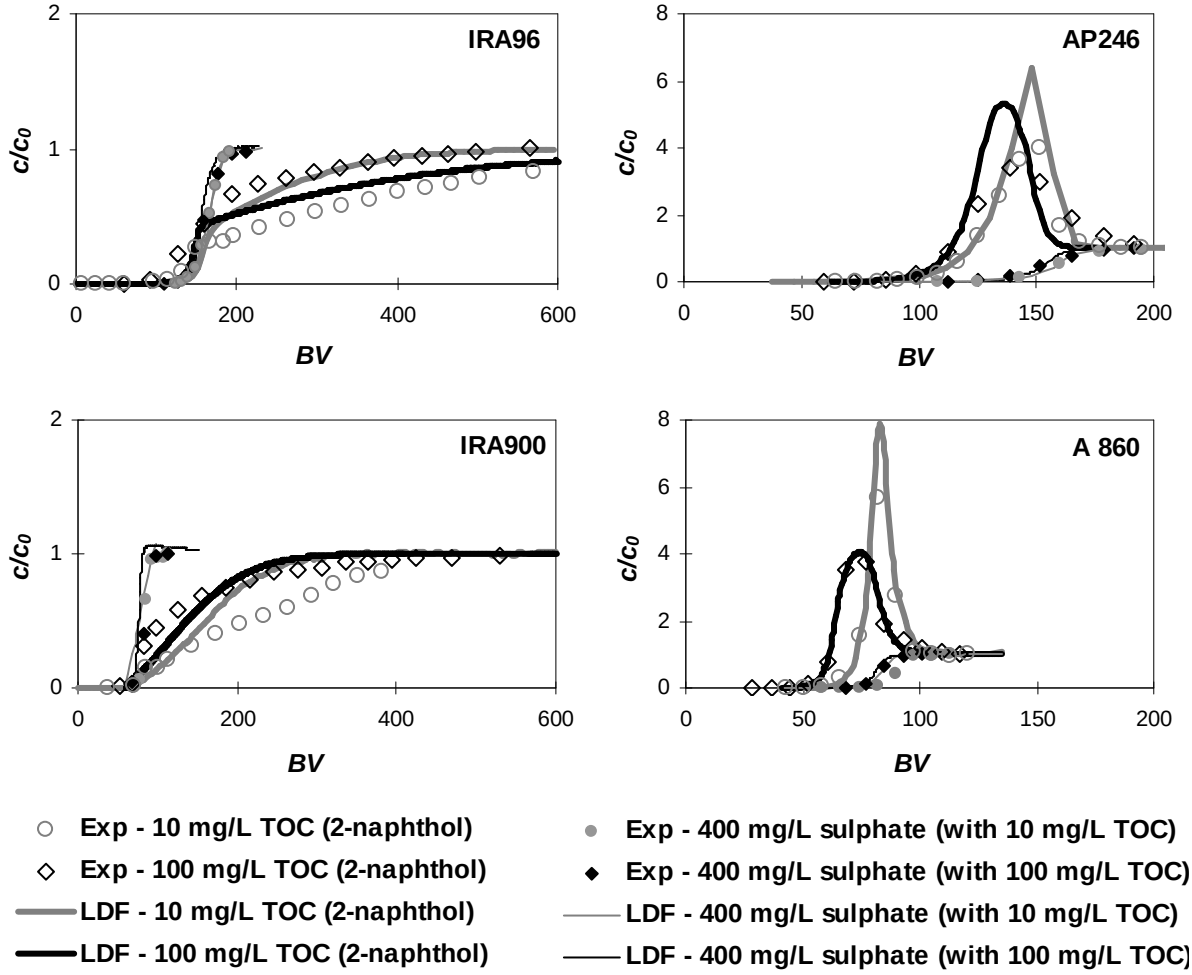

Figure 22. Breakthrough curves for TOC (2-naphthol) and sulphate onto four AERs (experimentally (Exp) determined and predicted by the linear driving force (LDF) model; c_0 = 10 and 100 mg/L TOC as well as 400 mg/L sulphate; pH 2.2).

The loading of 2-naphthol (pH 2.2) on the AERs depends strongly on the competitive uptake of the anion of the sulphuric acid (Figure 22). For MP polyacrylic medium and strong base AERs AP246 and A860, which seem to adsorb 2-naphthol mainly by ion-dipole and/or van der Waals interactions and less by π-π stacking and/or hydrophobic interactions, it follows that displacement effects take place and concentration overshoots (c/c_0 > 1) of the weaker adsorbed component 2-naphthol occur. To avoid TOC in the demineralised water, the loading

of these resins should be stopped before the 2-naphthol breakthrough. Thus, an increase of the TOC content in the demineralised water is a more suitable breaking off signal than the conductivity increase caused by (sulphate) ions. The best approach is to model the TOC breakthrough and to stop loading of the AER before the TOC content increases in the demineralised water. For this, the IAST combined with the LDF model is a suitable method. In our study, this model provides an excellent fit to the experimental data of the 2-naphthol adsorption onto MP polyacrylic AERs AP246 and A860 at acidic pH with c_0 = 10 and 100 mg/L TOC.

No concentration overshoots ($c/c_0 > 1$) were found for the adsorption of 2-naphthol (pH 2.2) onto the MP polystyrene weak and strong base AERs IRA96 and IRA900. Probably, these AERs adsorb 2-naphthol by ion-dipole and/or van der Waals interactions as well as π-π stacking and/or hydrophobic interactions. Consequently, these AERs were still able to remove some 2-naphthol after the sulphate breakthrough.

The LDF model tends to describe the experimental values in a very good manner up to the sulphate breakthrough for both TOC inlet concentrations. Therefore, as already mentioned above, the time of the loading stop for these AERs can be calculated by the LDF model to avoid leakage of TOC in the demineralised water. After the sulphate breakthrough, the LDF model approximated 2-naphthol (pH 2.2) capacities for AERs IRA96 and IRA900 with c_0 = 10 mg/L TOC, which were somewhat too low in comparison to the experimentally obtained data. Contrary, after the sulphate breakthrough, the LDF model predicted 2-naphthol (pH 2.2) uptakes for AERs IRA96 and IRA900 with c_0 = 100 mg/L TOC, which were slightly too high compared to experimental data. However, in sum, the LDF model combined with the IAST is able to predict the competitive uptake of 2-naphthol and sulphate for different AERs at acidic pH in satisfactory quality.

The breakthrough bed volumes (V_L/V_R) at c/c_0 = 0.05 for the adsorption of 2-naphthol at acidic pH was measured to be 128, 123, 75 and 61 (c_0 = 10 mg/L TOC) and 122, 110, 67 and 47 (c_0 = 100 mg/L TOC) for IRA96, AP246, IRA900 and A860, respectively. Thus, up to the initial 2-naphthol breakthrough, higher bed volumes and therefore longer running times can be obtained for weak and medium base AERs IRA96 and AP246 than for strong base AERs IRA900 and A860. In addition, longer operating times can be realised for MP polystyrene AERs IRA96 and IRA900 than for MP polyacrylic AERs AP246 and A860.

In conclusion, the MP polystyrene weak base AER IRA96 was found to be the most effective AER type for the elimination of 2-naphthol and probably also for other substances of the neutral NOM fraction in water of demineralisation plants.

4.3 Uptake of NOM from "real" water samples by anion exchange resins

4.3.1 Parameter estimation for breakthrough curve modelling of competitive NOM adsorption

Equilibrium parameters for competitive NOM adsorption at neutral pH

The experimental and calculated equilibrium data for NOM uptake (measured as DOC) from the "real" water sample after pre-treatment (coagulation, neutralisation/precipitation and filtration) onto four different AERs at pH 7 are shown in Figure 23.

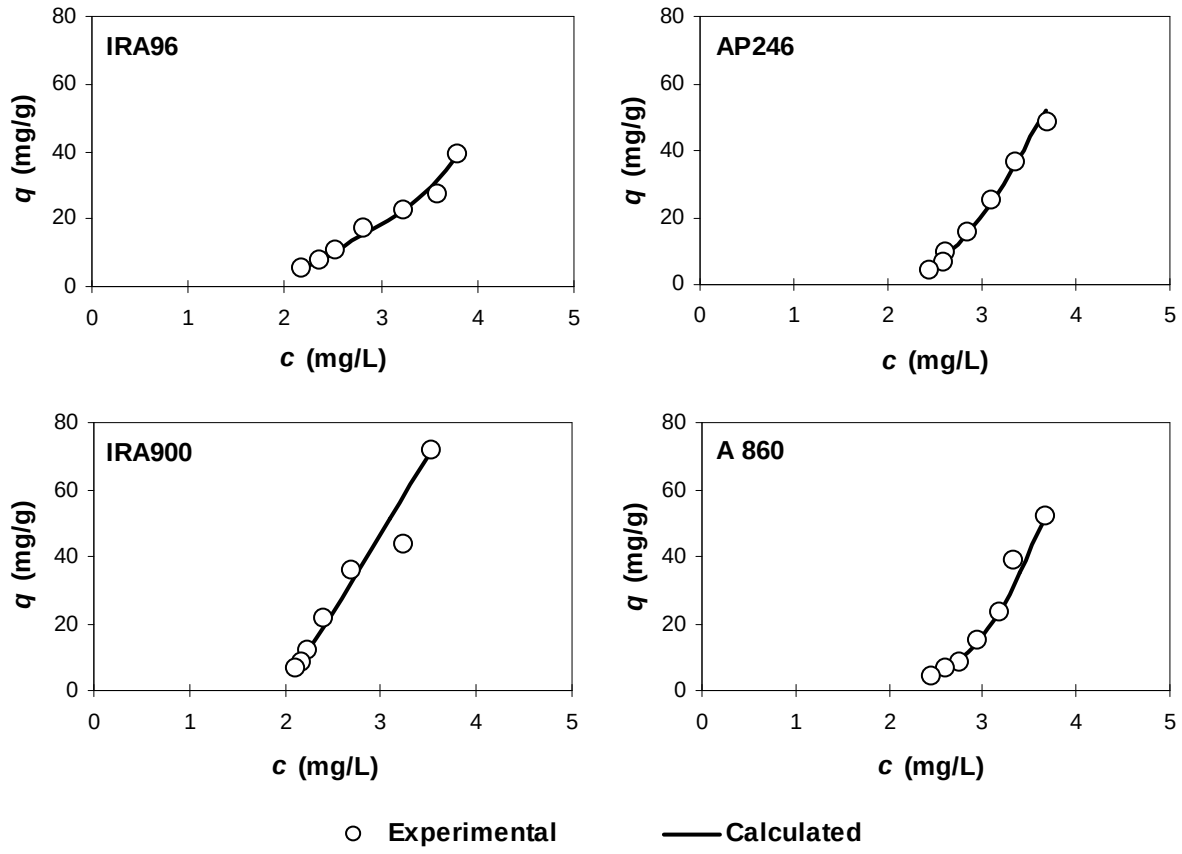

Figure 23. Experimental equilibrium data and calculated adsorption analysis results for NOM uptake (measured as DOC) from pre-treated water onto four AERs (c_0 = 4.08 mg/L DOC; pH 7).

Table 13 summarises the related concentration distributions found from the adsorption analysis of the different AERs.

Table 13. Adsorption analysis results of NOM uptake from pre-treated water onto four AERs (c_0 = 4.08 mg/L DOC; pH 7)

NOM fraction	Adsorption behaviour	K_F ((mg/g)/(mg/L)^n)	n (-)	Resin type			
				MP weak and medium base AERs		MP strong base AERs, type I	
				IRA96	AP246	IRA900	A860
				$c_{0,i}$ (mg/L DOC)			
1	non	0	-	1.94	2.33	2.02	2.27
2	weakly	5	0.5	0.54	0.29	0.11	0.59
3	moderately	20	0.5	1.22	0.71	0.67	0.45
4	strongly	80	0.5	0.37	0.75	1.28	0.76

$c_{0,i}$ = inlet concentration of the (NOM fraction) component i; mean percentage errors: 1.31 % (IRA96), 1.29 % (AP246), 2.49 % (IRA900) and 0.98 % (A860)

As can be seen in Figure 23, the selected Freundlich parameters (see Table 13) for the NOM fractions describe the DOC isotherms in satisfactory quality for the four AERs. Furthermore, the calculated inlet concentrations for the different NOM fractions ($c_{0,i}$) vary between the different AERs. A lower amount of the non-adsorbable NOM fraction was found for MP polystyrene resins IRA96 and IRA900 ($c_{0,1}$ = 1.94 and 2.02 mg/L DOC) than for MP polyacrylic resins AP246 and A860 ($c_{0,1}$ = 2.33 and 2.27 mg/L DOC).

The NOM adsorption behaviour characterised by the adsorption analysis can be taken as a quality measure in respect of the strength of the adsorption. The more the fictive component concentration distribution is shifted to the stronger adsorbable NOM fraction, the better NOM is adsorbed on the AER. In the case of MP polyacrylic medium and strong base AERs AP246 and A860, the concentrations of the different fictive components show only slight differences ($c_{0,2\text{-}4}$ = 0.29-0.76 mg/L DOC). That means that a considerable fraction of NOM is adsorbed moderately and strongly.

In case of MP polystyrene weak base AER IRA96, a larger fraction of NOM is moderately adsorbed ($c_{0,3}$ = 1.22 mg/L DOC), but only a small amount of NOM is strongly adsorbed ($c_{0,4}$ = 0.37 mg/L DOC). The MP polystyrene strong base AER IRA900 shows the best adsorption performances because most of the adsorbable NOM is strongly adsorbed ($c_{0,4}$ = 1.28 mg/L DOC) and the concentration of the weakly adsorbed NOM is very small ($c_{0,2}$ = 0.11 mg/L DOC).

These results prove that under neutral conditions the medium and strong base resins AP246, IRA900 and A860 have higher overall NOM capacities as well as a higher amount of strongly adsorbable NOM fraction than the weak base resin IRA96. This could be explained

by the quaternary amines of the medium and strong base AERs, which act as anion acceptors enabling strongly polar/ionic interactions with hydrophilic organics, whereas the tertiary amines of the weak base AER are in uncharged form and less polar/ionic interactions occur. This outcome is in accordance with results from earlier studies (e. g., Croué et al., 1999; Bolto et al., 2002; Tan et al., 2005; Boyer and Singer, 2008; Pürschel and Ender, 2008), in which polar/ionic interactions between quaternary amine functional groups and NOM adsorbates were also proposed as most important uptake mechanism under neutral pH conditions.

Furthermore, it was found that the efficiency of NOM fraction uptake at neutral pH also depends on the polymer composition of the AERs. It seems that humic substances, building blocks and LMW acids are preferentially removed by polar/ionic interaction between NOM acids/acidic components and the quaternary amines of the medium and strong base resins. In contrast, the NOM fractions of HOC, biopolymers and LMW neutrals could be primarily removed by physical adsorption (π-π stacking and/or hydrophobic interactions). As a consequence, the more hydrophobic polystyrene AERs are able to remove a higher amount of the HOC and hydrophobic neutrals fractions by physical adsorption than the polyacrylic resins (Humbert et al., 2005; Gottlieb, 1996). In contrast, AERs with polyacrylic structure tend to be more hydrophilic and they have a more open structure and higher water content (Boyer and Singer, 2008). Thus, they exhibit enforced removal of larger molecules, like biopolymers, than the polystyrene ones (Boyer and Singer, 2008; Pürschel et al., 2013a).

In the present study, the fraction of hydrophobic/neutral organic compounds was significant higher in the tested water than the fraction of larger molecules like biopolymers (see Table 6). Consequently, the MP polystyrene strong base polystyrene AER IRA900 with its more hydrophobic character is more efficient in overall NOM removal than the MP polyacrylic medium and strong base AERs AP246 and A860 with their more hydrophilic character.

Kinetic parameters for competitive NOM adsorption at neutral pH

Additionally to the adsorption analysis results, kinetic parameters are needed for BTC modelling. For the NOM uptake from pre-treated water on four different AERs, the volumetric film and intraparticle (solid) mass transfer coefficients ($k_F a_{VR}$ and k_S^*) were calculated by empirical correlations after Wilson and Geankoplis (1966) and Hess (2001) for

M = 1000 g/mol, v_F = 0.96 m/h and c_0 = 4.08 mg/L DOC. Both estimated mass transfer coefficients are given in Table 14 together with the calculated Biot numbers (*Bi*).

Table 14. $k_F a_{VR}$ and k_S^* values as well as *Bi* numbers for NOM fraction uptake from pre-treated water (pH 7) onto four AERs (M = 1000 g/mol, v_F = 0.96 m/h and c_0 = 4.08 mg/L DOC)

Parameters	**Resin type**			
	MP weak and medium base AERs		MP strong base AERs, type I	
	IRA96	**AP246**	**IRA900**	**A860**
$k_F a_{VR}$ (s^{-1})	0.5×10^{-1}	1.2×10^{-1}	0.6×10^{-1}	0.6×10^{-1}
k_S^* (s^{-1})	3.5×10^{-6}	4.0×10^{-6}	3.5×10^{-6}	3.4×10^{-6}
Bi (-)	13.4	16.3	7.2	8.8

After Hand et al. (1984), adsorption is controlled for $Bi \leq 0.5$ by the film mass transfer, for $0.5 < Bi \leq 30$ by the film and intraparticle mass transfer and for $Bi > 30$ by the intraparticle mass transfer.

The $k_F a_{VR}$ and k_S^* values for NOM adsorption at neutral pH were found to be 0.05-0.12 s^{-1} and 3.4-4.0 x 10^{-6} s^{-1}, respectively (Table 8). In addition, *Bi* values between 7.2 and 16.3 were estimated for NOM adsorption at pH 7. Therefore, NOM adsorption at pH 7 onto AERs is supposed to be controlled by both liquid film and intraparticle mass transfer rates under the given hydrodynamic conditions.

4.3.2 Fixed-bed adsorption of NOM at neutral pH

Figure 24 depicts the modelled BTCs for the NOM uptake from neutral "real" water samples onto IRA96, AP246, IRA900 and A860 together with the experimental BTC for IRA96.

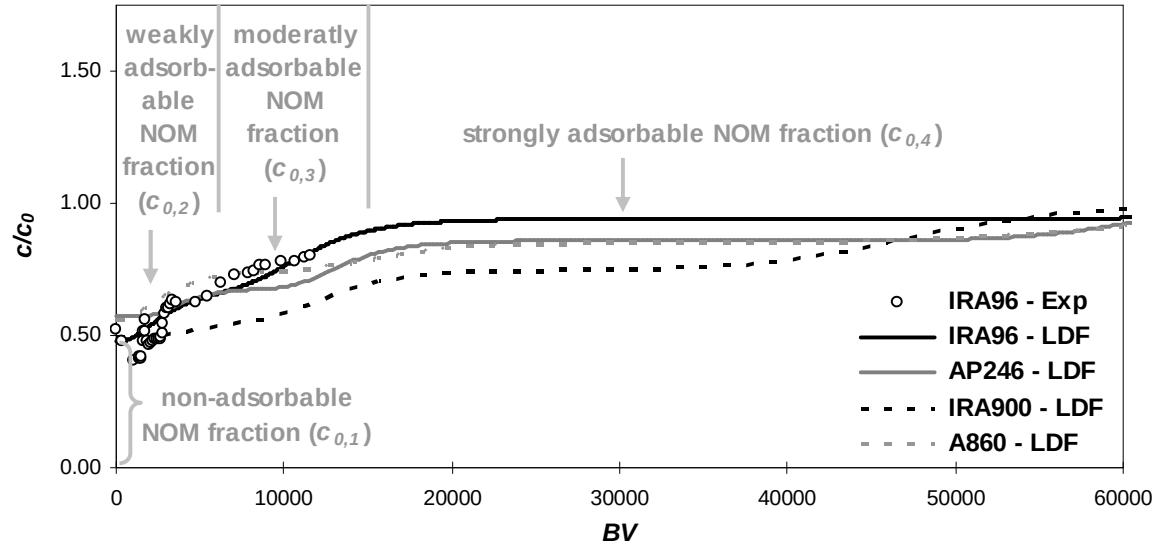

Figure 24. Breakthrough curves for NOM concentrations (measured as DOC) from pre-treated water onto four AERs (experimentally (Exp) determined and/or calculated by the LDF model with NOM fractions obtained by adsorption analysis; c_0 = 4.08 mg/L DOC; pH 7).

For AER IRA96, it could be proved that the prediction of the NOM breakthrough with the LDF model is successful (see Figure 24). Consequently, the empirical calculation of the intraparticle (solid) diffusion coefficient for NOM adsorption after Hess (2001) cannot only be applied for NOM uptake processes onto activated carbon but also onto AER material.

Applying the adsorption analysis on the experimental equilibrium data, the percentages on the non-adsorbable fraction were estimated to be about 49 % for IRA96 and IRA900 as well as about 56 % for AP246 and A860. As can be seen in Figure 24, the LDF model is able to predict the initial breakthrough of the non-adsorbable NOM fraction for all AERs. Further, the LDF model has the ability to estimate the uptake of the weakly, moderately and strongly adsorbed NOM fractions (see different breakthrough levels). Using the given equilibrium and kinetic parameters as input data, it was possible to estimate that all adsorbable NOM fractions are held back up to about 5000 BV. Furthermore, it was predicted that the moderately

adsorbable NOM fractions were removed up to about 15000 BV and only the strongly adsorbed NOM fraction could be retained between about 15000 and 60000 BV.

As a consequence, for MP polystyrene weak base AER IRA96, with its very low amount of strongly adsorbable NOM fraction, an almost total DOC breakthrough was estimated by LDF modelling at relative low bed volumes. Further, for MP polyacrylic weak and medium base AERs AP246 and A860 with their ability to uptake a considerable fraction of NOM moderately and strongly, higher overall NOM uptakes were obtained and thus longer running times were predicted than for IRA96.

In sum, at neutral pH conditions, the MP polystyrene strong base AER IRA900 removed the highest amount of the strongly adsorbable NOM fraction and shows the highest overall NOM capacity. This AER seems to be able to uptake more hydrophilic NOM fractions by polar/ionic interactions between NOM acids/acidic components and its quaternary amines as well as to remove more hydrophobic NOM fractions by π-π stacking and/or hydrophobic interactions on the polystyrene matrix.

4.3.3 Fixed-bed adsorption of NOM at acidic pH

For the "real" water sample collected after the cation exchange unit, the measured DOC and conductivity BTCs for the eight investigated AERs are shown in Figure 25.

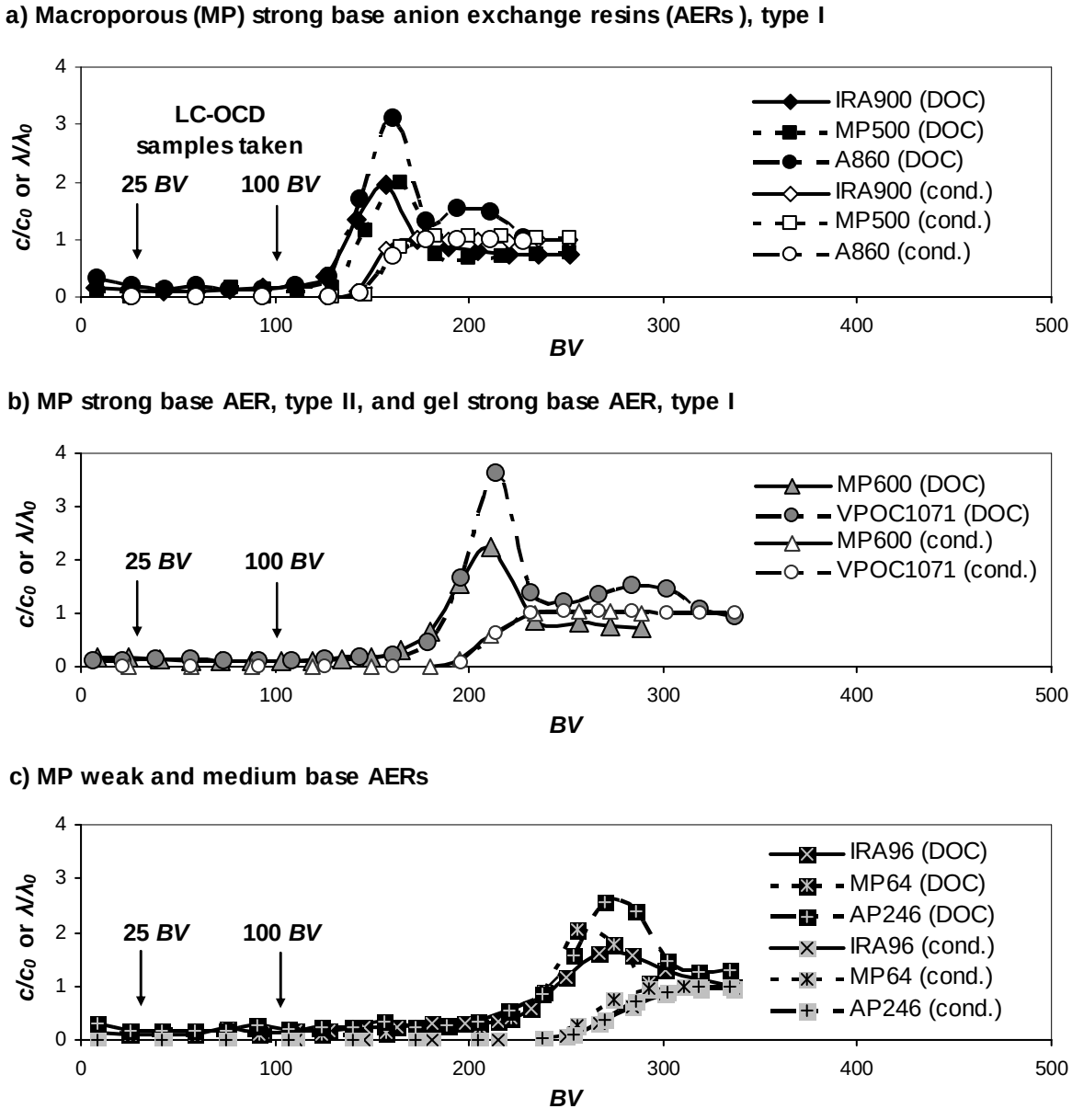

Figure 25. Experimentally determined breakthrough curves for NOM (measured as DOC) and anion concentrations (measured as conductivity (cond.; λ)) from pre-treated water after cation exchange onto eight AERs (c_0 = 3.96 mg/L DOC; pH 2.2).

Figure 25 shows that NOM (measured as DOC) as well as anions (indirectly measured by conductivity) were adsorbed in a good manner by all resins up to at least 100 BV ($c/c_0 < 0.3$). Between about 125 and 300 BV the weaker adsorbed NOM was displaced by the stronger adsorbed anion component (mainly sulphate). As a result of this competition and displacement, a concentration overshoot ($c/c_0 > 1$) can be observed for the weaker adsorbable NOM. The adsorption capacity of the resins was exhausted at about 175-300 BV, when $c/c_0 = 1$ for all components (NOM and anions).

From the BTC data shown in Figure 25, the lowest NOM uptakes (0.56-0.74 mg/g DOC) were estimated by integral mass balance equations for real BTCs for the MP strong base AERs of type I (IRA900, MP500 and A860), which also have the lowest *TVC*s (see also Table 2 and Table 3). Medium NOM capacities (0.89-0.91 mg/g DOC) were found for the MP strong base AER of type II (MP600) and the gel-type strong base AER (VPOC1071) with their intermediate *TVC*s. The highest NOM uptakes (0.84-1.26 mg/g DOC) were determined for the MP weak and medium base AERs (IRA96, MP64 and AP246), which also exhibits the highest *TVC*s. These results confirm that competitive uptake between weaker adsorbable NOM components and stronger adsorbable anions (mainly sulphate ions) occurs.

The matrix material and the structure of the AERs have also an impact on the NOM uptake. In the present work, it was found that MP polystyrene resins have NOM capacities, which are to some extent higher than those of MP polyacrylic resins, although their *TVC*s are nearly equal (IRA900 and MP500 versus A860 as well as IRA96 and MP64 versus AP246). Since polystyrene resins are more hydrophobic, they display an improved affinity for aromatic compounds than resins based on a polyacrylic structure (Humbert et al., 2005; Gottlieb, 1996; Pürschel et al., 2012). In contrast, AERs with polyacrylic structure tend to be more hydrophilic and they have a more open structure and higher water content (Boyer and Singer, 2008; Pürschel and Ender, 2008). Thus, they exhibit enforced removal of larger molecules, like biopolymers and fulvic acids, than the polystyrene ones (Boyer and Singer, 2008; Pürschel and Ender, 2013a).

In the present study, higher NOM capacities were found for MP polystyrene resins than for MP polyacrylic resins. Therefore, it can be concluded that the hydrophobic interactions have a significantly higher impact on the NOM uptake from the tested acidic water onto AERs than size-exclusion limitations. This could be expected, since the DOC concentration of the biopolymer fraction was significantly lower in the tested acidic water with 29 µg/L than the

DOC concentrations for HOC and LMW neutral fractions with 426 µg/L and 686 µg/L, respectively.

Due to their more hydrophobic character, MP polystyrene strong base AERs of type I should be more successful in the NOM uptake than those of type II with their ethanolic content in the quaternary ammonium group. However, the MP polystyrene strong base AER of type II (MP600) has a significantly higher *TVC*, so that the overall NOM capacity is increased in comparison to those of the MP polystyrene strong base AERs of type I (IRA900, MP500, A860). The *TVC* of the MP600 resin is comparable to that of VPOC1071, which is a gel-type polyacrylic strong base AER. The last one has a slightly higher NOM uptake despite its polyacrylic structure. This result is in accordance with results of Tan et al. (2005) and Cornelissen et al. (2008), who also found higher NOM removal with gel-type resins. This could be attributed to a higher swelling capacity of the gel-type resins in water. On the contrary, Bolto et al. (2002) reported that MP resins remove more NOM, since NOM components can diffuse more easily within the MP structure. The effect of MP versus gel-type structure on the adsorption of NOM should be investigated in more detail in a further study.

In demineralisation plants, the loading of the AER is generally stopped at a certain *BV* or at a point, where the conductivity or silicic acid concentration increase. In the present work and in Pürschel et al. (2013b), it could be shown that increase of the NOM content (measured as DOC) is a better alternative as switch-off criteria. Loading stop at the point of DOC increase avoids breakthrough of anions as well as of weaker adsorbed NOM components, which are considered as serious corrosion risk factor in the steam water cycle.

Furthermore, the NOM slip in the demineralised water up to the NOM breakthrough is of special interest. For that reason, the DOC concentration in the effluent samples was measured at about 25 and 100 *BV* throughput (before NOM and inorganic anion breakthrough occur, see Figure 25) for the eight investigated AERs. The results are presented in Table 15.

Table 15. DOC content in effluent samples at 25 and 100 *BV* throughput for eight AERs

Parameters	**Resin type**							
	MP strong base AERs, type I			MP strong base AER, type II	gel-type strong base AER, type I	weak and medium base AERs		
	IRA900	**MP500**	**A860**	**MP600**	**VPOC1071**	**IRA96**	**MP64**	**AP246**
DOC (at 25 *BV*; in µg/L)	227	155	268	283	159	265	138	292
DOC (at 100 *BV*; in µg/L)	376	292	377	289	256	260	240	332

It is shown in Table 15 that the DOC leakage increases in the effluent samples at 25 *BV* according to: MP64 < MP500 < VPOC1071 < IRA900 < IRA96 < A860 < MP600 < AP246. The order in the effluent samples at 100 *BV* is slightly different with MP64 < VPOC1071 < IRA96 < MP600 < MP500 < AP246 < IRA900 < A860. This might be explained with the beginning *TVC* exhaustion of the strong base AERs.

In conclusion, lower DOC escapes in the demineralised water were found for MP polystyrene AERs (e.g. MP64 and MP500) and gel-type polyacrylic AER (VPOC1071) than for MP polyacrylic AERs (AP246 and A860). All estimated DOC concentrations at 25 and 100 *BV* were above the recommended 100 ppb (VGB standard, 2011). However, for the AERs with lower DOC in the effluent (MP64, MP500, VPOC1071), there is an opportunity that the adjacent mixed-bed filter enables to meet this limit.

Additionally, LC-OCD analysis was performed to determine the extent to which different fractions of NOM were removed by the AERs (Figure 26).

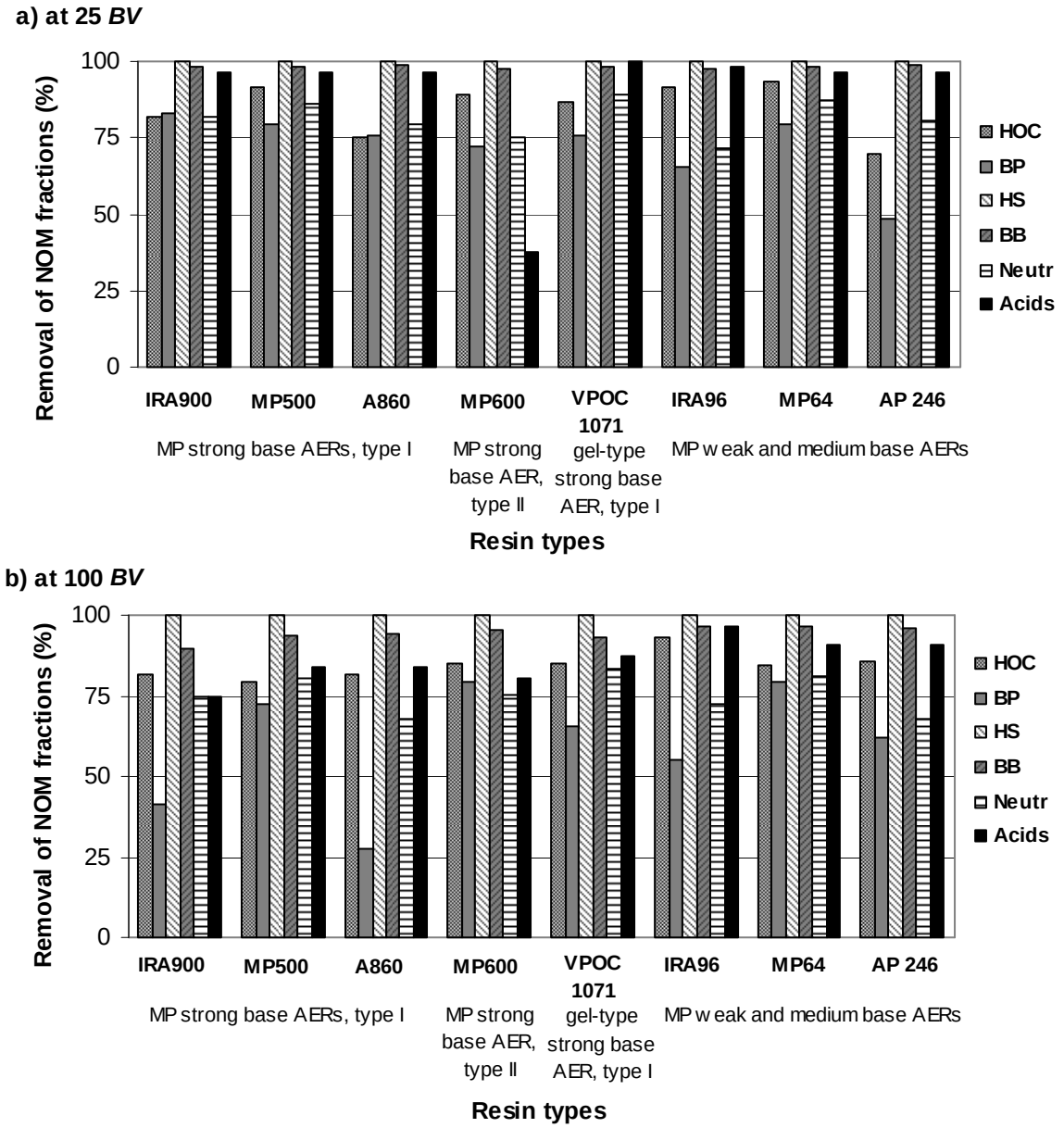

Figure 26. NOM fractions determined by LC-OCD in the effluent samples at 25 and 100 *BV* throughput for eight AERs (pH 2.2; HOC = hydrophobic organic carbon; BP = biopolymers; HS = humic substances; BB = building blocks; Neutr = low-molecular-weight (LMW) neutrals; Acids = LMW acids).

The results in Figure 26a/b show that humic substances (humic and fulvic acids) are removed up to 100 % at 25 and 100 *BV* throughput. At acidic pH, NOM components have a low charge density due to protonation of acidic functional groups (Ritchie et al., 2003; Boyer and Singer, 2008). Hence, the removal of humic substances at pH 2.2 occurs most likely by ion-dipole and/or van der Waals interactions between NOM components and the anionic resins (Croué et al., 1999) as well as by precipitation. Humic acid precipitation on the resin material

at pH values lower than pH 3.5 is a known effect and for example shown in the study by Ender et al. (2006b).

Further, it can be seen that in general building blocks and LMW acids were also preferentially removed by AERs at pH 2.2, whose uptake could also be based on ion-dipole and/or van der Waals interactions. In the effluent samples at 100 *BV*, the uptake of building blocks and LMW acids on the strong base AERs decreases to some extent, due to the beginning of the AERs exhaustion (Figure 26b).

The uptake of the HOC, biopolymer and LMW neutral fractions on the AERs is less efficient. Due to weaker interactions with the resin material, these fractions are in generally firstly displaced found in the AER filtrates (see Figure 26a/b).

Summing up, the most effective AER types for the removal of problematic NOM fractions were found to be MP500, IRA96 and MP64 for the HOC fraction, IRA900, MP500 and MP64 for the biopolymer fraction and MP500, VPOC1071 and MP64 for the LMW neutral fraction. The MP polystyrene medium base AER MP64 has a relatively high *TVC* and performs the best overall NOM fraction elimination within the examined resins. In addition, the gel-type polyacrylic strong base AER VPOC1071 was found to be the best working strong base AER regarding NOM uptake in the present study. In the case that MP polystyrene weak and strong base AERs have to be combined in the technical process, then the IRA96 and MP500 are the best tested choices to optimise NOM adsorption.

5. Conclusions

Different AERs were studied in their adsorption behaviour of NOM model substances and NOM from “real” water samples at neutral pH (pH 6 for model substances due to solution in Millipore water, and pH 7 for “real” water sample after pre-treatment procedure) and at acidic pH (pH 2.2 for model substances and “real” water sample after cation exchange unit) conditions.

The results of the present study demonstrate that under neutral and acidic pH conditions AERs are able to remove to some extent different types of starch, representing model substances for the biopolymer NOM fraction with medium to large molecular size in natural water.

Applying experimentally obtained equilibrium parameters and empirically calculated film and intraparticle (solid) diffusion coefficients, BTCs for the uptake of Merck starch at pH 6 onto AERs were predicted using the LDF model. The applicability of the BTC prediction model was verified with experimentally determined Merck starch (pH 6) BTCs for four AERs with different inlet concentrations.

It was found that size-exclusion is the main limiting mechanism for the removal of starch from water by AERs at neutral and acidic pH. As a consequence, the starch uptake by the resins rises with decreasing molecular size of the starch. In addition, the starch uptake also rises with increasing porosity, pore diameter and water content of the resin. It follows that the studied MP polyacrylic resins AP246 and A860 are more effective in starch removal than the MP polystyrene resins IRA96 and IRA900.

The uptake of starch onto AERs is further influenced by the functional groups of the resins. At neutral pH, the tertiary amines of weak and medium base AERs IRA96 and AP246 exist mainly in uncharged form. So, it is supposed that minor ion-dipole and/or van der Waals interactions occur in contrast to the strong base AERs IRA900 and A860 with their positively charged quaternary amines, leading to an earlier starch breakthrough for the weak and medium AERs. At acidic pH, ion-dipole and/or van der Waals interactions between starch and tertiary/quaternary amines could occur in the same manner. However, at this pH, the breakthrough of starch is additionally influenced by the uptake of sulphate, which acts as competing adsorbate. Thus, at acidic pH, the weak and medium base AERs IRA96 and AP246 with their higher *TVC*s should be more successful in removing starch through ion-

dipole and/or van der Waals interactions. However, to some extent this effect is superimposed by size-exclusion limitations.

In summary, at neutral and acidic pH, the most effective AER type for the elimination of the three types of starch and probably also for more substances of the biopolymer NOM fraction with medium to large molecular size, within the examined resins, was found to be the MP polyacrylic strong base AER A860 with its high water content.

The results indicate that MP polyacrylic strong base AERs (with high water content) are an alternative to the conventional adsorber resins for the removal of biopolymers from water in drinking water plants. For instance, Pürschel et al. (2013a) reported for four AERs at neutral pH higher Chemapol starch uptake capacities than for four adsorber resins. Furthermore, higher breakthrough bed volumes for high molecular weight starch molecules (pH 2.2) were found for the investigated MP polyacrylic AERs AP246 and A860 compared to the MP polystyrene AERs IRA96 and IRA900. In demineralisation plants, MP polyacrylic AERs (with high water content) are also a noteworthy option to the more regularly used MP polystyrene AERs in the elimination of the biopolymer fraction with large molecular size.

Furthermore, it was found that AERs can effectively remove 2-naphthol (pH 6 and 2.2), which was chosen as a model substance i) for the LMW neutral NOM fraction and ii) for phenolic organic pollutants.

BTCs for the uptake of 2-naphthol (pH 6) onto AERs were predicted using the LDF model as well as by applying the Glueckauf/Helfferich formulae. The applicability of both BTC prediction models was verified using experimentally obtained BTCs for 2-naphthol (pH 6) removal from water by four AERs at different inlet concentrations. It was found that the Glueckauf/Helfferich approach is not only a suitable tool for the fast calculation of BTCs for ions, but can also successfully be applied, after considering the Freundlich model for the mass balance, for the rapid prediction of BTCs for single-solute organic molecules. Further, for 2-naphthol (pH 2.2) BTC predictions, the IAST within the LDF model was applied. Calculated curves fit the experimental data in a good quality. Thus, the LDF model is an excellent tool for estimating the breakthrough bed volume of different AERs, to avoid leakage of TOC in the demineralised water caused by overloading.

The results of the present work show that at neutral pH higher 2-naphthol loadings were obtained for the more hydrophobic MP polystyrene AERs IRA96 and IRA900 than for the

less hydrophobic MP polyacrylic AERs AP246 and A860, probably due to stronger π-π stacking and/or hydrophobic interactions. Furthermore, at neutral pH, the quaternary amines of the medium/strong base AERs AP246, IRA900 and A860 are in positively charged form and seem to be able to remove 2-naphthol molecules additionally by ion-dipole and/or van der Waals interactions, whereas the tertiary amines of the weak/medium base AERs IRA96 and AP246 are mainly in uncharged form and should be less able to perform ion-dipole and/or van der Waals interactions with 2-naphthol molecules.

For 2-naphthol uptake at acidic pH, it was estimated that MP polystyrene AERs IRA96 and IRA900 remove 2-naphthol (pH 2.2) more successful than MP polyacrylic AERs AP246 and A860, which could be also caused by stronger π-π stacking and/or hydrophobic interactions. Furthermore, a higher 2-naphthol (pH 2.2) capacity was found for the MP polystyrene weak base AER IRA96 than for the MP polystyrene strong base AER IRA900, since it has a higher *TVC* (pH 2.2) and thus probably a higher amount of polar/ionic sites to perform ion-dipole and/or van der Waals interactions.

Comparing the uptake of 2-naphthol (pH 6) onto the MP polystyrene strong base AER IRA900 and onto conventional and hypercrosslinked adsorber resins, it was found that the MP polystyrene strong base AER is worth being considered as an alternative method for the removal of relative low concentrations of LMW aromatic organic compounds from aqueous solutions at neutral pH. Further, it was found that the usage of a weak base AER with MP polystyrene matrix (e.g., IRA96) is a good choice to optimise LMW neutral NOM fraction uptake in demineralisation plants at acidic pH.

The effectiveness of NOM elimination from “real” water samples (obtained from the water treatment station of a power plant) by different AERs was studied. In the present work, the fraction of hydrophobic/neutral organic compounds was significant higher in the tested water samples than the fraction of larger molecules like biopolymers (see Table 6).

At neutral pH, the BTCs for NOM uptake onto different AERs were predicted using the LDF model with the adsorption analysis results obtained from experimental equilibrium data as well as empirically calculated film and intraparticle (solid) diffusion coefficients. The applicability of the BTC prediction model was shown with the experimentally determined BTC for NOM uptake onto AER IRA96.

Higher overall NOM uptake capacities were predicted at neutral pH for medium and strong base AERs AP246, IRA900 and A860 than determined for the weak base AER IRA96. This could be explained by the positively charged quaternary amines of the medium and strong base AERs that allow polar/ionic interactions with the hydrophilic NOM fractions, whereas the tertiary amines of the weak AER are mainly in uncharged form and should be less able to perform polar/ionic interactions under neutral pH conditions. For strong base AERs, an enforced NOM capacity was estimated for the MP polystyrene resin IRA900 than for the MP polyacrylic resin A860, most probably due to an improved uptake of hydrophobic/neutral NOM components onto the MP polystyrene matrix by π-π stacking and/or hydrophobic interactions and low impact of size-exclusion limitation due to NOM composition in the "real" water sample.

Under acidic pH conditions, the NOM sorption occurs predominantly by weaker ion-dipole and/or van der Waals interactions, whereas the anion uptake is based on stronger ionic interactions. The different adsorption strengths of NOM and sulphate onto AERs result in displacement effects and leads to concentration overshoots ($c/c_0 > 1$) of the weaker adsorbed NOM components. As a consequence, it was found that the higher the *TVC* of the AER, the higher the overall NOM uptake is.

Further, the NOM leakage up to the switch off signal caused by conductivity or the more sensitive DOC concentration increase is very important. It was found that humic substances were completely removed by all resins at acidic pH, surely attributable to precipitation processes and ion-dipole and/or van der Waals interactions between NOM components and the anionic resins. Also, each AER showed high uptake affinities for building blocks and LMW acids at pH 2.2, which could be also removed by ion-dipole and/or van der Waals interactions. Lower uptakes were found for HOC, biopolymer and LMW neutral fractions at acidic pH, due to weaker interactions with the resin material. As a main result of the present study, the most effective AER types for the removal of problematic NOM fractions at pH 2.2 were found to be MP500, IRA96 and MP64 for the HOC fraction, IRA900, MP500 and MP64 for the biopolymer fraction and MP500, VPOC1071 and MP64 for the LMW neutral fraction.

In view of these results, the application of MP polystyrene strong base AERs is an option to remove specific NOM fractions, especially the HOC, low to medium molecular size biopolymers as well as the LMW neutrals, from water in drinking water treatment plants.

Furthermore, at acidic pH conditions, it was found that the MP polystyrene medium base AER MP64 performs the best overall NOM fraction removal within the examined resins. Further, the gel-type polyacrylic strong base AER VPOC1071 is the best tested strong base AER concerning NOM uptake. If MP polystyrene weak and base strong base AERs have to be integrated in the technical process, than the IRA96 and MP500 are the best tested alternatives to optimise NOM adsorption.

In future studies, the influence of resin structure (MP or gel-type), resin size and water content should be investigated in more detail. Additionally, regeneration experiments should be conducted for all AERs under neutral and acidic pH conditions to study their specific fouling character.

References

Aiken, G.R., Thurman, E.M., Malcolm, R.L., 1979. Comparison of XAD macroporous resins for the concentration of fulvic acid from aqueous solution. Analytical Chemistry 51, 1799-1803.

Aiken, G.R., McKnight, D.M., Thorn, K.A., Thurman, E.M, 1992. Isolation of hydrophilic organic acids from water using non-ionic macroporous resins. Org. Geochem. 18, 567-573.

Anderson, C.T., Maier, W.J., 1979. Trace organics removal by anion exchange resins. J. Am. Water Works Assoc. 71, 278-283.

Boening, P.H., Beckmann, D.D., Snoeyink, V.L., 1980. Activated carbon versus resin adsorption of humic substances, J. Am. Water Works Assoc. 72, 54-59.

Bolto, B., Dixon, D., Eldridge, R., King, S., Linge, K., 2002. Removal of natural organic matter by ion exchange. Water Res. 36, 5057-5065.

Bosholm, J., 1972. Zur Berechnung von Durchbruchskurven an Ionenaustauscherkolonnen (Calculation of breakthrough curves in ion-exchange columns). Chem. Techn. 24, 30-33.

Boyer, T.H., Singer, P.C., 2008. Stoichiometry of removal of natural organic matter by ion exchange. Environ. Sci. Technol. 42, 608-613.

Boyer, T.H., Singer, P.C., Aiken, G.R., 2008. Removal of dissolved organic matter by anion exchange: Effect of dissolved organic properties. Environ. Sci. Technol. 42, 7431-7437.

Caetano, M., Valderrama, C., Farran, A., Cortina, J.L., 2009. Phenol removal form aqueous solution by adsorption and ion exchange mechanisms onto polymeric resins. Journal of Colloid and Interface Science 338, 402-409.

Christman, R.F., Ghassemi, M., 1966. Chemical nature of organic color in water. J. Am. Water Works Assoc. 58, 723.

Cornelissen, E.R., Moreau, N., Siegers, W.G., Abrahamse, A.J., Rietveld, L.C., Grefte, A., Dignum, M., Amy, G, Wessels, L.P., 2008. Selection of anionic exchange resins for removal of natural organic matter (NOM) fractions. Water Res. 42, 413-423.

Crittenden, J.C., Berrigan J.K., Hand, D.W., 1986. Design of rapid small-scale adsorption tests for a constant surface diffusivity. J Water Pollut control Fed 58, 312-319.

Crittenden, J.C., Berrigan J.K., Hand, D.W., Lykins, B., 1987. Design of rapid small-scale adsorption tests for a nonconstant diffusivities. J Environ Eng - ASCE 113, 243-259.

Croué, J.-P., Violleau, D., Bodaire, C., Legube, B., 1999. Removal of hydrophobic and hydrophilic constituents by anion exchange resin. Water Sci. Technol. 40, 207-214.

Ender, V., Kettner, B., Schumann, T., Hajdamowicz, S., 2006a. The influence of temperature on the removal of organics from natural waters by ion exchange – laboratory and pilot plant experiments. PowerPlant Chemistry 8, 117-125.

Ender, V., Schumann T., Sachs, S., Bernhard, G., 2006b. On the uptake mechanisms of organics from natural water – Investigations with strong and weak base ion exchangers and their corresponding copolymers. PowerPlant Chemistry 8, 541-549.

Fettig, J., 2005. Modelling the uptake of natural organic matter (NOM) by different granular sorbent media. J. Water Supply Res. Technol.-AQUA 54, 83-93.

Fu, P.L.-K., Symons, J.M., 1990. Removing aquatic organic substances by anion exchange resins. J. AWWA 82, 70-77.

Genz, A., Baumgarten, B., Goernitz, M., Jekel, M., 2008. NOM removal by adsorption onto granular ferric hydroxide: Equilibrium, kinetics, filter and regeneration studies, Water Res. 42, 238-248.

Glueckauf, E., 1955a. Theory of chromatography: Pt. 10. Formulae for diffusion into spheres and their application to chromatography. Trans. Faraday Soc. 51, 1540-1551.

Glueckauf, E., 1955b. Principles of operation of ion-exchange columns. In: “Ion exchange and its application”, Soc. chem. Ind., London, 34-46.

Goto, M., Hayashl, N., Goto, S., 1986. Adsorption and desorption of phenol on anion-exchange resin and activated carbon. Environ. Sci. Technol. 20, 463-467.

Gottlieb, M., 1996. The reversible removal of naturally occurring organics using resins regenerated with sodium chloride. Ultrapure Water 11, 53-58.

Guimarães, D., Leão, V.A., 2011. Studies of sulphate ions removal by the polyacrylic anion exchange resin Amberlite IRA458: batch and fixed-bed column studies. In: “Mine Water – Managing the Challenges”, Aachen (Germany), 337-341.

Hand, D.W., Crittenden, J.C., Thacker, W.E., 1984. Simplified models for design of fixed-bed adsorption systems. J. Environ. Eng.-ASCE 110, 440-456.

Heese, C., Worch, E., 1997. Eine neue anwenderorientierte Methode zur Vorausberechnung von Stoffübergangskoeffizienten für die Adsorbermodellierung (A new user-oriented method for prediction of intraparticle mass transfer coefficients for adsorber modelling). Vom Wasser 89, 373-391.

Heijman, S.G.J., van Paassen, A.M., van der Meer, W.G.J., Hopman, R., 1999. Adsorptive removal of natural organic matter during drinking water treatment. Water Sci. Technol. 40, 183-190.

Helfferich, F., 1962. Ion exchange. McGraw-Hill Book Company, Inc., New York.

Hess, F., 2001. Entwicklung praxisorientierter Berechnungsgrundlagen für die Kinetik der Aktivkohlefiltration in der Trinkwasseraufbereitung (Development of practice-oriented design fundamentals for activated carbon filtration in drinking water treatment). PhD thesis, Dresden University of Technology, Dresden (Germany).

Hongve, D., Baann, J., Becher, G., Beckmann, O.A., 1999. Experiences from operation and regeneration of an anionic exchanger for natural organic matter (NOM) removal. Water Science and Technology 40, 215-221.

Huang, J., Yuan, B., Wu, X., Deng, S., 2012. A comparative adsorption study of β-naphthol on four polymeric adsorbents from aqueous solution. Journal of Colloid and Interface Science 380, 166-172.

Huber, S.A., Frimmel, F.H., 1996. Size-exclusion chromatography with organic carbon detection (LC-OCD): a fast and reliable method for the characterisation of hydrophilic organic matter in natural waters. Vom Wasser 86, 277-290.

Huber, S.A., Gluschke, M., 1998. Chromatographic characterisation of TOC in process water treatment. Ultrapure Water 3, 48-52.

Huber, S.A., 2006. The behaviour of natural organic matter in water treatment and the water water/steam cycle: deeper insights. PowerPlant Chemistry 8, 105-116.

Hübner, P., 2011. Organics removal in water treatment plants. PowerPlant Chemistry 13, 426-435.

Humbert, H., Gallard, H., Suty, H., Croué, J.-P., 2005. Performance of selected anion exchange resins for the treatment of a high DOC content surface water. Water Res. 39, 1699-1708.

Jain, A.K., Gupta, V.K., Jain, S., Suhas, S., 2004. Removal of chlorophenols using industrial wastes. Environ. Sci. Technol. 38, 1195-2000.

Janoš, P., 2003. Separation methods in the chemistry of humic substances. J. Chromatogr. A. 983, 1-18.

Johannsen, K., Worch, E., 1994. Eine mathematische Methode zur Durchführung von Adsorptionsanalysen (A mathematical method for evaluation of adsorption analysis). Acta Hydrochim. Hydrobiol. 22, 225-230.

Karagas, M., Villanueva, C.M., Nieuwenhuijsen, M.J., Weisel, C.P., Cantor, C.P., Kogevinas, M., 2008. Disinfection by-products and skin cancer: a hypothesis. Cancer Cause Control 19, 547-548.

Krasner, S.W., Amy, G., 1995. Jar-test evaluations of enhanced coagulation. Journal American Water Works Association 87, 93-107.

Kümmel, R., Worch, E., 1990. Adsorption aus wässrigen Lösungen (Adsorption from aqueous solutions). VEB Deutscher Verlag für Grundstoffindustrie, Leipzig.

Küster, F.W., Thiel, A., 2008. Rechentafeln für die chemische Analytik (Tables for chemical analysis). De Gruyter, Berlin/New York.

Leenheer, J.A., 1994. Chemistry of dissolved organic matter in rivers, lakes, and reservoirs. In: Baker, L. A. (Ed.), Environmental Chemistry of Lakes and Reservoirs. American Chemical Society, Washington, D.C., 195-221.

Leenheer, J.A., Croué, J.P., 2003. Characterizing aquatic dissolved organic matter. Environmental Science and Technology 37, 18a-26a.

Li, P., Sengupta, A.K., 2004. Sorption of hydrophobic ionizable organic compounds (HIOCs) onto polymeric ion exchangers. Reactive and functional Polymers 60, 27-39.

Luukkonen, T., Hukkanen, R., Pellinen, J., Rämö, J., Lasse, U., 2012. Reduction of organic carbon in demineralised make-up water with activated carbon. PowerPlant Chemistry 14, 112-119.

Mattaraj, S., Kilduff, J.E., 2003. Using reverse osmosis to remove natural organic matter from power plant makeup water. PowerPlant Chemistry 5, 31-35.

McDonald, S., Bishop, A.G., Prenzler, P.D., Robards, K., 2004. Analytical chemistry of freshwater humic substances. Analytica Chimica Acta 527, 105-124.

Moon, H., Lee, W.K., 1986. A lumped model for multicomponent adsorptions in fixed-beds. Chem. Eng. Sci. 41, 1995-2004.

Myers, A.L., Prausnitz, J.M., 1965. Thermodynamics of mixed-gas adsorption. Am. Inst. Chem. Eng. J. 11, 121-127.

Nouri, S., Dolat Abad, R.M., Bahram, M., 2012. Adsorption studies of β-naphthol by untreated and treated activated carbon [optimizing of adsorption by central composite design (CCD)]. Journal of the Iranian Chemical Society 9, 397-405.

Pan, B.C., Meng, F.W., Chen, X.Q., Pan, B.J., Li, X.T., Zhang, W.M., Zhang, X., Chen, J.L., Zhang, Q.X., Sun, Y., 2005. Application of an effective method in predicting breakthrough curves of fixed-bed adsorption onto resin adsorbent. Journal of Hazardous Materials B124, 74-80.

Peuravouri, J., Pihlaja, K., 1997. Molecular size distribution and spectroscopic properties of aquatic humic substances. Analytical Chimica Acta 337, 133-149.

Peuravouri, J., Monteiro, A., Eglite, L, Pihlaja, K., 2005. Comparative study for separation of aquatic humic-type organic constituents by DAX-8, PVP and DEAE sorbing solids and tangential ultrafiltration: elemental composition, size-exclusion chromatography, UV-vis and FT-IR. Talanta 65, 408-422.

Pürschel, M., Ender, V., 2008. Sorption of natural organic matter by adsorber and ion exchange resins – Investigations with starch and phenylalanine as model substances. In: 15th International Conference on the Properties of Water and Steam (15th ICPWS), 07.-11.09.2008, Berlin (Germany), ISBN 978-3-931384-64-7.

Pürschel, M., Worch, E., Ender, V., 2012. Uptake of low-molecular-weight neutrals NOM fraction by different anion exchange resins – Equilibrium data and modelling of breakthrough curves. In: 3rd International Conference "Interaction of organics and organic plant cycle treatment chemicals with water, steam and materials". 21.-23.05.2012, Heidelberg (Germany).

Pürschel, M., Sachs S., Bernhard, G., Ender, V., 2013a. Uptake of multi-disperse starch by anion exchangers. Journal of Physical Science and Application 3, 147-155.

Pürschel, M., Worch, E., Ender, V., 2013b. Uptake of NOM fractions by anion-exchange resins in demineralization plants. Desalination and Water Treatment, DOI 10.1080/19443994.2013.825884, in press.

Radke, C.J., Prausnitz, J.M., 1972. Thermodynamics of multisolute adsorption from dilute liquid solutions. Am. Inst. Chem. Eng. J. 18, 761-768.

Ritchie, J.D, Perdue, E.M., 2003. Proton-binding study of standard and reference fulvic acids, humic acids, and natural organic matter. Geochimica et Cosmochimica Acta 67, 85-96.

Sachs, S., Bubner, M., Schmeide, K., Choppin, G.R., Heise, K.H., Bernhard, G., 2002. Carbon-13 NMR spectroscopic studies on chemically modified and unmodified synthetic and natural humic acids. Talanta 57, 999-1009.

Schley, H., Markert, A., 2004. Reverse osmosis as part of the makeup water treatment in the Lippendorf Power Station. In: Proc. Zittau Power Plant Symposium "Application of ion exchange and membrane techniques to makeup boiler water treatment in power plants", 16.-17.10.2004, Oybin (Germany).

Schönfelder, T., Lutat, A., 2000. Chemistry of steam water cycles of the Rostock Power Station with special viewing to organic ingredients. In: Proc. Zittau Power Plant Chemistry Symposium "TOC in steam water cycles", Zittau (Germany), Scientific Reports of the University of Applied Sciences Zittau/Görlitz 67, 26-43.

Schumann, T., 2005. Untersuchungen zur Entfernung organischer Wasserinhaltsstoffe mit Ionenaustauschern (Investigations for the removal of NOM by ion exchangers). Diploma thesis, University of Applied Sciences Zittau/Görlitz, Zittau (Germany).

Sontheimer, H., 1975. Verfahrenstechnische Grundlagen von Adsorption und Ionenaustausch (Process principals of the functional operation of adsorption and ion-exchange). Lecture script, Karlsruhe University of Technology, Karlsruhe (Germany).

Sontheimer, H., Crittenden, J.C., Summers, R.S., 1988. Activated Carbon for Water Treatment. DVGW Forschungsstelle, Karlsruhe.

Sperlich, A., Schimmelpfennig, S., Baumgarten, B., Genz, A., Amy, G., Worch, E., Jekel, M., 2008. Prediction anion breakthrough in granular ferric hydroxide (GFH) adsorption filters. Water Res. 42, 2073-2082.

Svoboda, R., Denk, J., Maggi, C., 2003. Influence of carbon dioxide on corrosion in steam turbines. PowerPlant Chemistry 5, 581-586.

Tan, Y., Kilduff, J.E., Kitis, M., Karanfil, T., 2005. Dissolved organic matter removal and disinfection byproduct formation control using ion exchange. Desalination 176, 189-200.

Tan, Y., Kilduff, J.E., 2007. Factors affecting selectivity during dissolved organic carbon matter removal by anion-exchange resins. Water Research 41, 4211-4221.

Van der Kooij, D., 2003. Biodegradable compounds and biofilm formation in water treatment and distribution. In: Watanabe, Y., Funimizu, N. (Eds.), Water Resources and Water Supply in the 21st Century. Hokkaido University Press, Sapporo.

VGB standard, 2011. “Guidelines for Feed Water, Boiler Water and Steam Quality for Power Plants / Industrial Plants.” 3th Edition, instruction sheet VGB-S-010-T-00;2011-12.DE. VGB PowerTech Service GmbH, Essen (Germany).

Villanueva, C.M., Cantor, K.P., Grimalt, J.O., Malats, N., Silverman, D., Tardon, A., Garcia-Closas, R., Serra, C., Carrato, A., Castano-Vinyals, G., Marcos, R., Rothman, N., Real, F.X., Dosemeci, M., Kogevinas, M., 2007. Bladder cancer and exposure to water disinfection by-products through ingestion, bathing, showering and swimming in pools. Am. J. Epidemiol. 165, 148-156.

Williamson, J.E., Bazaire, K.E., Geankoplis, C.J., 1963. Liquid-phase mass transfer at low Reynolds numbers. Ind. Eng. Chem. Fundam. 2, 126-129.

Wilson, E.J., Geankoplis, C.J., 1966. Liquid mass transfer at very low Reynolds numbers in packed beds. Ind. Eng. Chem., Fundam. 5, 9-14.

Worch, E., 1991a. Zur Vorausberechnung der Gemischadsorption in Festbettadsorbern Teil 1: Mathematisches Modell (Prediction of mixture adsorption in fixed-bed adsorbers Pt. 1: Mathematical model). Chem. Tech. 43, 111-113.

Worch, E., 1991b. Zur Vorausberechnung der Gemischadsorption in Festbettadsorbern Teil 2. Anwendung des Berechnungsmodells auf experimentell untersuchte Systeme (Prediction of mixture adsorption in fixed bed adsorbers: Pt. 2: Application of the calculation model to experimentally investigated systems. Chem. Tech. 43, 221-224.

Worch, E., 1993. Eine neue Gleichung zur Berechnung von Diffusionskoeffizienten gelöster Stoffe (A new equations for the calculation of diffusion coefficients for dissolved substances). Vom Wasser 81, 289-297.

Worch, E., 2012. Adsorption Technology in Water Treatment. Fundamentals, Processes and Modeling. De Gruyter, Berlin/Boston.

Zhang, W., Changhong, H., Pan, B., Zhang, Q., Jiang, P., Jia, K., 2009. Sorption enhancement of 1-naphthol onto a hydrophilic hyper-cross-linked polymer resin. J. Hazard. Mater. 163, 53-57.

Zhaoyi, X., Zhang, Q., Chen, J., Wang, L., Anderson, G.K., 1997. Adsorption of naphthalene derivatives on different macroporous polymeric adsorbents. Chemosphere 35, 2269-2276.